

**THE ROLE OF LYSOSOMAL ACID LIPASE IN  
HEPATIC CHOLESTEROL METABOLISM AND  
NON-ALCOHOLIC FATTY LIVER DISEASE**

A DISSERTATION

SUBMITTED TO THE FACULTY OF  
THE UNIVERSITY OF MINNESOTA BY

**MICHAEL LOPRESTI**

IN PARTIAL FULFILLMENT OF THE REQUIREMENTS  
FOR THE DEGREE OF  
DOCTOR OF PHILOSOPHY

DR. DOUGLAS MASHEK, ADVISOR

DECEMBER 2021

© Michael Lopresti 2021

## **Acknowledgements**

I would like to thank my advisor Dr. Doug Mashek for his support, guidance, and understanding throughout my PhD. Thank you for pushing me when I needed it; I'll do my best to make you famous. Thank you to the rest of the Mashek Lab during my time here, especially Mara Mashek for always making time for any and all questions I had. I'm thankful for the perspective and shared experience provided by my fellow graduate students: Jonas Alvarez and Mahima Devarajan. Special thanks to Dr. Wenqi Cui for lots of coffee trips and countless hours talking about lipophagy. Thank you to Arnav Desai for being an excellent mentee and for reminding me why I do what I do. I would like to acknowledge my thesis committee and thank them for their support and expertise: Dr. Do-Hyung Kim, Dr. Deborah Ferrington, and Dr. Thomas Neufeld. I would also like to thank the Proteomics of Aging training grant for funding support.

I would like to thank my parents, John and Mary Beth, and my siblings, Sophia and Anthony, for their unending support and love, even from a thousand miles away. Thank you to my entire family for reminding me what's important when grad school was difficult. I would like to acknowledge the entire Meyerhoff (M23) class, as I would not have made it this far without our shared experiences; specifically, Dr. Ifeolu Akinnola and Yves Nazon for being the best/worst roommates of all time, respectively. Thank you to Michael Pereira for providing much needed perspective and encouragement. Thank you to my friends and classmates at the U for always being down talk and grab a drink at Stubs pre-2020, and for countless hours on Zoom during and after 2020. I would also like to thank Doug Petrie for helping me make some truly life altering realizations.

Lastly, I would like to acknowledge my wife, Natalie, and the home that we have made together. I would like to thank Roxanne for being the perfect pet throughout my degree, and Percival, Blizzard, and Chuk for being a close second(s). Nat, thank you for reminding me when I needed a break and for listening as I rambled about lipids. There's no one I would rather cry about grad school stressors and big life changes with. Thank you for loving me no matter who I am.

## **Abstract**

Non-alcoholic fatty liver disease (NAFLD) is characterized by the accumulation of lipid droplets (LD) in hepatocytes. NAFLD development and progression is associated with an increase in hepatic cholesterol levels and decreased autophagy and lipophagy flux. Previous studies have shown that the expression of lysosomal acid lipase (LAL, encoded by the gene LIPA), which can hydrolyze both triglyceride and cholesteryl esters, is inversely correlated with the severity of NAFLD. Here, we examine how LAL dysfunction promotes the unregulated synthesis of cholesterol and whether LAL overexpression protects against the development of NAFLD. We used a combination of LAL inhibition and knockdown to evaluate how cholesterol liberated from LAL regulates sterol regulatory element binding protein 2 (SREBP2). Our data indicates that the lysosomal cholesterol pool that regulates SREBP2 is heavily reliant on exogenous lipid sources and is converted into oxysterols to provide negative feedback. We also predicted that overexpressing LIPA in the livers of mice fed a Western diet would prevent the development of NAFLD. As expected, mice fed the Western diet exhibited numerous markers of NAFLD, including hepatomegaly, lipid accumulation, and inflammation. Unexpectedly, LAL overexpression did not attenuate steatosis and had only minor effects on neutral lipid composition. However, LAL overexpression exacerbated inflammatory gene expression and infiltration of immune cells in mice fed the Western diet. LAL overexpression also resulted in abnormal phagosome accumulation and lysosomal lipid accumulation depending upon the dietary treatment. Overall, we show a disconnect in the regulation of cholesterol resulting from LAL knockdown versus overexpression. While knockdown results in a broken feedback loop, the overexpression of LAL does not significantly alter cholesterol pools. Ultimately, hepatic overexpression of LAL drives immune cell infiltration and inflammation and does

not attenuate the development of NAFLD, suggesting that targeting LAL expression may not be a viable route to treat NAFLD in humans.

## **Table of Contents**

<b>Acknowledgements</b> .....	i
<b>Abstract</b> .....	ii
<b>List of Figures</b> .....	vi
<b>Chapter One: The Role of Lysosomal Acid Lipase in Lipid Metabolism</b> .....	1
Non-alcoholic fatty liver disease (NAFLD) .....	2
The Liver.....	2
Hepatic lipid synthesis .....	3
Lipid droplets (LDs).....	5
Liver distribution of lipoproteins.....	6
Cellular nutrient sensing.....	8
Cellular regulation of lipid metabolism.....	10
Mechanisms of lipophagy.....	12
Lysosomal Acid Lipase (LAL).....	17
LAL mutations result in severe clinical phenotypes .....	17
NAFLD and LAL.....	18
Goals and objectives.....	19
<b>Chapter Two: Lysosomal Acid Lipase Dysfunction Indirectly Promotes Cholesterol</b>	
<b>Synthesis</b> .....	21
Summary .....	22
Introduction.....	23
Materials and Methods.....	25
Results.....	29
Discussion .....	41
<b>Chapter Three: Hepatic Lysosomal Acid Lipase Overexpression Worsens Hepatic</b>	
<b>Inflammation in Mice Fed a Western Diet</b> .....	45
Summary .....	46
Introduction.....	47
Materials and Methods.....	48
Results.....	55
Discussion .....	82

Data availability.....	84
Acknowledgements.....	84
<b>Chapter Four: Conclusions and Perspectives .....</b>	<b>86</b>
<b>Bibliography .....</b>	<b>92</b>

**List of Figures**

**Chapter One: The Role of Lysosomal Acid Lipase in Hepatic Lipid Metabolism**

**Figure 1.1:** LAL function in the lysosome.....16

**Chapter Two: Lysosomal Acid Lipase Dysfunction Indirectly Promotes Cholesterol Synthesis**

**Figure 2.1:** LAL regulates cholesterol synthesis .....31

**Supplemental Figure 2.1:** LIPA mRNA expression correlates with SREBP2 targets 32

**Figure 2.2:** Lysosomal cholesterol regulates SREBP2 via oxysterol levels.....34

**Figure 2.3:** SREBP2 activity is controlled in part by insulin signaling.....36

**Figure 2.4:** LDL absence ablates LAL inhibition effect under certain conditions .....38

**Figure 2.5:** Extracellular free cholesterol decreases LAL activity .....40

**Figure 2.6:** Model of the role of LAL in regulating SREBP2 activity .....42

**Chapter Three: Hepatic Lysosomal Acid Lipase Overexpression Worsens Hepatic Inflammation in Mice Fed a Western Diet**

**Figure 3.1:** LAL overexpression alters hepatic LD size distribution.....57

**Supplemental Figure 3.1:** Female mice data corresponding to Figure 1. ....59

**Figure 3. 2:** LAL overexpression modifies hepatic lipid species.....64

**Supplemental Figure 3.2:** Change in body mass .....61

**Figure 3.3:** Whole body treatment effects.....68

**Supplemental Figure 3.3:** Hepatic lipids and peripheral analyses in female mice ....65

**Figure 3.4:** LAL overexpression altered the hepatic transcriptome .....71

**Supplemental Figure 3.4:** Gene ontology analysis of transcriptomic data .....72

**Figure 3.5:** LAL overexpression promoted immune cell infiltration and inflammation .75

**Supplemental Figure 3.5:** Immune measurements in females and systemic infiltration in males .....77

<b>Figure 3.6:</b> LAL overexpression alters autophagosome abundance. ....	80
<b>Supplemental Figure 3.6:</b> Autophagic measurements in females.....	81

# CHAPTER ONE

## The Role of Lysosomal Acid Lipase in Hepatic Lipid Metabolism

Michael Lopresti wrote this chapter in its entirety

## **Non-alcoholic fatty liver disease (NAFLD)**

NAFLD is characterized by the excessive accumulation of lipids in the liver and is intricately linked with the development of metabolic syndrome. Accumulation of lipid in the liver results in liver damage and metabolic abnormalities throughout the body that increase the risk of numerous diseases including Type 2 Diabetes and cardiovascular disease. If untreated, NAFLD can progress into non-alcoholic steatohepatitis (NASH), which is characterized by increased cholesterol accumulation, hepatocyte ballooning, and cell death. The damage to the liver resulting from NASH may lead to the formation of scar tissue and liver fibrosis, which can further develop into hepatocellular carcinoma. NAFLD is a major health issue affecting 1 in 4 people worldwide<sup>1</sup>. In the US alone, NAFLD drives medical costs of about \$103 billion, without factoring in societal costs<sup>2</sup>. Unfortunately, there are no FDA approved drugs for treating NAFLD, so it is essential to improve our understanding of liver lipid breakdown and synthesis.

## **The Liver**

The liver is an incredibly heterogenous organ, with hepatocytes comprising 60% of the cells in the liver, and the rest being hepatic stellate cells, Kupffer cells, endothelial cells, and infiltrating immune cells<sup>3</sup>. The functional unit in the liver is the lobule, a hexagonal structure made of hepatocytes centered around a central vein and surrounded by portal triads. The portal triad is composed of a portal vein, hepatic artery, and bile duct. These structural differences result in heterogenous delivery of oxygen and nutrients, which likely contributes to the zonation of gene expression profiles and metabolism in hepatocytes across the liver. As a whole, the liver is a major metabolic hub that regulates whole-body metabolism by providing glucose, lipids, and ketone bodies to other tissues.

The liver plays a large role in controlling blood glucose levels. The liver responds to changes in circulating glucose levels by adjusting gluconeogenesis and glycogenolysis in response to changes in insulin and glucagon. Gluconeogenesis converts metabolic byproducts, like lactate and glycerol, into glucose to maintain blood sugar levels. Simultaneously, glycogen, the storage form of glucose that is present in large quantities in the liver, can also be broken down and released into the blood as glucose. Both processes are inhibited by the increased insulin that accompanies high blood glucose, resulting in glucose storage as glycogen. In times of decreasing blood glucose, glucagon initiates gluconeogenesis and glycogen breakdown, resulting in the large release of glucose from the liver.

### **Hepatic lipid synthesis**

The liver plays a major role in numerous facets of whole lipid metabolism, including *de novo* lipogenesis of fatty acids (FA), synthesizing triacylglycerol (TAG) and cholesterol, and regulating the circulating pool of lipoproteins. The production of various lipid species from acetyl-CoA, termed *de novo* lipogenesis, is upregulated in response to nutrient rich conditions, and can produce up to a third of hepatic TAG<sup>4</sup>.

The first step of *de novo* FA synthesis is the carboxylation of acetyl-CoA by acetyl-CoA carboxylase (ACC) to produce malonyl-CoA. The FA synthase complex repeatedly combines malonyl-CoAs with the starting acetyl-CoA via an NADPH dependent redox reaction until a FA is produced. The primary endpoint is palmitic acid (16:0), though both myristate (14:0) and medium chain FAs may be formed. Longer and more complex FAs are produced by additional enzymes. Elongation of the acyl chain past 16 carbons is initiated by the seven members of the Elovl (Elongation of Very Long chain FAs) elongase family. Additionally, FA desaturases introduce single double bonds to form

monounsaturated FAs but are unable to produce polyunsaturated FAs *de novo*. Long chain polyunsaturated FAs like arachidonic, eicosapentaenoic, or docosahexaenoic acids require 18 carbon precursors such as linoleic and  $\alpha$ -linolenic acid, respectively.

As FAs are highly lipotoxic when unesterified, synthesized FAs are stored as TAG. In the liver, this process begins in the ER with the esterification of a FA and glycerol-3-phosphate by a glycerol-3-phosphate acyltransferase (GPAT) enzyme, resulting in the formation of lysophosphatidic acid. Acyl-CoA: acylglycerol-3-phosphate acyltransferases add a second acyl group to the lysophosphatidic acid, producing phosphatidic acid. For TAG synthesis, the phosphate group is then removed from phosphatidic acid by phosphatidic acid phosphatase, or lipin, to produce diacylglycerol. Diacylglycerol acyltransferases perform the final reaction, combining diacylglycerol with a final FA molecule. The produced TAGs accumulate in the ER before being budding off the ER membrane as LDs.

As with other lipid synthetic pathways, sterol biosynthesis begins with acetyl-CoA, which is converted to mevalonate by the activities of acetoacetyl-CoA synthetase, 3-hydroxy-3-methylglutaryl-CoA (HMG-CoA) synthase, and HMG-CoA reductase (HMGCR), the latter of which is the rate-limiting step in cholesterol biosynthesis. Another series of enzymes convert mevalonate into squalene, and then lanosterol. The final conversion of lanosterol to cholesterol is carried out by a series of dehydrogenases and reductases. Cholesterol can then be shuttled to the cell membranes, further modified to produce other sterols, or converted into cholesteryl esters (CE) by acyl-CoA:cholesterol acyltransferases for storage. The produced CE, as well as TAG, can be stored in cellular lipid droplets (LDs) for storage or released from the liver into the circulatory system as lipoproteins.

## **Lipid droplets (LDs)**

Storage of lipids in LDs is essential for proper cell function. LDs provide an energy reserve of lipid storage, but also play a large role in regulating cell signaling. The structure of LDs consists of a neutral lipid core consisting of CE and TAG that is surrounded by a phospholipid monolayer and a protein coat. LD formation occurs in the endoplasmic reticulum (ER) and begins with neutral lipid synthesis. CE and TAG accumulate inside the ER until the droplet buds off from the ER as a mature LD.

LD coat proteins regulate additional TAG synthesis, LD fusion, organelle interactions, lipolysis, and signaling. After LD creation, TAG synthetic enzymes, like GPAT, localize from the ER to the LD<sup>5</sup> to continue LD growth. LD fusion is mediated by the cell death-inducing DNA fragmentation Factor- $\alpha$ -like effector family of proteins<sup>6</sup>. LDs have been shown to interact with numerous organelles including the ER, mitochondria, and autophagic machinery. The perilipin (PLIN) family of proteins play a key role in regulating LD dynamics and breakdown. The expression of PLIN proteins varies by tissue with PLIN2, PLIN3, and PLIN5 being present in the liver<sup>7</sup>. PLIN proteins provide structure to the LD and regulate lipolysis<sup>8,9</sup>, which can occur via two pathways: classical lipolysis and lipophagy – the latter will be discussed in detail later in this chapter.

Classical lipolysis is performed by lipases that reside on the LD surface, including adipose triacylglycerol lipase (ATGL), hormone sensitive lipase, and monoacylglycerol lipase. These lipases break down TAG, DAG, and MAG respectively, as they cleave acyl groups off TAG to produce FAs and a glycerol. FAs released from TAG are largely sent to the mitochondria for  $\beta$ -oxidation to produce acetyl-CoA for the citric acid cycle. However, in the liver, incomplete  $\beta$ -oxidation produces ketone bodies, like  $\beta$ -hydroxybutyrate and acetoacetate, that are released into circulation. This process is

stimulated by increased blood glucagon and catecholamines, resulting in the release of ketone bodies which can be rapidly utilized to produce ATP by other tissues.

As ATGL is the first step in this series of reactions, it is heavily regulated by cellular nutrient status. In addition to directly breaking down LDs, ATGL also initiates the activation of lipophagy, the bulk degradation of LDs by autophagy<sup>10</sup>. PLIN5 plays a key signaling role by carrying FAs cleaved by ATGL to the nucleus, where it binds and activates sirtuin 1 (SIRT1) to drive lipophagy<sup>11,12</sup>. Ultimately, hepatic LD breakdown provides substrate for  $\beta$ -oxidation, ketone release, lipid mediated signaling, and lipoprotein synthesis<sup>13</sup>.

### **Liver distribution of lipoproteins**

The liver regulates whole body lipid metabolism by altering circulating lipids. The mechanisms of lipoprotein uptake and release by the liver work with lipogenesis to properly distribute lipids through the body. Due to the insolubility of fats in aqueous solutions, lipid transport through the body is carried out by packaging lipids in complex particles called lipoproteins. Lipoproteins have a central core of the hydrophobic neutral lipid species CE and TAG. This core is surrounded by a membrane of phospholipids and free cholesterol studded with apolipoproteins, which solubilizes the lipoprotein, allowing it to move through the circulatory system. There are several classes of apolipoproteins that bind lipoproteins, but the specifics are outside the scope of this review. Briefly, apolipoproteins aid in lipoprotein formation, provide structure to the particle, and regulate uptake and metabolism of the lipid core.

After a meal, dietary lipids are absorbed in the intestine and packaged into large lipoproteins called chylomicrons, which move through the lymphatic system to begin

circulating in the blood for uptake by extrahepatic tissues. Lipoprotein lipase (LPL) on the surface of endothelial cells catabolizes the TAG carried by various lipoproteins, including chylomicrons, to provide FAs for tissue uptake. After chylomicrons are broken down, the chylomicron remnants are uptaken by the liver, where the remaining TAG and CE are metabolized before being distributed to the rest of the body<sup>14</sup>.

The liver distributes TAG and CE to other tissue by releasing very low-density lipoproteins (VLDL). VLDL particles are incredibly TAG rich and are circulated through the bloodstream to provide TAG to peripheral tissues. As TAGs are cleaved by LPL on endothelial cells, the TAG content of the VLDL decreases and the relative amount of cholesterol increases, resulting in the lipoprotein becoming LDL (low-density lipoprotein).

LDL is a small, cholesterol rich lipoprotein commonly called “bad cholesterol” due to its association with heart disease and atherosclerosis<sup>15</sup>. Circulating LDL can be endocytosed by cells expressing the LDL receptor (LDLR)<sup>16</sup>. The endosome containing the lipoprotein then fuses with the lysosome, where the stored CE are broken down in lysosomes as discussed in more detail later. Ultimately, roughly 70% of LDL is removed from the circulatory system by the liver<sup>16</sup>. As such, hepatic LDL uptake is important to prevent cholesterol accumulation in peripheral tissues. Additionally, the liver regulates whole body cholesterol levels by secreting high density lipoproteins (HDL). HDL circulates through the blood and absorbs cholesterol released from peripheral tissues to carry it back to the liver.

HDL particles are the smallest lipoprotein complex and move through the blood collecting exported cholesterol from other tissues and circulating lipoproteins. As HDL collects cholesterol, the lipoprotein increases in size until it returns to the liver for

conversion into bile or is delivered to steroidogenic tissues like the adrenal glands or the gonads. While the mechanisms of liver lipid metabolism have been summarized above, the cellular regulation of these mechanisms will be discussed below.

### **Cellular nutrient sensing**

Cellular lipid metabolism is intricately tied to the nutrient status and energetic balance of the cell. As high levels of cellular cholesterol and FAs can lead to cytotoxicity and cell death, lipid metabolism is highly regulated. However, lipid metabolism is not only regulated by lipid availability, but also through a complex network of nutrient sensing proteins that evaluate metabolite availability and cellular energy levels before lipid metabolism is altered.

Cellular levels of ATP (adenosine triphosphate) are a key indicator of energy status, and as such play a direct role in the activation AMP (adenosine monophosphate) kinase (AMPK). The binding of AMP to AMPK activates the AMPK kinase domain even at concentrations 100x less than the ATP concentration<sup>17</sup>, as such, AMPK is incredibly sensitive to changes in AMP concentrations. Once activated, AMPK phosphorylates a host of proteins involved in lipid metabolism<sup>18</sup>, glycolysis<sup>19,20</sup>, mitochondrial homeostasis<sup>21</sup>, and autophagy<sup>22</sup>. One such target is the mechanistic target of rapamycin complex 1 (mTORC1), which is inhibited by AMPK activation<sup>23,24</sup>.

Often called the “master nutrient regulator”, mTORC1 integrates input from a variety of sources and drives key cell growth pathways<sup>25</sup>. At the core of the complex is mTOR, a serine/threonine protein kinase. However, the regulation of mTOR activity by other proteins that sense specific nutrients is what makes mTORC1 so integral to nutrient sensing, as shown above with AMPK.

To be activated, mTORC1 must localize to the lysosome<sup>26</sup>. This process is controlled by the Rag GTPases, which bind mTORC1, and the Ragulator complex, which senses lysosomal amino acids and serves as a lysosomal anchor<sup>27,28</sup>. When amino acids are plentiful, these proteins bind mTORC1 and localize it to the lysosome. However, activation of mTORC1 also requires input from extracellular growth factors<sup>29</sup>. Extracellular insulin activates the insulin receptor, leading to the activation of Akt, a kinase that inhibits the tuberous sclerosis complex (TSC) via phosphorylation<sup>30,31</sup>. Under fasting conditions, TSC prevents Rheb activation, but when TSC is phosphorylated, Rheb is activated and promotes mTORC1 activity. In this way, mTORC1 activation relies on both amino acid and growth factor signaling.

Additional regulation of mTORC1 after both conditions have been met helps to fine tune its activity. As previously stated, AMP regulates AMPK dependent inhibition of mTORC1, providing information about the overall cellular energy levels. mTORC1 has recently been shown to respond to changes in lysosomal cholesterol levels by the arginine gated SLC38A9 (solute carrier family 38 member 9 protein)<sup>32</sup>. SLC38A9 communicates lysosomal levels of cholesterol and arginine to mTORC1, resulting in its activation<sup>33</sup>.

Once activated, mTORC1 activates a host of pathways involved in cell growth, some of which have already been discussed. In addition to driving cell growth, mTORC1 activation inhibits the initiation of autophagy, the bulk degradation of cellular components via the lysosome. The effect of mTORC1 on many downstream pathways are well characterized; mTORC1 directly phosphorylates ribosomal S6 kinase 1 (S6K) and eukaryotic translation initiation factor 4E-binding protein 1 (4E-BP1) to promote ribosome biogenesis and protein synthesis<sup>34,35</sup>. After activation, mTORC1 can translocate to the

nucleus to drive mitochondrial biogenesis by complexing with the transcription factor peroxisome proliferator-activated receptor gamma coactivator 1-  $\alpha$  (PGC1 $\alpha$ )<sup>36</sup>. However, some mechanisms are less well understood, like how mTORC1 activates the sterol response element binding proteins (SREBP) proteins to drive lipid synthesis<sup>37</sup>.

### **Cellular regulation of lipid metabolism**

While mTORC1 is the master nutrient sensor, the SREBP transcription factors are master regulators of lipid metabolism. The SREBP family consists of SREBP1a, SREBP1c, and SREBP2, though only SREBP1c and SREBP2 are abundant in the liver<sup>38</sup>. All family members share a similar domain structure, with the amino-terminal binding to sterol regulatory elements in DNA, the middle region of two hydrophobic transmembrane regions, and the regulatory carboxy-terminal domain<sup>39</sup>.

Under unstimulated conditions, SREBP proteins reside in the ER, where they are bound to SREBP cleavage activating protein (SCAP). SCAP has both a sterol sensing domain and a SREBP binding domain; when ER sterols drop below 5% of the total membrane lipid pool, SCAP mediates the translocation of SREBP to the Golgi apparatus<sup>40</sup>.

However, this process can be prevented if SCAP is bound to an INSIG (insulin induced gene) protein. INSIG binding with SCAP is induced at high cholesterol or oxysterol levels<sup>41</sup>. In the Golgi apparatus, site-1 and site-2 proteases cleave the SRE binding domain of SREBP from the transmembrane regions, allowing it to translocate to the nucleus and facilitate transcription of the target genes. On top of this mechanism, each SREBP has additional regulation and specific targets.

SREBP1c activation drives *de novo* FA lipogenesis and TAG synthesis. Mechanistically, SREBP1c translocation to the nucleus drives the transcription of FA synthase and ACC

to increase lipogenesis<sup>42</sup>. However, SREBP1c also promotes the expression of numerous elongases, desaturases, and GPAT, driving FA modifications and TAG synthesis<sup>42,43</sup>. SREBP1c translocation to the Golgi is also regulated by feedback inhibition of unsaturated FAs. FAF2 (FA synthase associated factor 2) binding to INSIG prevents the association of INSIG with SCAP, allowing SREBP activation<sup>44</sup>. However, when unsaturated FAs are present, they bind to FAF2 and prevent INSIG binding, allowing INSIG to bind to SCAP and prevent SREBP cleavage<sup>44</sup>. Lastly, insulin and mTORC1 drives SREBP1c cleavage, though as previously stated, the mechanism isn't understood<sup>45,46</sup>.

SREBP2 activation drives *de novo* cholesterol biosynthesis and promotes LDL uptake. In the nucleus, SREBP2 drives transcription of several cholesterologenic genes including HMGCR, which performs the rate limiting step in mevalonate synthesis<sup>47</sup>. SREBP2 also promotes hepatic cholesterol uptake by increasing LDLR expression. SREBP2 activation is more sensitive than SREBP1c to changes in cellular cholesterol<sup>48</sup>. Additionally, INSIG can promote the degradation of HMGCR when bound to oxysterols, providing another feedback mechanism to regulate cholesterol<sup>49</sup>.

As previously stated, the regulation of lipid synthesis is a tightly controlled process to protect the cell from lipotoxicity. SREBP activation requires multiple conditions be met and relies on signals from additional nutrient sensing machinery. As such, the release of FAs and cholesterol from their storage forms via lipolysis is also highly regulated.

On a tissue level, LD breakdown is activated when circulating  $\beta$ -catecholamine levels increase and insulin decreases in response to fasting<sup>50</sup>. Cellularly, this results in increases in ATGL protein due to inhibition of mTORC1<sup>51</sup> that drives lipolysis. As

previously stated, ATGL-catalyzed lipolysis promotes lipophagy via SIRT1 activation<sup>11</sup>. SIRT1 is a deacylase that is activated under conditions of nutrient limitation, and plays a major role in promoting autophagy by regulating the activity of autophagic proteins<sup>52</sup>.

Activation of autophagy requires input from multiple nutrient sensing proteins, including AMPK, mTORC1, and SIRT1. The major signaling node in autophagy initiation is unc-51-like autophagy activating kinase 1 (ULK1). ULK1 drives the formation of two key complexes that regulate autophagosome formation and are discussed below. AMPK directly phosphorylates ULK1 at Ser317 and Ser777<sup>22</sup> to promote activation of ULK1, whereas mTORC1 phosphorylation of ULK1 at Ser757 is inhibitory<sup>53</sup>. Inhibition of autophagy has been shown to significantly reduce LD breakdown, emphasizing the importance of this ATGL induced lipophagy<sup>54</sup>. Rab7 has been identified as a key regulator of lipophagy in hepatocytes, localizing to LDs and promoting both autophagosome and lysosome interactions<sup>55</sup>.

### **Mechanisms of lipophagy**

PLIN proteins serve as a physical barrier to prevent lipophagy and, as such, the degradation of PLIN proteins by chaperone mediated autophagy (CMA) is the first step for LD breakdown<sup>56-58</sup>. During CMA, the chaperone protein HSC70 (heat shock-cognate chaperone 70 kDa) binds to proteins containing a KFERQ amino acid sequence and escorts them to lysosomes for degradation<sup>59</sup>. At the lysosome, HSC70 interacts with lysosomal associated membrane protein 2A to import proteins into the lysosome for degradation<sup>60,61</sup>. Once the PLIN proteins have been removed from the LD surface, portions of the LD can be engulfed for degradation by lysosomes or phagophores.

At this point LD breakdown can proceed via either micro- or macrolipophagy. During microlipophagy, lysosomes directly interact with and engulf portions of LDs. The mechanics behind this process in the liver are still largely unelucidated<sup>62</sup>. Recent work suggests that microlipophagy targets smaller LDs<sup>63</sup>, though specific proteins involved still haven't been identified.

Macrolipophagy utilizes the core autophagic machinery to engulf portions of the LD and deliver it to the lysosome<sup>54</sup>. There are several autophagy related genes (ATG) that play a role in autophagosome formation, but it begins with ULK1 activation. As previously stated, the process of autophagosome formation involves two protein complexes. The ULK1 complex contains FIP200 (focal adhesion kinase family-interacting protein of 200 kDa), ATG13, and ULK1 and localizes to the ER to play a key role in elongation of the isolation membrane, the initial step in autophagosome formation<sup>64,65</sup>. The second complex is composed of beclin 1 (BECN1), VPS34 (vacuolar protein sorting protein 34), VPS15, and ATG14<sup>66</sup>; this complex is also necessary for elongation of the isolation membrane. ULK1 also phosphorylates BECN1 to promote its activity, a necessary step for full autophagic induction<sup>67</sup>.

As the phagophore forms, additional proteins localize to that phagophore assembly site. Of note is the recruitment and activation of the mammalian ATG8 homologue, LC3 (microtubule-associated protein 1A/1B-light chain 3). LC3 is a small, soluble protein that resides in the cytosol as LC3-I. However, LC3 is cleaved by ATG4<sup>68</sup>, resulting in the exposure of a post translational lipidation site. When autophagosome formation occurs, LC3-I is lipidated with a phosphatidylethanolamine by ATG7 and ATG3<sup>69</sup> to produce LC3-II. This lipidation associates LC3-II to the autophagosome membrane. After engulfing part of an LD, a process still poorly characterized, the lipid containing

autophagosome fuses with a lysosome to initiate breakdown. This process is dependent on a host of tether and adaptor proteins and SNARE (soluble NSF attachment protein receptor) complexes<sup>70</sup>. While the mechanisms behind the regulation of these two lipophagic pathways remains largely unknown, both are involved important for hepatic LD degradation and result in the accumulation of LD contents in lysosomes.

Once in the lysosome, the core of the LD composed of TAG and CE is broken down by lysosomal acid lipase (LAL=protein/LIPA=gene) (Figure 1.1). LAL hydrolyzes TAG and CE to produce FAs and glycerol or FAs and cholesterol, respectively<sup>71</sup>. As the lysosome is the site of breakdown in both lipophagy and endocytosis, LAL is responsible for hydrolyzing lipids from both LDs and LDL<sup>72</sup>. The cleavage of these lipid species results in the accumulation of FAs and cholesterol within the lysosome. The export of FAs from the lysosome occurs via lysosomal exocytosis<sup>73</sup>. As this process releases content from the lumen of the lysosome outside the cell, it results in secretion of LAL, dispensing it into circulation.

Cholesterol export from the lysosome is regulated by the Niemann-Pick type C (NPC) proteins. NPC2 is soluble and localized inside the lysosome, where it binds cholesterol and transfers it to NPC1<sup>74</sup>. NPC1 resides in the lysosomal membrane, and transport cholesterol through the membrane, although the mechanism is still undiscovered<sup>75</sup>. Both NPC1 and NPC2 are essential for proper lysosomal cholesterol export, as their ablation leads to excessive cholesterol synthesis<sup>76,77</sup>. A portion of lysosomal derived cholesterol is converted into oxysterols to regulate SREBP2 in the ER<sup>78</sup>, and without this feedback SREBP2 is trapped in an active state. LAL is responsible for liberating cholesterol in the lysosome, yet the effect of LAL modulation on SREBP2 activity has not been

determined. Additionally, most NPC focused studies do not examine the role of lipophagy in the cholesterol accumulation, instead focusing on LDL<sup>79,80</sup>.

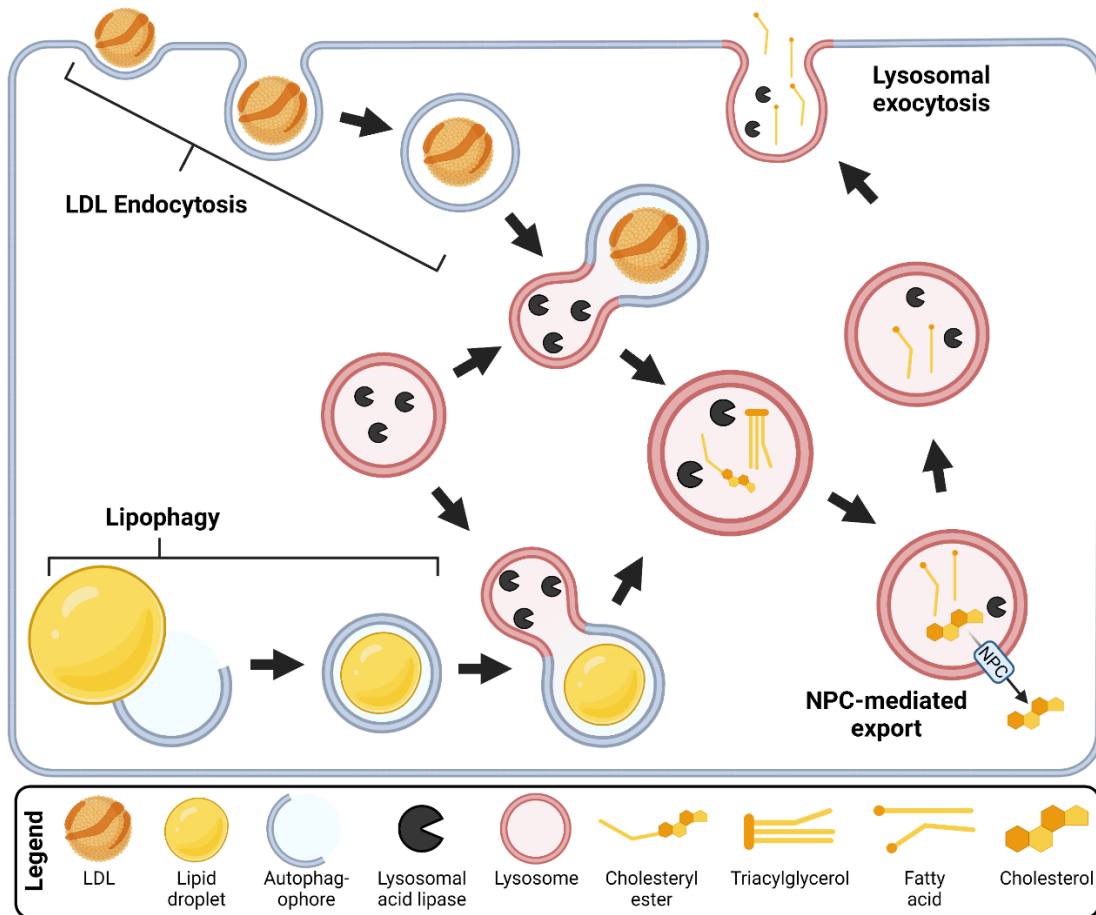


**Figure 1.1: LAL function in the lysosome.**

LAL degrades both TAG and CE from exogenous and endogenous lipid sources.

Cholesterol and fatty acids are exported from the lysosome by either the NPC proteins or lysosomal exocytosis, respectively.

## **Lysosomal Acid Lipase (LAL)**

LAL is a member of the  $\alpha/\beta$  hydrolase superfamily, with a classical catalytic triad of Ser153, His353, Asp324 and an oxyanion hole in the active site<sup>81,82</sup>. Prior to post-translational modification, the predominant LAL isoform is 399 residues, containing a 21-residue signal peptide to localize to lysosomes, and has a molecular mass of 43 kDa. LAL consists of a core and cap domain. Within the cap domain (residues 184-308) there is a lid region (residues 215-244) that covers the active site, preventing substrate access. Mutation of Cys227 reduces TAG cleavage while completely preventing CE breakdown, indicating the importance of this region in maintaining substrate specificity<sup>83</sup>. The lid is moved by conformational changes at Pro214 and Gly245, but the regulation of this change is not known. At neutral pH, there is a predicted hydrogen bond formation between Asp361 and Asn250 that locks the lid in the closed formation. While it appears to primarily block access to the active site, the lid is essential for proper enzymatic function, as its deletion leads to a 3000-fold reduction in LAL activity<sup>82</sup>. LAL is glycosylated at six distinct sites, which increases the molecular mass of the mature protein to 51kDa. Two of these glycosylation sites, N134 and N246, are essential for LAL secretion and function<sup>84</sup>. There is some conflict in the field as to whether LAL requires any proteolytic cleavage for proper maturation<sup>85</sup>.

## **LAL mutations result in severe clinical phenotypes**

LAL is moderately expressed in most tissues but is most highly expressed in adipose tissue and macrophages. However, despite its low expression, LIPA plays a significant role in the liver, as evidenced by knockout (KO) or lack of function phenotypes. A complete loss of LAL function results in Wolman's disease, which is usually fatal within a year of birth, due to excessive hepatic and splenic lipid accumulation ultimately leading to liver failure<sup>86</sup>. However, mutations that result in 1-12% of residual activity of LAL

lipolysis lead to cholesteryl ester storage disease (CESD)<sup>87,88</sup>. CESD is characterized by the accumulation of CEs in various tissues, dyslipidemia, hepatosplenomegaly, and hepatic fibrosis and cirrhosis. Notably, the disruption of LAL activity in CESD results in abnormal HDL release<sup>89</sup>. CESD is treatable by providing patients with recombinant LAL injections. The injected LAL is endocytosed into cells, resulting in its accumulation in lysosomes, where it functions normally<sup>90,91</sup>. Mutations leading to LAL deficiency are estimated to affect roughly 1 in 175,000 people<sup>92</sup>. Often the mutations that lead to Wolman's and CESD are on residues that are less solvent accessible, driving conformational changes<sup>93,94</sup>.

While the complete loss of LAL in humans is fatal, knockout mice can survive with severe metabolic dysfunction, providing a model system to investigate the role of LAL in whole body lipid metabolism. Mice with a whole body knockout have reduced adipose tissue coupled with severe hepatosplenomegaly, indicating widespread dysfunction in how lipid is distributed and utilized by metabolic tissues<sup>95</sup>. Cholesterol homeostasis specifically is disrupted, with significant increases in hepatic and intestinal cholesterol synthesis, resulting in significant accumulation of cholesterol in the liver<sup>96,97</sup>. Additional studies characterizing the effects of hepatocyte specific LAL KO reveal similar accumulations of CE<sup>98</sup>, and increased hepatic inflammation<sup>99</sup>.

### **NAFLD and LAL**

Even in individuals lacking LAL mutations, LAL appears to play a role in preventing the development of liver disease. Serum levels of LAL are inversely correlated to the severity of liver disease and NAFLD<sup>100,101</sup>. Additional studies have shown that FA treatment reduces LAL activity in cell culture<sup>102</sup>, and that advanced NAFLD is associated with impaired lipophagy<sup>103</sup>. As NAFLD progresses to NASH, cholesterol synthesis

becomes dysregulated and cholesterol crystals begin to accumulate in LDs<sup>104,105</sup>. The involvement of cholesterol accumulation with NASH development is well established<sup>105-107</sup>, with some studies suggesting that cholesterol accumulation and not steatosis is the driving factor behind liver inflammation<sup>108</sup>.

### **Goals and objectives**

Based on the reduction of LAL with NAFLD and the correlated dysregulation of cholesterol metabolism, we sought to further evaluate the role of LAL in regulating cholesterol metabolism and the progression of fatty liver disease. It is imperative to improve our understanding of how alterations in LAL may contribute to the development of NAFLD and NASH by promoting unregulated cholesterol synthesis. To address this, this thesis contains two primary objectives: to determine the mechanism by which LIPA dysfunction promotes SREBP2 activation and to test whether hepatic LAL overexpression could prevent the progression of NAFLD in mice on a high fat diet.

The first objective, contained within Chapter 2, relies on *in vitro* cell culture models to determine how LAL knockdown or inhibition affects cellular cholesterol synthesis. While the effect of dysfunctional NPC proteins on cholesterol metabolism has been extensively studied, research on LAL inhibition has not been. LAL dysfunction would result in CE accumulation in the lysosome, whereas NPC inhibition results in cholesterol accumulation. As mTORC1 senses lysosomal cholesterol and can drive SREBP activation, better characterizing this system while LAL is dysregulated may reveal additional pathways of SREBP regulation. Ultimately, the results indicate that LAL inhibition modulates SREBP2 through the same pathways as NPC dysfunction and depends on LDL as a source of lysosomal cholesterol.

The second objective, contained within Chapter 3, utilizes an LAL overexpression mouse model to evaluate the efficacy of increased hepatic LAL to prevent NAFLD on a high fat diet. Prior to 2021, overexpression of LAL in a mouse model as a potential treatment for diet induced metabolic syndrome hadn't been assessed. As LAL is a key lysosomal lipase, hepatic lipid content and changes in autophagy machinery were two of the primary endpoints for this study. Inflammatory markers and immune cells were also quantified, as the progression of NAFLD to NASH is accompanied by drastic increases in inflammation. Strikingly, LAL did not alter hepatic lipid content, but did drive autophagy. The overexpression of LAL, even on the control diet, resulted in large increases in immune cell infiltration into the liver suggesting that overexpression of LAL is not a viable option to treat NAFLD.

## CHAPTER TWO

# Lysosomal Acid Lipase Dysfunction Indirectly Promotes Cholesterol Synthesis

Michael Lopresti wrote this chapter in its entirety

## Summary

The progression of non-alcoholic fatty liver disease to non-alcoholic steatohepatitis is a key point in the worsening of liver disease and is strongly correlated with unregulated hepatic cholesterol synthesis. Lysosomal derived cholesterol has previously been identified as a key feedback mechanism for cholesterol biosynthesis. As lysosomal acid lipase (LAL) is the only known lysosomal enzyme capable of breaking down cholesteryl esters, we investigated the role of LAL in regulating sterol regulatory element binding protein 2 (SREBP2) activation. The connection between LAL deficiency and cholesterol accumulation is established, but the signaling pathways involved have not been well characterized. Using a combination of LAL knockdown and inhibition, we tested how sensitive SREBP2 was to fluctuations in lysosomal cholesterol metabolism. Our data demonstrates that LAL released cholesterol is a significant regulator of SREBP2, though cholesterol levels are not directly responsible for the increases in SREBP2, instead acting through oxysterol metabolism. We also show that the lysosomal cholesterol pool that regulates SREBP2 is heavily reliant on exogenous lipid sources. Overall, we establish that LAL dysfunction induced changes in cholesterol synthesis are due to disrupted lipoprotein breakdown and decreased oxysterol signaling.

## Introduction

Cellular cholesterol levels are highly regulated, as excessive free cholesterol can result in lipotoxicity and cell death, is associated with a wide range of diseases<sup>109</sup>, and is thought to be one of the driving forces behind the development of non-alcoholic steatohepatitis<sup>110</sup>. The major sources of cellular cholesterol are low-density lipoprotein (LDL) uptake and *de novo* cholesterol synthesis. As the liver uptakes LDL and is responsible for roughly 50% of cholesterol synthesis in the body, alterations in hepatic cholesterol can have severe whole-body effects.

Circulating LDL is predominately composed of cholesteryl esters (CE) and binds with the LDL receptor (LDLR) on the plasma membrane, initiating endocytosis of the lipoprotein. LDL moves through the endocytic pathway, ultimately ending in the lysosome where lysosomal acid lipase (LAL) degrades the LDL to produce cholesterol and an acyl chain. Free cholesterol is then exported into the cytosol via the NPC1 (Niemann-Pick type C1) and NPC2 cholesterol transporters that span the lysosomal membrane.

The production of cholesterol synthesizing proteins is regulated by the activation of the transcription factor SREBP2 (sterol regulatory element binding protein 2). Under normal conditions, SREBP2 resides in the endoplasmic reticulum (ER), and translocates to the Golgi with stimulation. This step is regulated by ER levels of cholesterol<sup>40</sup>, oxysterols<sup>41</sup>, and mTORC1 (molecular target of rapamycin complex 1) activation<sup>111</sup>. In the Golgi, SREBP2 is cleaved by proteases to release the soluble DNA binding region which localizes to the nucleus and promotes transcription. mRNAs increased with SREBP2 activation include LDLR and HMGCR (3-hydroxy-3-methylglutaryl coenzyme A reductase), the rate limiting enzyme for cholesterol biosynthesis, which both act through independent mechanisms to increase cellular cholesterol levels.

The disruption of LAL or NPC1/2 function drives the activation of SREBP2 and results in the production of excessive cholesterol that contributes to liver disease. LAL and NPC1/2 KO mice all show increased hepatic cholesterol accumulation and synthesis, though LAL KO resulted in a 1.5 to 2-fold change in cholesterol synthesis over NPC1/2 KO mice<sup>77</sup>. Additionally, the excessive cholesterol synthesis LAL KO mice cannot be completely rescued by a low cholesterol diet or inhibition of intestinal sterol uptake<sup>96,97</sup>.

Further investigation into how disrupted lysosomal cholesterol metabolism leads to SREBP2 activation showed that NPC<sup>78</sup> and LIPA mutations<sup>112</sup> led to reduced cellular oxysterol secretion of 25-hydroxycholesterol (25-HC) and 27-hydroxycholesterol (27-HC). Interestingly, oxysterol treatment reduces total cholesterol in WT and NPC1 mutants, suggesting that lysosomal cholesterol is vital for oxysterol feedback inhibition of SREBP2<sup>78</sup>. Similar results have been shown in models of LAL deficiency, with reductions in cellular production of 27-HC<sup>89</sup>. As LAL and NPC both regulate the release of lysosomal cholesterol, it makes sense that they would both modulate SREBP2 activity in the same way. However, as the LAL KO has a more severe cholesterol accumulation phenotype, additional regulatory mechanisms may be at work that have yet to be identified.

Additional studies on the interplay of lysosomal cholesterol and SREBP2 activation show that lysosomal cholesterol regulates mTORC1 activity via the amino acid transporter SLC38A9 (solute carrier family 38 member 9)<sup>32</sup>. Inhibition of mTORC1 in NPC KO cells restores lysosomal function but doesn't alter lysosomal cholesterol, although overall cholesterol synthesis was unmeasured in this study<sup>32</sup>. This and related work confirms that NPC proteins regulate both cholesterol transport and sensing<sup>113</sup>, but the role of LAL

in this interplay remains untested. The importance of endogenous vs exogenous pathways in providing CE for lysosomal degradation and regulating cellular cholesterol has not been investigated. However, the ability of NPC KO cells to rescue SREBP2 activity with supplemented oxysterol and not LDL shows that NPC is required for LDL to affect SREBP2, and suggests that LDL is an important source of cholesterol<sup>78</sup>. The goal of this chapter is to evaluate whether LAL and NPC affect SREBP2 and cholesterol biosynthesis via the same mechanisms, or whether LAL acts through additional pathways to produce a more severe phenotype.

## **Materials and Methods**

### *Primary hepatocyte isolation and cell culture*

Wildtype male mice (C57BL/6J) aged 8-12 weeks were fasted for 4 hours prior to perfusion. Primary hepatocytes were isolated with a collagenase perfusion then plated on collagen-coated plates. Immediately following isolation, hepatocytes were cultured in M199 media supplemented with 10 nM dexamethasone, 1 mM carnitine, 100 nM insulin, and 10% FBS. After 5 hours, M199 media supplemented with 10 nM dexamethasone, 1 mM carnitine, and 10 nM insulin was used. Hepatocytes were transfected with either Mission scrambled control siRNA or siRNA targeting mouse LIPA (Millipore Sigma, EMU075891) using Effectene Transfection Reagent (Qiagen, cat. no. 301425). Experiments were performed 24 hours after transfection.

### *Immortalized cell culture*

HepG2 cells were cultured in MEM (ThermoFisher, cat. no. 11095), DMEM (ThermoFisher, cat. no. 11995), or Advanced DMEM (AddMEM) (ThermoFisher, cat. no. 12491) for at least 2 weeks prior to experiments. Fetal bovine serum (FBS) was added to both MEM and DMEM to comprise 10% of the total volume, and 2% in AddMEM.

AML12 cells were cultured in DMEM:F12 (ThermoFisher, cat. no. 11330032) with 10% FBS. For experiments in a 12 well plate, cells were plated at a density of 350,000/well. For experiments in a 24 well plate, cells were plated at a density of 175,000/well.

#### *Cell Culture Experimental Conditions*

Human LDL (Lee BioSolutions, Maryland Heights, MO) was added to cell culture at a final concentration 50 µg/mL unless specified otherwise. 0.1% (w/v) β-methylcyclodextrin (MCD) and 50 µM cholesterol were complexed at 37°C for as described<sup>32</sup>. Chemical inhibitors and concentrations used were 5 µg/mL 25-HC (Cayman Chemical, cat. no.), 5 µg/mL 27-HC (Cayman Chemical, cat. no. 11097), 10 µM NPCi (U18666A, Sigma Aldrich, cat. no. 662015), 20 µM AKTi (Ly294002, Cayman Chemical, cat. no. 70920) for the specified time length. For LALi studies, cells were treated with 10 µM LAListat 1 (Tocris, cat. no. 6098) or an equal volume of DMSO for 16 hours prior to the start of the assay, and throughout the assay.

#### *Lentiviral production and shRNA knockdown*

Hek293-T cells cultured in DMEM with 10% FBS were transfected with lentiviral construction plasmids psPAX2 (Addgene, Plasmid #12260), pMD2.G (Addgene, Plasmid #12259), and either a scrambled shRNA control or shRNA targeting the human LIPA gene (Millipore Sigma, TRCN0000029245) with a CMV promoter and puromycin resistance. The next day, fresh media was added. After 48 hours, lentivirus containing media was collected and filtered through a 0.22 µm filter. One-tenth of the lentiviral media (roughly 1 mL) was added to a 10 cm dish of HepG2s and left for 48 hours. HepG2s were then cultured in media containing 4 mg/mL puromycin for 4 days before being used in experiments.

### *RNA isolation and analysis*

RNA was isolated from cells using a Trizol based purification. cDNA was synthesized using Superscript Vilo cDNA Synthesis Kit (Invitrogen, Waltham, MA) and qPCR was performed using SYBR Green Master Mix (ThermoFisher, cat. no. 4309155). All data shown were normalized using the  $\Delta\Delta CT$  method with the reference gene indicated and expressed as a fold change of the control group.

### *Acetate [<sup>14</sup>C] Pulse chase*

Hepatocytes and HepG2 cells were pulsed with 1  $\mu$ Ci [<sup>14</sup>C] acetate per mL media to label lipids produced via *de novo lipogenesis*. After 2 hours, cell lipids were extracted using a methanol:chloroform extraction as described<sup>114</sup>. Extracted cell lipids were separated into different fractions by thin layer chromatography on 0.25 mm silica gel G plates in a hexane:ethyl ether:acetic acid (80:20:2, v/v/v) solvent system. Cholesterol and CE fractions were identified and measured by an AR-2000 radio-TLC imaging scanner. Total radiolabeled lipids were quantified by scintillation counter after the addition of Bio-Safe II cocktail.

### *Luciferase assay*

Cells were plated and transfected with pLDLR-Luc (Addgene, Plasmid #14940) and pRL-SV40 (Promega, cat. no. E2231). The next day, media was changed. One day post transfection, cells were exposed to experimental conditions for 12-16 hours, at which point luciferase activity was assessed using the Dual-Luciferase Reporter Assay (Promega, cat. no. E1910) kit and associated protocols. Firefly luciferase activity driven by SREBP2 was normalized to Renilla luciferase activity driven by the SV40 promoter.

### *Protein isolation and Western blotting*

Cells were lysed in Lysis B buffer (150mM NaCl, 10mM Tris, pH 7.4, 0.1% Triton X-100) containing protease (Sigma, cat. no. P8340) and phosphatase (Sigma, cat. no. P5726 and P0044) inhibitors and clarified. Protein concentration was determined via BCA assay (Thermo Fisher Scientific, cat. no. 23225). Ponceau staining was used as a protein loading control. Antibodies used were LAL (Origene, TA309730), phospho-S6K (Cell Signaling, 9205S), and S6K (Cell Signaling, 9202).

#### *mTORC1 Activity*

Cells were cultured in Hank's balanced saline solution (HBSS) without glucose for 4 hours to deplete ribosomal S6 kinase 1 (S6K) phosphorylation before treatment for 1 hour with HBSS or the complete media described. Cells were then lysed and mTORC1 activity was measured by Western blotting for phospho-S6K and total S6K.

#### *Lysosomal acid lipase activity assay*

Cell lysates were added to 200 $\mu$ M 4-methylumbelliferyl oleate (4-MUO) in 100 mM acetate buffer pH 4 with 1% Triton X-100. Fluorescence (excitation/emission - 320/460 nm) was measured every 10 minutes for two hours and molarity was determined by comparing to a standard curve of 4-methylumbelliferone (4-MU). Enzymatic activity was determined by averaging the difference in 4-MU generation every 10 minutes. LAL activity was normalized to total protein concentration in the lysate.

#### *Statistical analyses*

All data are presented as individual values overlaid with means  $\pm$  SEM. Statistical significance was declared at  $p < 0.05$ . The statistical tests used are included in the figure legends.

## Results

### *LAL inhibition and knockdown increase cholesterol synthesis*

Initial experiments validated that our cell-based models produced a similar phenotype as the LAL KO mice. siRNA mediated KD of LIPA in primary mouse hepatocytes resulted in a significant increase in mRNA expression of the SREBP2 target genes HMGCS1 (3-hydroxy-3-methylglutaryl coenzyme A synthase), MVD (mevalonate diphosphate decarboxylase), and LDLR (Figure 2.1A). siLIPA treatments with more than 50% of LIPA mRNA of the siCtrl group were excluded. When all siRNA treatments were plotted together, a significant negative correlation was observed between LIPA mRNA and the expression of each measured SREBP2 target gene (Supplemental Figure 2.1A-C).

Additionally, chemical inhibition of LAL activity resulted in a significant increase in *de novo* cholesterol biosynthesis, and a trend toward increased CE synthesis (Figure 2.1B-C). These findings were also replicated and confirmed with a lentiviral shRNA mediated LIPA KD in HepG2 cells (Figure 2.1D-F, Supplemental Figure 2.1D-E). Similar gene expression changes were observed in the HepG2s, though we see differences in the ratio of cholesterol to CE synthesis between the primary hepatocytes and HepG2s, which has been previously characterized<sup>115</sup>. These data confirm that LAL dysfunction, whether induced by inhibition or KD, drives cholesterol synthesis by increasing SREBP2 activity. This is in line with NPC regulation of SREBP2, so next examined whether lysosomal derived oxysterols were responsible for the LAL induced change, or if another mechanism was at work.

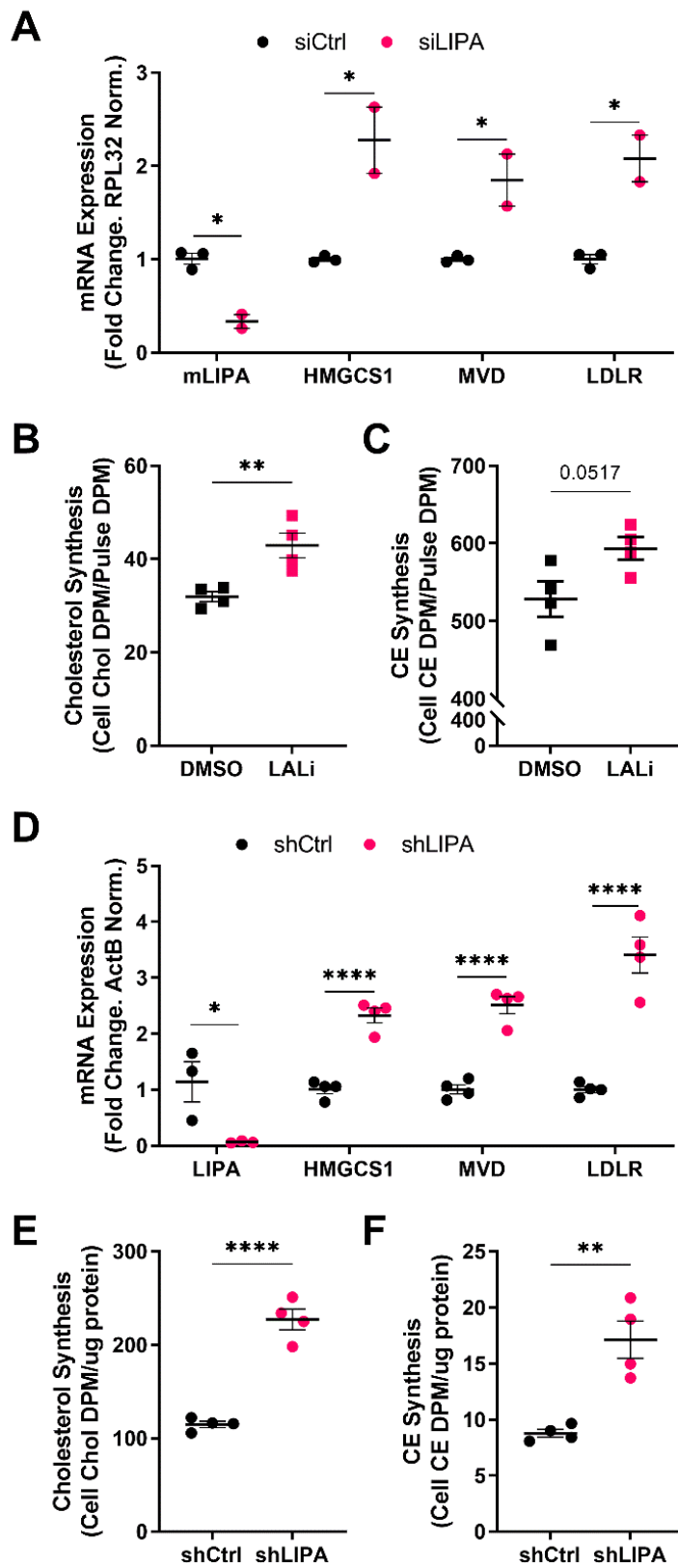
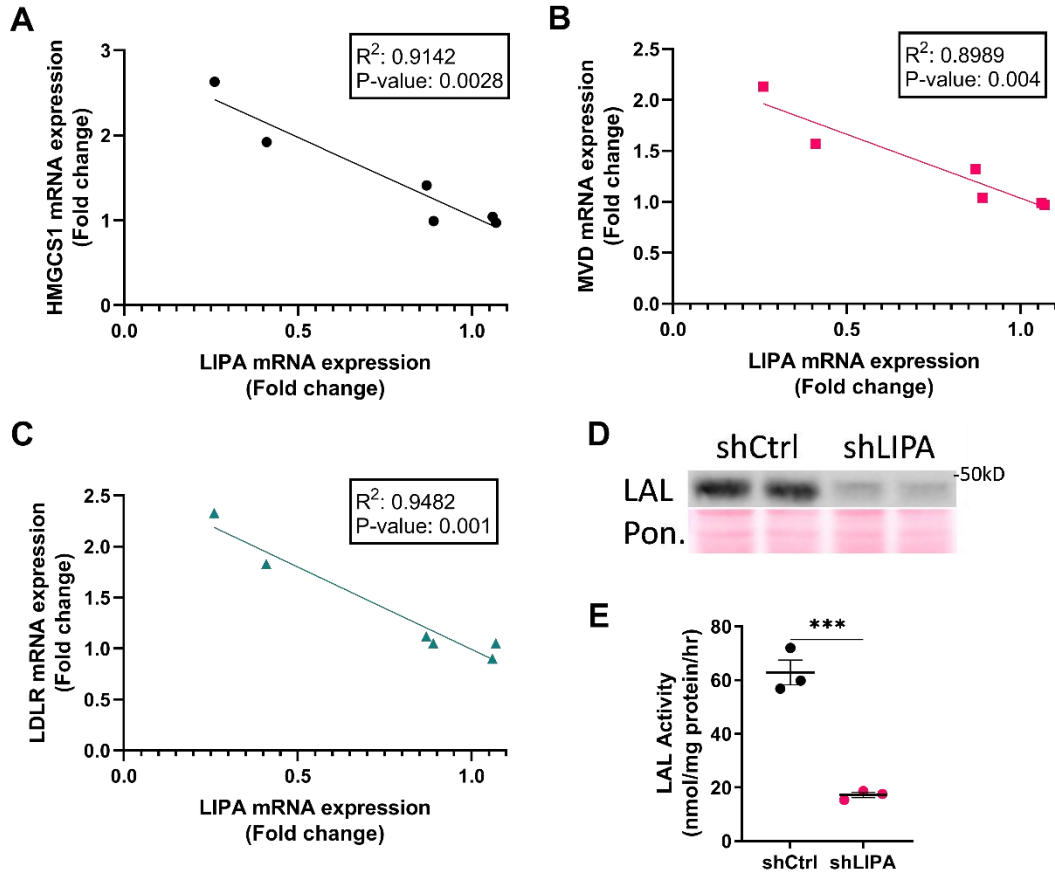


**Figure 2.1: LAL regulates cholesterol synthesis.**

(A) mRNA expression of cholesterol biosynthetic genes in primary mouse hepatocytes after siRNA KD of LIPA. Incorporation of labeled acetate into (B) cholesterol and (C) cholesteryl ester in primary mouse hepatocytes treated with LALi. (D) mRNA expression of cholesterol biosynthetic genes in LIPA KD HepG2s. Incorporation of labeled acetate into (E) cholesterol and (F) cholesteryl ester in LIPA KD HepG2s. Differences between groups were determined using unpaired t-tests. Statistical comparisons are indicated by horizontal lines and significant values are depicted as \*P < 0.05, \*\*P < 0.01, \*\*\*P < 0.005, \*\*\*\*P < 0.001.



**Supplemental Figure 2.1: LIPA mRNA expression correlates with SREBP2 targets.**

mRNA expression of LIPA plotted against expression of (A) HMGCS1, (B) MVD, and (C) LDLR in primary mouse hepatocytes after siRNA KD of LIPA. (D) Western blot validation of shLIPA KD in HepG2s. (E) LAL activity assay confirming shLIPA KD in HepG2s.

Differences between groups were determined using unpaired t-tests. Statistical comparisons are indicated by horizontal lines and significant values are depicted as \*P < 0.05, \*\*P < 0.01, \*\*\*P < 0.005, \*\*\*\*P < 0.001.

*LAL regulation of SREBP2 is dependent on lysosomal derived oxysterols, not cholesterol*

SREBP2 activation was measured using a luciferase reporter containing the SRE promoter region of the LDLR gene. Cells were treated with an LAL inhibitor, an NPC inhibitor, and both in combination to establish whether they displayed an additive effect on SREBP2 activity. LAL inhibition had a mild effect on SREBP2 activation, while NPC had a robust effect (Figure 2.2A). The combination drug treatment did not have an additive effect, suggesting that whatever cholesterol is produced by LAL must move through the NPC transporters to alter SREBP2, as expected.

Next, we confirmed that LAL dysfunction affected SREBP2 via modulation of oxysterols. When cellular cholesterol was depleted using MCD, the effect of LALi on SREBP2 activity was ablated, but cholesterol rescue into the media did not prevent the effect of LAL (Figure 2.2B). The reduction of SREBP2 activity in both DMSO and LALi treated cells with the addition of cholesterol suggests that LAL may alter SREBP2 via a separate mechanism than diminishing ER cholesterol. Previous work has characterized the role of lysosomal derived oxysterols in SREBP2 activation<sup>78</sup>, leading us to suggest that LAL drives SREBP2 by modulating these oxysterols. If so, the addition of oxysterol should completely blunt the effect of LALi.

As the lysosomal cholesterol transported by NPC regulate cellular oxysterol levels, we examined whether modulation of oxysterols ablated the effect of LAL dysfunction. When LIPA KD HepG2s were treated with 25-HC and 27-HC, the effect of LIPA KD on SREBP2 activity was completely ablated (Figure 2.2C). These data suggest, as expected, that LAL impairment alters SREBP2 signaling via the same mechanism as NPC deficiency.

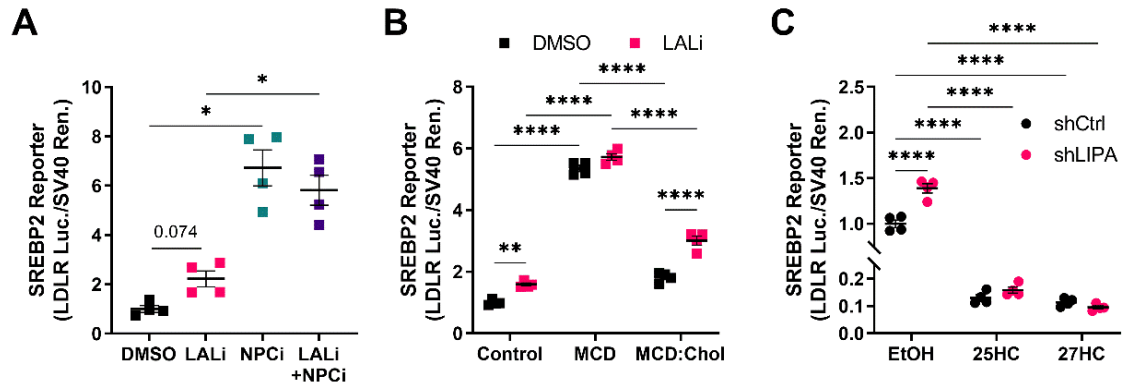


**Figure 2.2: Lysosomal cholesterol regulates SREBP2 via oxysterol levels.**

(A) Changes in SREBP2 activity in response to inhibition of LAL and NPC1/2. (B) Changes in SREBP2 activity in response to oxysterol treatment. (C) Changes in SREBP2 activity in response to cellular cholesterol levels. All experiments were performed on HepG2 cells. Differences between groups were determined using (A) Welch ANOVA test or (B-C) two-way ANOVAs followed by Tukey's post hoc comparisons. Statistical comparisons are indicated by horizontal lines and significant values are depicted as \* $P < 0.05$ , \*\* $P < 0.01$ , \*\*\* $P < 0.005$ , \*\*\*\* $P < 0.001$ .

*SREBP2 activity is regulated by both LAL and insulin signaling*

While our data suggest that the cholesterol products of LAL activity play a key role in regulating SREBP2, the role of mTORC1 and insulin signaling needs to be evaluated. To evaluate this, HepG2 cells were treated with LALi in the presence or absence of insulin (Figure 2.3A). The addition of insulin did not alter the induction of SREBP2 by LALi, though the DMSO treatment group did show a trend for increased SREBP2 activation with insulin addition. The presence of insulin attenuated the difference between DMSO and LALi treated cells. Upon Akt inhibition we observed the opposite effect. Again, there was no difference in the effect of LALi as compared to the DMSO treated group, but there was a significant reduction of the LALi group with Akt inhibition as compared to the control (Figure 2.3B). The reduction in LALi results in a decrease in the difference between DMSO and LALi treated cells. These reductions in the difference between activation of DMSO and LALi suggest that LALi treatment mimics the effect of insulin treatment and relies on Akt activity, at least in part, for SREBP2 induction. Together, these results indicate that LAL produced cholesterol and insulin signaling work in combination to promote SREBP2.

To directly assess whether LAL dysfunction alters mTORC1 activation, cells were treated with LALi and the phosphorylation status of S6K (Thr389) was measured after nutrient deprivation and addition. The addition of complete DMEM to the cells significantly increased S6K phosphorylation status, and this was completely unaffected by LAL inhibition (Figure 2.3C-D). To confirm that LAL inhibition was not affecting this, we repeated this assay using the lentiviral HepG2 LIPA KD cells, as they exhibit a more robust phenotype. Again, we did not see any effect of LIPA KD on mTORC1 activity (Figure 2.3E-F) suggesting that the changes in gene expression observed as result of LIPA inhibition are not due to alterations in mTORC1 signaling.

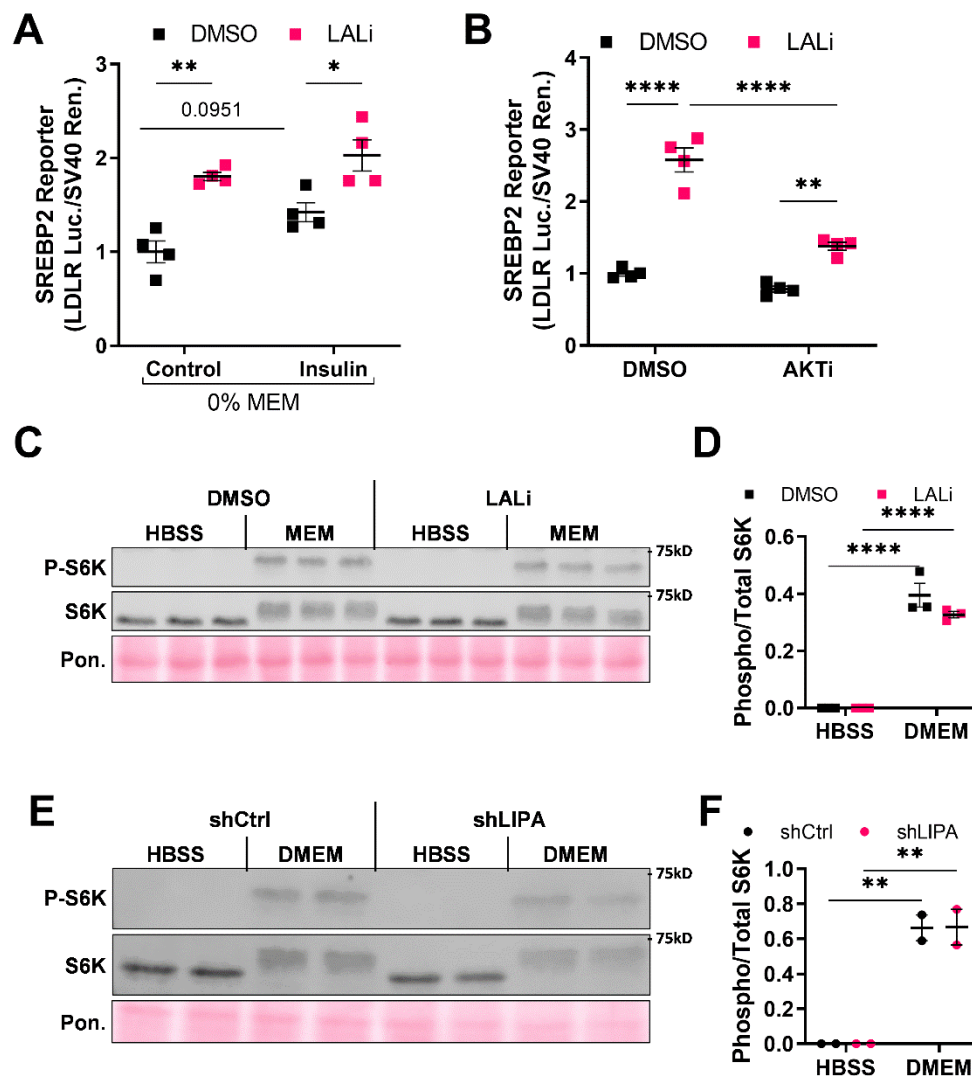


**Figure 2.3: SREBP2 activity is controlled in part by insulin signaling.**

Changes in LALi-induced SREBP2 activity in response to (A) insulin treatment and (B) inhibition of Akt activity. (C) Western blot and (D) quantification of S6K phosphorylation with LAL inhibition. (E) Western blot and (F) quantification of S6K phosphorylation with LIPA KD. All experiments were performed on HepG2 cells. Differences between groups were determined using two-way ANOVAs followed by Tukey's post hoc comparisons. Statistical comparisons are indicated by horizontal lines and significant values are depicted as \*P < 0.05, \*\*P < 0.01, \*\*\*P < 0.005, \*\*\*\*P < 0.001.

*LAL regulation of SREBP2 is dependent on extracellular cholesterol sources*

We then examined the reliance of LAL produced cholesterol on exogenous lipoproteins as a source for CE to regulate SREBP2 activity. HepG2s were cultured in complete media, serum free media, or serum free media supplemented with 50 µg/mL LDL. The depletion of serum significantly increased the activation of SREBP2 under both conditions but did not alter the difference between DMSO and LALi (Figure 2.4A). Addition of LDL into the media reduced the SREBP2 activity closer to baseline and increased the effects of LALi on inducing SREBP2 activity.

As FBS is a highly heterogeneous media supplement, HepG2s were cultured in Advanced MEM (AdMEM). AdMEM contains insulin and other growth factors, allowing reductions in the amount of FBS needed for cell culture. This approach allowed us to minimize potential confounding factors present in serum. Under these conditions, we observed similar changes in SREBP2 in response to serum depletion and LDL addition, but the absence of serum ablated the effect of LALi on SREBP2 activity (Figure 2.4B). To evaluate this LDL dependency in a non-cancerous cell line, we repeated this experiment in AML12 cells. Again, we saw a robust increase in SREBP2 activation with LALi when LDL was present, but this difference was ablated without FBS or LDL (Figure 2.4C). This suggests that LDL is the primary source of cholesterol released from LAL-mediated hydrolysis that signaling to govern SREBP2 activity in hepatocytes.

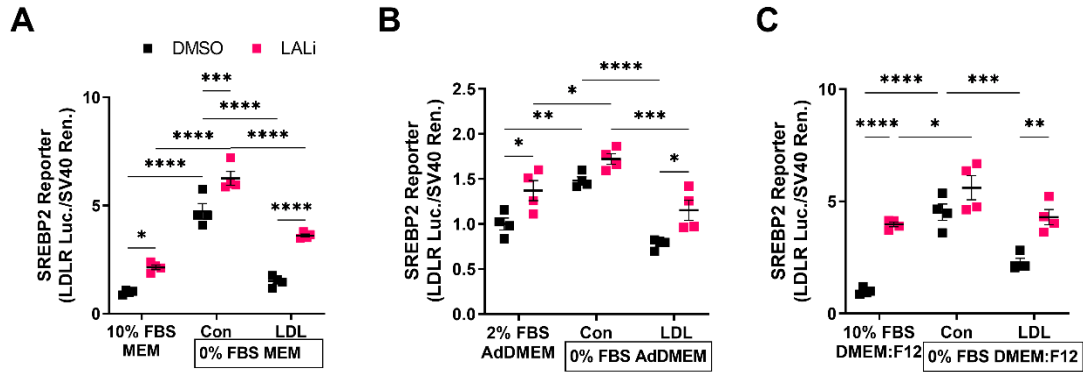


**Figure 2.4: LDL absence ablates LAL inhibition effect under certain conditions.**

(A) SREBP2 activation in HepG2s cultured in MEM with varying extracellular LDL. (B) SREBP2 activation in HepG2s cultured in Advanced DMEM (AdDMEM) with varying extracellular LDL. (C) SREBP2 activation in AML12s cultured in DMEM:F12 media with varying extracellular LDL. Differences between groups were determined using two-way ANOVAs followed by Tukey's post hoc comparisons. Statistical comparisons are indicated by horizontal lines and significant values are depicted as \* $P < 0.05$ , \*\* $P < 0.01$ , \*\*\* $P < 0.005$ , \*\*\*\* $P < 0.001$ .

*Extracellular free cholesterol and LDL have opposing effects on LAL activity*

Having shown that LAL regulation of SREBP2 is reliant on LDL, we evaluated whether LAL expression and activity responds to changing extracellular LDL. After 48 hours of LDL exposure, there was a mild trend toward increased LAL activity and expression at the highest LDL dose (Figure 2.5A-C). To determine whether the increase in LAL activity is due to the increase in LAL expression, LAL activity was normalized to expression (Figure 2.5D). This revealed that activity per LAL was unchanged at the 1000  $\mu\text{g/ml}$  LDL when compared to the control but was increased at the lowest dose of 250  $\mu\text{g/ml}$ . This could indicate that low expression of LDL drives post translational modifications of LAL that increase its activity.

As we previously showed differences in the effect of LAL inhibition on SREBP2 under conditions of exogenous LDL or cholesterol, we also examined the potential effect of free cholesterol on LAL activity. MCD was used to solubilize the cholesterol and thus was included alone as a control. We observed an increase in LAL activity with MCD exposure, but the addition of cholesterol up to 50  $\mu\text{M/mL}$  reduced activity while having no change on LAL expression (Figure 2.5E-G). When normalized to LAL expression, even just 5  $\mu\text{M/mL}$  cholesterol trended toward a reduction in activity per LAL protein (Figure 2.5H). As with the LDL, this robust change in LAL activity separate from LAL expression suggests that these interventions could be altering LAL activity via some unidentified post translational modification. No change was observed in the LAL banding pattern, though a subtle change in molecular weight would likely be undetectable using a Western blot due to the variable glycosylation status of LAL.

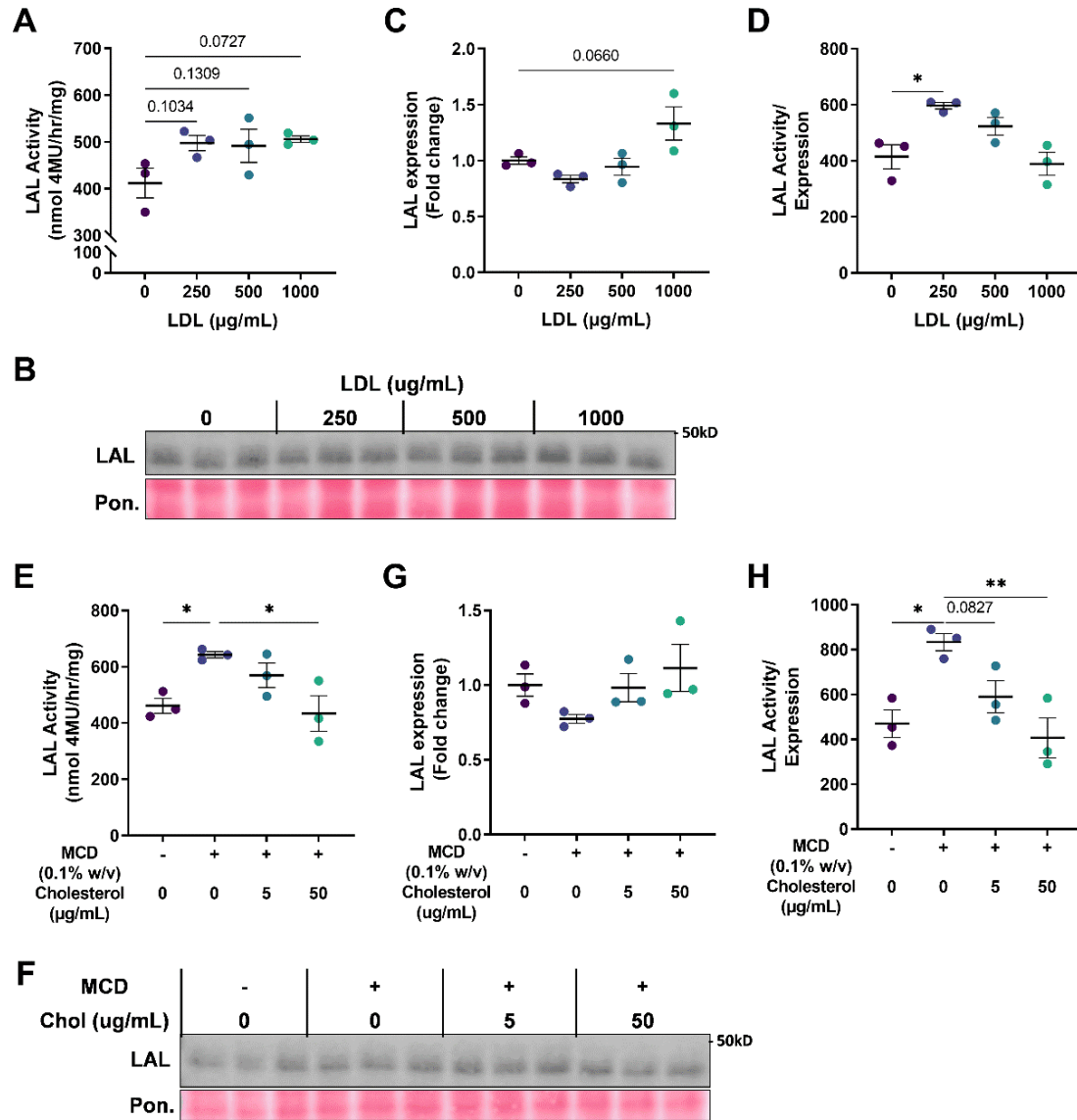


**Figure 2.5: Extracellular free cholesterol decreases LAL activity.**

(A) LAL activity assay, (B) Western blot, and (C) quantified LAL expression in HepG2s treated with varying LDL concentrations for 48 hours. (D) LAL activity normalized to LAL expression under LDL treatment. (E) LAL activity assay, (F) Western blot, and (G) quantified LAL expression in HepG2s treated with varying cholesterol concentrations for 48 hours. (H) LAL activity normalized to expression level under cholesterol treatments. Differences between groups were determined using a one-way ANOVA followed by Dunnett's post hoc comparisons. Statistical comparisons are indicated by horizontal lines and significant values are depicted as \* $P < 0.05$ , \*\* $P < 0.01$ , \*\*\* $P < 0.005$ , \*\*\*\* $P < 0.001$ .

## Discussion

The goal of these experiments was to specifically evaluate the role of LAL in regulating and responding to cellular cholesterol levels. We determined that dysfunction in both LAL and NPC promotes SREBP2 activation that is unchanged with the addition of free cholesterol but reduced with oxysterol supplementation, and that the regulation of SREBP2 by lysosomal cholesterol is dependent on LDL as a CE source. This was expected, as disruptions of both LAL and NPC prevent the proper lysosomal degradation and release of cholesterol. However, it is important to note that LAL dysfunction promotes lysosomal CE accumulation, whereas NPC inhibition results in lysosomal cholesterol accumulation. As such, the disruption of both proteins induces SREBP2 via the same pathways, but the buildup of these lipid species may have different effects on lysosomal function or signaling that have yet to be explored.

These results further emphasize the importance of lysosomal cholesterol in regulating cholesterol homeostasis and indicate that lysosomal cholesterol must be metabolized into an oxysterol to suppress SREBP2 signaling (Figure 2.6). Although further studies characterizing the cholesterol byproducts of lysosomal cholesterol are necessary to better understand whether the lysosomal cholesterol pool is selectively converted to specific oxysterol species. As these dysfunctions can significantly increase hepatic cholesterol synthesis, regardless of alterations in dietary cholesterol uptake, the use of oxysterol derivatives to suppress SREBP2 activity could be investigated for patients with drug resistant hypercholesterolemia. However, considerable modifications may be required to prevent undesirable off target effects.

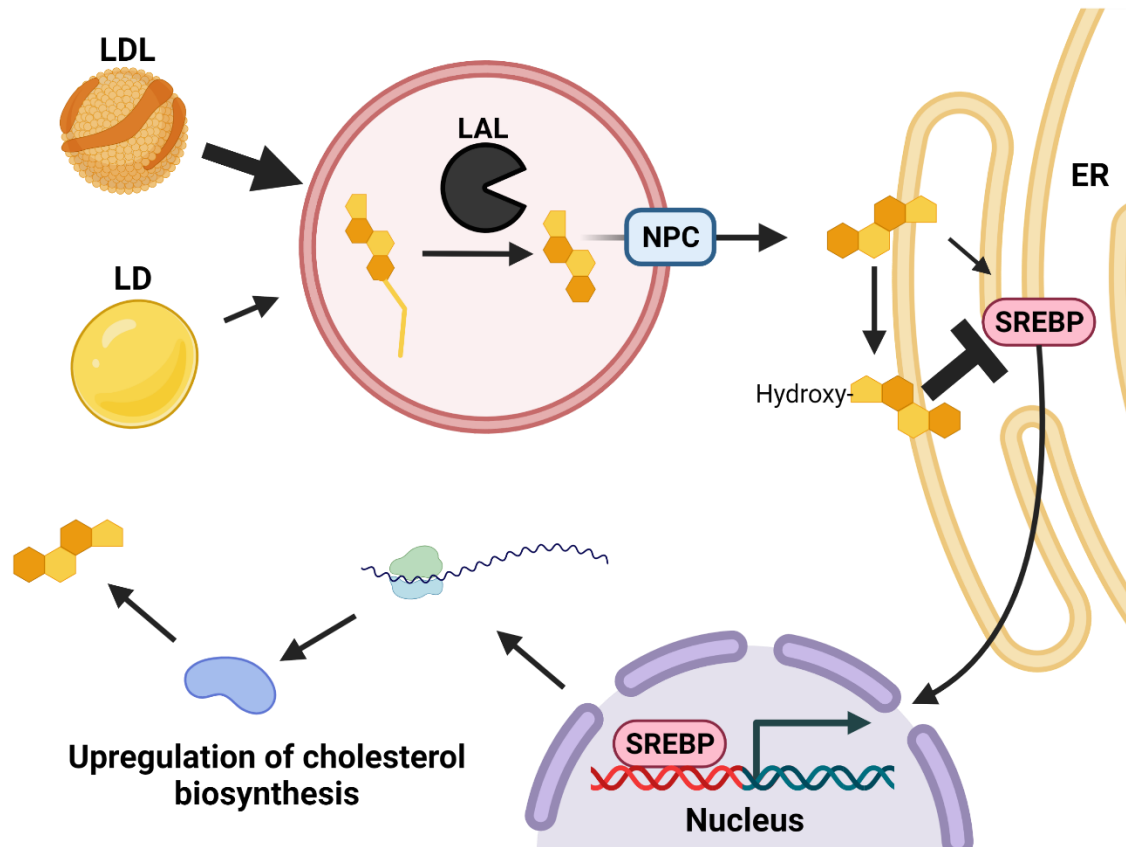


**Figure 2.6: Model of the role of LAL in regulating SREBP2 activity.**

LDL is the predominant CE source for LAL catabolized cholesterol. After export from the lysosome, this cholesterol pool is converted to oxysterols to inhibit SREBP2 and reduce cellular cholesterol synthesis.

The presented results show that LAL inhibition driving SREBP2 is largely dependent on LDL, though this varied with cell type and culture conditions. The loss of effect due to LAL inhibition in HepG2s in Advanced DMEM could be a result of altered cholesterol homeostasis due to prolonged low FBS conditions. As such, the reliance of cells on LDL could be highly dependent on their previous culture conditions and would likely be different in hepatocytes with large stores of CE, such as those in NAFLD. We attempted to answer this question by performing long term lipid loading to induce a cell culture NASH model as described<sup>116</sup>, but were unsuccessful in replicating the protocol.

Surprisingly, we found no significant effect of LAL inhibition on mTORC1 activity, despite seeing altered SREBP2 activation with insulin and Akt inhibition under conditions of blocked LAL. This result was unexpected, as it has been shown that SLC38A9 and NPC1 sense lysosomal cholesterol resulting in increased mTORC1 activity<sup>32</sup>. Therefore, we expected that preventing the cleavage of CE and the subsequent release of cholesterol inside the lysosome would reduce mTORC1 activity, but that wasn't the case. One possibility is that CE and cholesterol may bind similarly to the lysosomal cholesterol sensor. Previous work only directly examined cholesterol and oxysterol binding to SLC38A9<sup>32</sup> and the cholesterol depletion conditions used, like MCD, would have driven lysosomal CE localization and breakdown<sup>117</sup> so it isn't possible to determine the potential role of CE in activating SLC38A9. In contrast, other studies conducted in macrophages have shown that LAL KO promotes mTORC1 activation<sup>118</sup>, suggesting that much more work remains to be done on defining the regulation of mTORC1 by LAL.

After evaluating the role of LAL inhibition on cholesterol synthesis, we examined how extracellular cholesterol and LDL supplementation alter LAL activity. The data show that low levels of LDL increase LAL activity, whereas free cholesterol reduces LAL activity.

However, neither change is correlated with altered LAL expression. With no change in expression, LAL activity is likely regulated either by a direct inhibition or a post translational modification. LAL is a heavily glycosylated protein, but no specific post translational modifications have been identified that alter activity.

Overall, this work demonstrates the important role of LAL and lysosomal CE metabolism in directly regulating cellular cholesterol synthesis via SREBP2 activation. The reliance of SREBP2 on extracellular lipoproteins suggests that the CE reserves stored in the LD are not utilized to a sufficient extent under conditions of cholesterol depletion. The alterations in LAL activity and expression in response to varying extracellular cholesterol indicates that there are additional pathways regulating lysosomal CE metabolism that need identification.

## CHAPTER THREE

# Hepatic Lysosomal Acid Lipase Overexpression Worsens Hepatic Inflammation in Mice Fed a Western Diet

Michael W. Lopresti<sup>1</sup>, Wenqi Cui<sup>1</sup>, Breann Abernathy<sup>1</sup>, Gavin Fredrickson<sup>2</sup>, Fanta Barrow<sup>2</sup>, Arnav S. Desai<sup>1</sup>, Xavier S. Revelo<sup>2</sup>, Douglas Mashek<sup>1,3</sup>

<sup>1</sup> Department of Biochemistry, Molecular Biology, and Biophysics,  
University of Minnesota, Minneapolis MN

<sup>2</sup> Department of Integrative Biology and Physiology,  
University of Minnesota, Minneapolis MN

<sup>3</sup> Department of Medicine, Division of Diabetes, Endocrinology and Metabolism,  
University of Minnesota, Minneapolis MN

This chapter contains an original research article previously published.

Michael Lopresti wrote this manuscript and generated the data  
(with the exception of Figure 3.2 and Figure 3.5D-P).

Reproduced with permission from Journal of Lipid Research  
(<https://doi.org/10.1016/j.jlr.2021.100133>)

Copyright 2021.

## Summary

Non-alcoholic fatty liver disease (NAFLD) is characterized by the accumulation of lipid droplets (LD) in hepatocytes. NAFLD development and progression is associated with an increase in hepatic cholesterol levels and decreased autophagy and lipophagy flux. Previous studies have shown that the expression of lysosomal acid lipase (LAL, encoded by the gene LIPA), which can hydrolyze both triglyceride and cholesteryl esters, is inversely correlated with the severity of NAFLD. In addition, ablation of LAL activity results in profound NAFLD. Based on this, we predicted that overexpressing LIPA in the livers of mice fed a Western diet would prevent the development of NAFLD. As expected, mice fed the Western diet exhibited numerous markers of NAFLD, including hepatomegaly, lipid accumulation, and inflammation. Unexpectedly, LAL overexpression did not attenuate steatosis and had only minor effects on neutral lipid composition. However, LAL overexpression exacerbated inflammatory gene expression and infiltration of immune cells in mice fed the Western diet. LAL overexpression also resulted in abnormal phagosome accumulation and lysosomal lipid accumulation depending upon the dietary treatment. Overall, we found that hepatic overexpression of LAL drove immune cell infiltration and inflammation and did not attenuate the development of NAFLD, suggesting that targeting LAL expression may not be a viable route to treat NAFLD in humans.

## Introduction

Lysosomal acid lipase (gene=*LIPA*, protein=LAL) is the only identified lipase in the lysosome and plays a key role in lipid metabolism. Triacylglycerols (TAG) and cholesteryl esters (CE) hydrolyzed in lysosomes are derived from two pathways: the endocytosis of circulating lipoproteins or the autophagic engulfment of lipid droplets (LD), the latter of which is termed lipophagy<sup>119,120</sup>. Released fatty acids (FA) are largely effluxed via lysosomal exocytosis and reuptaken as needed<sup>73</sup>, whereas cholesterol is transported out of the lysosome via the NPC1/2 proteins<sup>74</sup>. Cholesterol produced via LAL plays a key role in regulating cellular cholesterol synthesis by inhibiting SREBP2 activation<sup>97</sup>.

Deficiency or loss of *LIPA* leads to cholesteryl ester storage disease (CESD) or Wolman Disease, respectively<sup>87</sup>. CESD is characterized by an enlarged fatty liver, hypercholesterolemia, and hypertriglyceridemia, whereas Wolman Disease is fatal for humans early in life. Whole body knockout of *Lipa* in mice results in accumulation of lipids in autophagosomes, severe hepatomegaly, fatty liver, and increased cholesterol synthesis<sup>95,97,121</sup>. Further, liver specific KO promotes hepatic inflammation and lipid accumulation<sup>99</sup>. However, hepatocyte specific expression of human *LIPA* in a whole body mouse KO model is able to rescue liver inflammation and ameliorate KO induced effects in peripheral tissues<sup>122</sup>, indicating that hepatic *LAL* expression is a key player in regulating whole body metabolism.

Serum LAL activity has repeatedly been shown to decrease with the development of non-alcoholic fatty liver disease (NAFLD)<sup>100,101</sup>, and is correlated with reduced hepatic LAL activity<sup>102</sup>. In addition to reduced LAL expression, autophagy as a whole is downregulated in response to various high fat diet models<sup>123,124</sup>, in part due to inhibition

of autophagic flux<sup>125</sup> and the prevention of acidification of lysosomes<sup>126</sup>. Recent work also identifies lipophagy inhibition in clinical samples of NAFLD patients<sup>103</sup>, leading some to suggest testing LAL replacement therapy as a potential treatment for diet-induced liver disease<sup>127</sup>. A mouse model of LAL overexpression in adipose tissue prevented diet-induced weight gain and lowered circulating cholesterol<sup>128</sup>. However, the potential impacts of liver specific overexpression of LAL are unknown.

During the development of NAFLD, lipid accumulation leads to hepatocyte ballooning and apoptosis<sup>129</sup>. In response, Kupffer cells, the resident macrophages in the liver, encircle the dying cells to degrade them, forming crown-like structures that accumulate cholesterol, resulting in a phenotypic change that recruits other immune cells and promotes inflammation<sup>116,130,131</sup>. As this occurs, the Kupffer cell pool is depleted and recruited monocytes to fill the niche, but these monocyte-derived replacements are more inflammatory than Kupffer cells<sup>132,133</sup>. B cells are also recruited to the liver, where they drive inflammation and fibrogenesis<sup>134</sup>. Multiple studies have demonstrated that preventing this recruitment of additional immune cells or removal of Kupffer cells slows the progression of NAFLD, indicating that immune cell infiltration is a key step in disease progression<sup>134–138</sup>.

As the dysregulation of lipid metabolism is a driving force in NAFLD, we examined whether the hepatic overexpression of human *LIPA* could protect mice from developing NAFLD on a Western diet. In contrast to expectations, these studies revealed that LAL overexpression exacerbated NAFLD and the associated pro-inflammatory phenotype.

## **Materials and Methods**

### *AAV creation*

pAAV.TBG.PI.eGFP.WPRE.bGH was a gift from James M. Wilson (Addgene plasmid # 105535). The *LIPA* gene, which codes for human LAL, was cloned into this plasmid to replace eGFP. A similar system has previously been used to overexpress a transgene specifically in hepatocytes<sup>139</sup>. The GFP and *LIPA* containing plasmids were packaged in AAV8 viral particles by the University of Minnesota Viral Vector and Cloning Core.

#### *Mice and diets*

Seven-week-old male and female C57BL/6J mice were purchased from Jackson Labs and housed under controlled temperature (22°C) and lighting conditions (14:10h light-dark cycle). To promote NAFLD, we used a high fat diet with additional fructose, palmitate, and cholesterol (FPC diet)<sup>140</sup>. Purified diet (TD.94048) and FPC diet (TD.190142) were purchased from Envigo (Indianapolis, IN). Mice fed the FPC diet also received fructose-glucose water (23.1 g/L d-fructose, 18.9 g/L d-glucose). Mice were acclimatized for 1 week prior to retroorbital injections with  $5 \times 10^{11}$  viral copies/mouse of AAV harboring GFP or *LIPA*. After 1 week, dietary treatments were initiated for 16 weeks, and body weights were collected weekly. At week 17, mice were sacrificed following a 4 hour fast and tissues were collected. All animal protocols were approved by the University of Minnesota Institutional Animal Care and Use Committee.

#### *Lysosomal Lipase Activity Assay*

Biological samples (tissue lysate or serum) were added to 200uM 4-methylumbelliferyl oleate (4-MUO) in 100 mM acetate buffer pH 4 with 1% Triton X-100. Fluorescence (excitation/emission - 320/460 nm) was measured for 3 hours and enzymatic activity was determined by comparing to a standard curve of 4-methylumbelliferone. Tissue lysate samples were normalized to total protein, and serum samples were normalized per volume.

### *Western Blotting*

Liver, iWAT, and heart tissue was homogenized in RIPA buffer containing protease and phosphatase inhibitors and clarified. Protein concentration was determined via BCA assay (23225, Thermo Fisher Scientific, Waltham, MA). Ponceau staining was used as a protein loading control, representative images are shown in figures, but the entire lane was used for quantification. Antibodies used were LAL (TA309730, Origene, Rockville, MD), CD45 (ab10558, Abcam, Cambridge, United Kingdom), F4/80 (ab74383, Abcam, Cambridge, United Kingdom), Phospho-ULK1 (6888, Cell Signaling Technology, Danvers, MA), ULK1 (8054, Cell Signaling Technology, Danvers, MA), Atg5 (12994, Cell Signaling Technology, Danvers, MA), and LC3 (PM036, MBL International Corporation, Woburn, MA).

### *Imaging and staining*

Livers were preserved in formaldehyde and then paraffin embedded for H&E and PicroSirius Red staining. For Oil Red O staining (ORO), liver samples were preserved by OCT. All staining and sectioning were done by the UMN Histology Core. LD size analyses was performed using a CellProfiler pipeline to analyze H&E images and Oil Red O stain<sup>141</sup>. Images were collected from liver sections from 3 mice per group, providing 2-6 images per liver for CellProfiler analyses. LDs with a diameter smaller than 2.75  $\mu\text{m}$  were unable to be reliably quantified and were excluded, as well as objects with a compactness >2 or eccentricity >0.94. PicroSirius Red stain was imaged using polarized light and quantified using a CellProfiler pipeline on images excluding central veins and portal triads.

### *Lipid Quantification*

Total hepatic lipids were extracted using chloroform:methanol (2:1), dried under N<sub>2</sub> gas, and quantified gravimetrically. Free cholesterol (for both males and females) and CE (for females) were determined enzymatically<sup>142</sup>. TAG, CE, free cholesterol, and FA composition of TAG/CE for male mice was quantified via gas chromatographic analysis by the Vanderbilt University Hormone Assay and Analytical Services Core. Briefly, lipid classes are separated by thin layer chromatography using Silica Gel 60 A plates developed in petroleum ether, ethyl ether, acetic acid (80:20:1) and visualized by rhodamine 6G. TAG and CE are scraped from the plates and methylated using BF<sub>3</sub>/methanol. Gas chromatographic analysis is performed on an Agilent 7890A gas chromatograph equipped with flame ionization detectors and a capillary column (SP2380, 0.25 mm x 30 m, 0.20 μm film, Supelco, Bellefonte, PA).

#### *Serum metabolites*

At sacrifice, blood was collected from the heart and serum was isolated after centrifugation for 10 min at 5,000 G. TAG (SB-2100-430, Stanbio Laboratory, Boerne, TX), glucose (997-03001, Wako Diagnostics, Lexington, MA), ketone bodies (415-73301, Wako Diagnostics, Lexington, MA), NEFAs (999-34691, Wako Diagnostics, Lexington, MA), and cholesterol (999-02601, Wako Diagnostics, Lexington, MA) were measured using 96 well plate formats as per manufacturer's instructions.

#### *RNA Sequencing*

RNA was isolated from liver tissue using a combined TRIzol (15596026, Invitrogen, Waltham, MA)/RNeasy kit (74004, Qiagen, Hilden, Germany) extraction and were submitted to the UMN Genomics Core for RNAseq analysis. Briefly, total RNA samples were converted to Illumina sequencing libraries using Illumina's (San Diego, CA) TruSeq RNA Sample Preparation Kit (Cat. # RS-122-2001 or RS-122-2002) or Stranded mRNA

Sample Preparation Kit (Cat. # RS-122-2101). The libraries are then loaded onto the NovaSeq paired end flow cell and clustering occurs on board the instrument. Base call (.bcl) files for each cycle of sequencing are generated by Illumina Real Time Analysis (RTA) software. The base call files and run folders are streamed to servers maintained at the Minnesota Supercomputing Institute. Primary analysis and de-multiplexing are performed using Illumina's bcl2fastq v2.20.

#### *Differential Expression Analysis of RNAseq*

2 x 150bp FastQ paired-end reads (n=37.1 million average per sample) were trimmed using Trimmomatic (v 0.33) enabled with the optional "-q" command; 3bp sliding-window trimming from 3' end requiring minimum Q30. Quality control on raw sequence data for each sample was performed with FastQC. Read mapping was performed via Hisat2 (v2.1.0) using the mouse genome (GRCm38) as reference. Gene quantification was done via Feature Counts for raw read counts. Differentially expressed genes were identified using the edgeR (negative binomial) feature in CLCGWB (Qiagen, Redwood City, CA) using raw read counts. We filtered the generated list based on a minimum 2x Absolute Fold Change and FDR corrected  $p < 0.05$ . Data were analyzed through the use of Ingenuity Pathway Analysis (IPA; QIAGEN Inc., <https://www.qiagenbioinformatics.com/products/ingenuitypathway-analysis>)<sup>143</sup> and the Gene Ontology database<sup>144</sup>.

#### *qPCR*

RNA was isolated from liver tissue using a combined Trizol/RNeasy kit extraction, as previously described. cDNA was synthesized using Superscript Vilo cDNA Synthesis Kit (Invitrogen, Waltham, MA) and qPCR was performed using SYBR Green Master Mix. All

data shown were normalized to Cyc1 and TBP expression using an extended  $\Delta$ CT method<sup>145</sup>.

#### *Immune Cell Isolation*

Livers were collected and at least 1 g was homogenized in RPMI media using a gentleMACS dissociator (Miltenyi Biotech, Bergisch Gladbach, Germany). A cell pellet was obtained by differential centrifugation using a 37.5% Percoll (Sigma-Aldrich, St. Louis, MO) gradient<sup>146</sup>. Red blood cells were removed using a lysis buffer (Biolegend, San Diego, CA) and the cells were washed before counting with a Muse cell analyzer (Millipore Sigma, Burlington, MA).

#### *Mass Cytometry*

Immune cells were stained with 5  $\mu$ M cisplatin to discriminate between viable and dead cells. Cisplatin staining was quenched with maxpar cell staining buffer and non-specific binding was blocked with TruStain FcX Plus (Biolegend, San Francisco, CA). Staining for cell surface markers was performed with 5  $\mu$ g of metal-conjugated primary antibodies for 30 mins at 4°C. Cells were then fixed with 1.6% formaldehyde (ThermoFisher, Waltham, MA) and incubated with 0.5  $\mu$ M intercalator solution in Fix and Perm buffer overnight. Cells were washed, re-suspended in maxpar water and data acquired on a CyTOF2 cytometer (DVS Sciences, Sunnyvale, CA). For intracellular staining, cells were fixed and permeabilized with maxpar buffers and stained with metal-conjugated intracellular antibodies. Mass cytometry data was analyzed using Cytobank<sup>134</sup>. Immune cells were determined as a percent of total CD45+ cells, which was normalized to Western Blots for CD45 to provide the total amount of each cell type per liver sample. All reagents for the mass cytometry analysis were from Fluidigm (San Francisco, CA) unless otherwise noted.

### *Electron microscopy*

Samples approximately 1-2 mm<sup>3</sup> were initially placed in a fixative solution of 3% paraformaldehyde, 1.5% glutaraldehyde, and 2.5% sucrose in 0.1 M sodium cacodylate buffer with 5mM calcium chloride and 5mM magnesium chloride (pH 7.4) and kept at RT for 30 minutes, then stored for at least 24 hrs at 4°C. They were rinsed in buffer (10 min, 3x), then placed in 1% osmium tetroxide and 0.1 M sodium cacodylate buffer (pH 7.4) overnight at 4°C. Specimens were rinsed in ultrapure water (NANOpure Infinity®; Barnstead/Thermo Fisher Scientific; Waltham, MA) (10 min, 3x), en bloc stained with 1% aqueous uranyl acetate for 2 hrs, and rinsed in ultrapure water (10 min, 3x). They were then dehydrated in an ethanol series (25%, 50%, 75%, 95% (2x) and 100% (3x); 20 min for each change) and embedded in Embed 812 resin (Electron Microscopy Sciences, Hatfield, PA). Ultrathin sections 80–100 nm thick were cut on a Leica Ultracut UCT microtome using a diamond knife and collected on formvar/carbon-coated copper 200-mesh grids (Electron Microscopy Sciences, Hatfield, PA). They were stained with 3% aqueous uranyl acetate for 20 min, rinsed in ultrapure water (10 sec, 5x), stained with Sato's triple-lead stain<sup>147</sup> for 3 min, and rinsed in ultrapure water (10 sec, 5x). Sections were examined with a JEOL JEM1400-Plus transmission electron microscope operating at 60 kV. Images were recorded with a Maxim DL digital capture system. TEM image quantification is based on 4-7 images collected from 3 mice per group.

### *Statistical analyses*

All data are presented as individual values overlaid with means  $\pm$  SEM. Differences between groups were determined using either a two-way ANOVA followed by Turkey's post hoc test or multiple unpaired t-tests. Statistical significance was declared at  $p < 0.05$ .

## Results

### *FPC diet-induced hepatomegaly was unaffected by hepatic LAL overexpression*

After 16 weeks on diet (Figure 3.1A), hepatic protein lysates from mice that received the *LIPA* AAV had significantly higher hepatic LAL activity (Figure 3.1B) and LAL expression (Figure 3.1C-D, Supplemental Figure 3.1A-B) when compared to groups that received the GFP AAV. No significant changes were observed in body weight gain across the male groups (Figure 3.1E), although the FPC diet did significantly increase body weight gain in females (Supplemental Figure 3.1C, Supplemental Figure 3.2). Regardless of sex and LAL expression, the livers of mice on the FPC diet weighed significantly more than mice on the purified diet (Figure 3.1F, Supplemental Figure 3.1D), though no changes in fibrosis were observed (Supplemental Figure 3.1H-I). While the diet did not elicit the changes in body weight originally seen by Wang et al<sup>140</sup>, the diet promoted severe hepatomegaly, resulting in a non-obesogenic NAFLD model.

Histological staining of livers revealed variations in fat accumulation and LD populations across groups resulting from both LAL overexpression and the FPC diet (Figure 3.1G-I, Supplemental Figure 3.1E-G). As expected, the FPC diet significantly increased the percent of total area stained by ORO, though this was unaffected by LAL expression (Figure 3.1H, Supplemental Figure 3.1F). After binning LDs by diameter and examining the percent of LDs in each size range (Figure 3.1I, Supplemental Figure 3.1G), we observed a significant reduction in LDs with a diameter between 2.75 and 5  $\mu\text{m}$  and an increase in LDs between 10-15  $\mu\text{m}$  in the CON-LIPA group. While similar trends were present in FPC fed mice, the significance was lost. This shift in LD size could indicate that LAL overexpression drives increased breakdown of smaller LDs, which are thought to be the preferred lipophagic substrates<sup>63</sup>. These data show that while LAL

overexpression did not prevent hepatomegaly or steatosis, it did have more subtle effects on hepatic LD size in mice on the control diet.

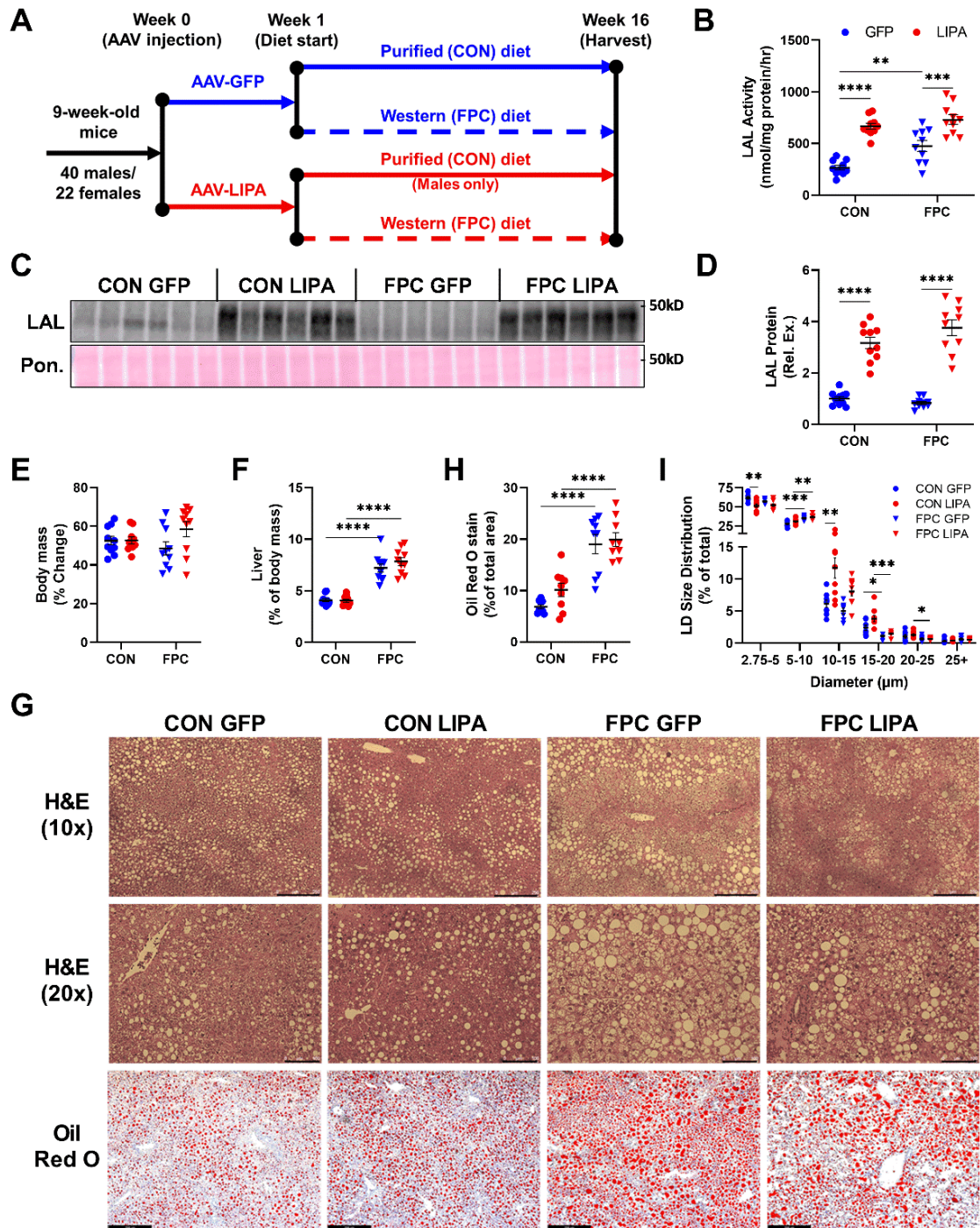
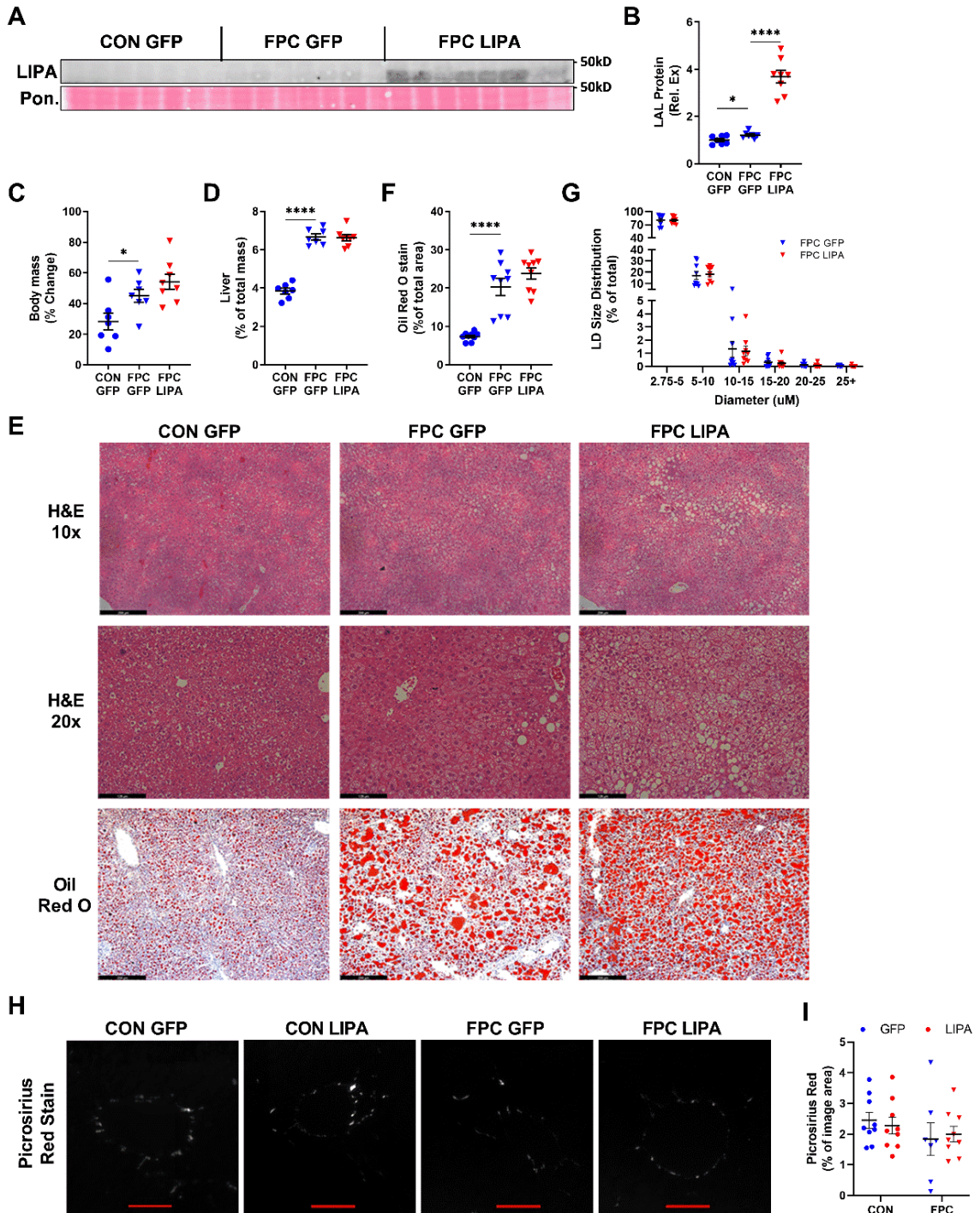


**Figure 3.1: LAL overexpression alters hepatic LD size distribution.**

(A) Experimental timeline. (B) Hepatic LAL activity measured via 4-MUO hydrolysis assay. (C) Representative western blot for hepatic LAL expression and (D) quantification. (E) Percent body weight change from Week 1 to Week 16. (F) Liver weights normalized to body weight. (G) Representative images for H&E 10x (250 μm

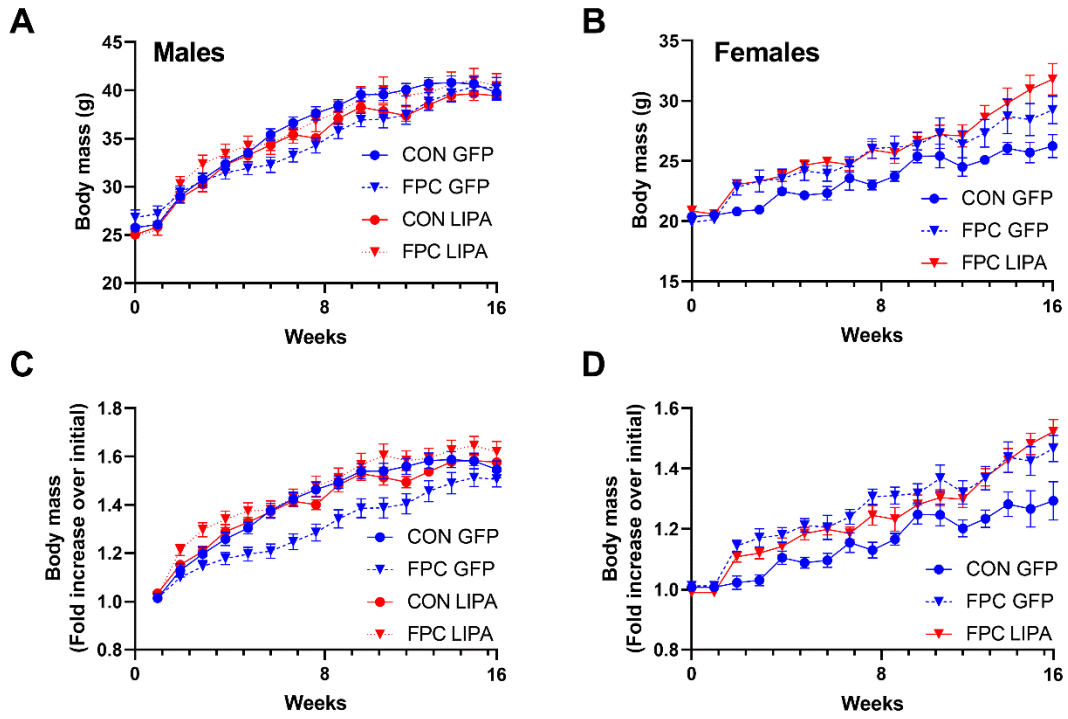
scale bar), 20x (100  $\mu\text{m}$  scale bar) and Oil red O (256  $\mu\text{m}$  scale bar) staining for liver sections. (H) Percent of total image area occupied by Oil Red O staining. (I) Percent of hepatic LDs within each size group. All data shown are from male mice. Statistical comparisons are indicated by horizontal lines and significant values are depicted as \*P < 0.05, \*\*P < 0.01, \*\*\*P < 0.005, \*\*\*\*P < 0.001.



**Supplemental Figure 3.1: Female mice data corresponding to Figure 1.**

(A) Western blot for hepatic LAL expression and (B) quantification. (C) Percent body weight change from Week 1 to Week 16. (D) Liver weights normalized to body weight. (E) Representative images for H&E 10x (250 µm scale bar), 20x (100 µm scale bar) and

Oil red O (256  $\mu\text{m}$  scale bar) staining for liver sections. (F) Percent of total image area occupied by Oil Red O staining. (G) Percent of hepatic LDs within each size group. (I) Representative images for PicroSirius Red staining containing portal triads (50  $\mu\text{m}$  scale bar). (H) Quantification of PicroSirius Red stain. Data in A-E are from female mice, I-H are male mice. Statistical comparisons are indicated by horizontal lines and significant values are depicted as \* $P < 0.05$ , \*\* $P < 0.01$ , \*\*\* $P < 0.005$ , \*\*\*\* $P < 0.001$ .



**Supplemental Figure 3.2: Change in body mass.**

Weekly measures of body mass for (A) male and (B) female mice. Body mass as a fold change compared to week 1 for (C) male and (D) female mice.

*LAL overexpression alters hepatic cholesterol stores*

Measurements of total hepatic lipids further confirm that the hepatomegaly is largely the result of lipid accumulation in mice on the FPC diet and was unaltered by LAL expression in both males (Figure 3.2A) and females (Supplemental Figure 3.3A). Hepatic TAG, CE, and free cholesterol levels rose in mice receiving the FPC diet and were largely unaffected by LAL expression (Figure 3.2B-D, Supplemental Figure 3.3B-C).

In addition to measuring total lipid levels, we analyzed the acyl chains present in both TAG and CE in the male mice (Figure 3.2E-F). Significant changes were observed in the composition of TAG acyl groups in response to the FPC diet (Figure 3.2E), with increases in 18:1( $\omega$ -9) and 18:1( $\omega$ -7), and decreases in 16:0, 18:2, and 18:0. However, no significant changes due to LAL expression were observed. In contrast, the acyl groups stored in CE were significantly altered in response to the FPC diet and to LAL overexpression alone (Figure 3.2F). The FPC diet, regardless of LAL expression, significantly increased 16:1, 18:1( $\omega$ -9), and 18:1( $\omega$ -7), while 16:0, 18:0, and 18:2 were reduced. Notably, the pools of CE containing saturated fatty acids 14:0, 16:0, and 18:0 were all significantly reduced with LAL overexpression on the control diet, while there was a trend for increased 16:1. However, these LIPA driven changes in the CE pool disappeared on the FPC diet.

To better visualize the changes in FA partitioning, we sorted this data into saturated (SFA), monounsaturated (MUFA), and polyunsaturated (PUFA) FAs for both the TAG and CE pools (Figure 3.2G-H). The changes in mole percent of TAG composition in mice on FPC diet are similar to those seen in humans with NAFLD (Figure 3.2G)<sup>106</sup>, while LAL overexpression reduced the percent of CE containing SFA and increased MUFA on the

control diet (Figure 3.2H). As with the changes in LD size distribution, this change was lost in mice on the FPC diet.

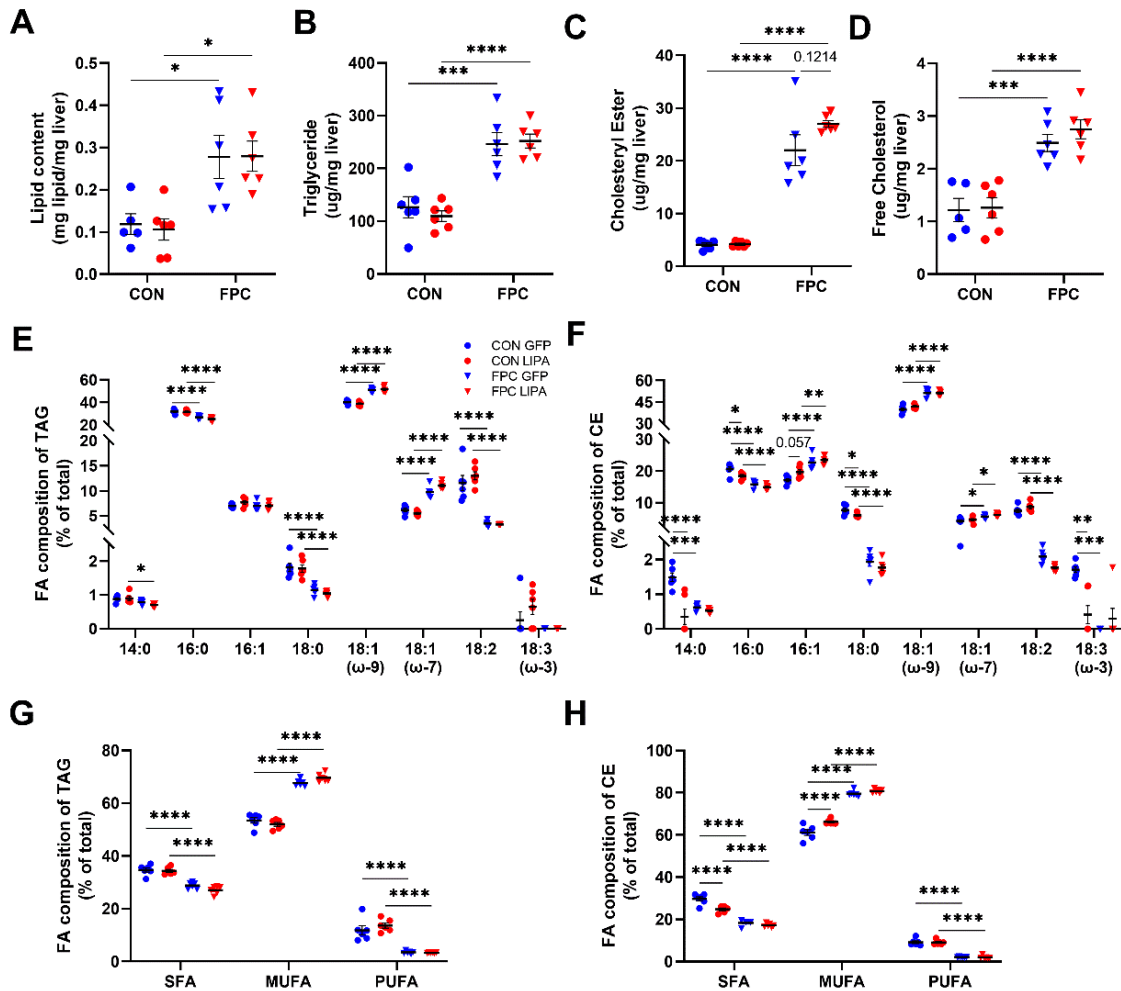
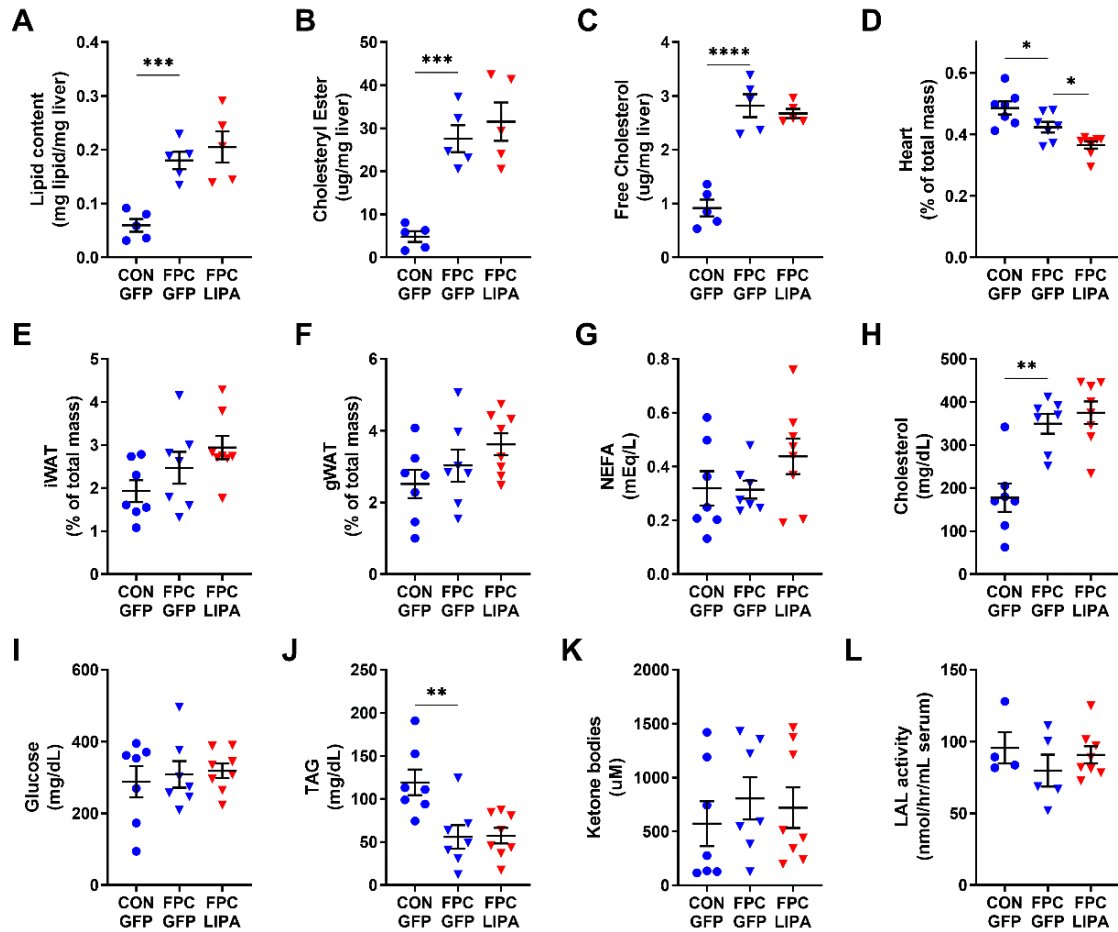


**Figure 3.2: LAL overexpression modifies hepatic lipid species.**

(A) Mass of all hepatic lipids per mg of liver. (B) Mass of triglycerides per mg of liver. (C) Mass of cholesterol per mg of liver. (D) Mass of cholesterol esters per mg of liver. (E) Percent composition of TAG pool categorized by acyl group. (F) Percent composition of CE pool categorized by acyl group. (G) Percent composition of the TAG pool categorized by FA type. (H) Percent composition of the CE pool categorized by FA type. All data shown are from male mice. Statistical comparisons are indicated by horizontal lines and significant values are depicted as \* $P < 0.05$ , \*\* $P < 0.01$ , \*\*\* $P < 0.005$ , \*\*\*\* $P < 0.001$ .



**Supplemental Figure 3.3: Hepatic lipids and peripheral analyses in female mice.**

(A) Hepatic lipids per mg of tissue. (B) Mass of cholesteryl esters per mg of liver. (C) Mass of free cholesterol per mg of liver. Weights for (D) heart, (E) iWAT, and (F) gWAT normalized to body weight. Serum levels for (G) NEFA, (H) cholesterol, (I) fasting glucose, (J) TAG, and (K) ketone bodies. (L) Serum LAL activity measured via 4-MUO hydrolysis assay. All data shown are from female mice. Statistical comparisons are indicated by horizontal lines and significant values are depicted as \*P < 0.05, \*\*P < 0.01, \*\*\*P < 0.005, \*\*\*\*P < 0.001.

*LAL overexpression and FPC diet promote changes in the heart and adipose depots*

As liver LAL expression plays a key role in regulating metabolic changes throughout the body, we measured the weights of the heart, inguinal white adipose tissue (iWAT), and gonadal white adipose tissue (gWAT), as well as the concentrations of several serum metabolites (Figure 3.3, Supplemental Figure 3.3D-K). Heart mass was significantly reduced in male and female mice on the FPC diet with LAL overexpression when compared to the FPC-GFP control (Figure 3.3A, Supplemental Figure 3.3D). We were unable to identify any previously reported heart specific phenotypes in LIPA KO models outside of atherosclerosis based studies, although polymorphisms in LIPA that increase expression are associated with impaired endothelial function and increased susceptibility to coronary artery disease<sup>148</sup>.

iWAT depots from male mice in the FPC-LIPA group were significantly larger than those in the CON-LIPA and FPC-GFP groups (Figure 3.3B). However, gWAT depots did not exhibit the same trend, with only the LIPA groups showing a significant increase on the FPC diet (Figure 3.3C). Despite differences in body weight, female mice did not have any significant differences in WAT depots (Supplemental Figure 3.3E-F).

No significant changes from LAL expression in serum NEFA, cholesterol, or fasting glucose levels were observed in male mice, whereas female mice had a significant increase in serum cholesterol in response to the FPC diet (Figure 3.3D-F, Supplemental Figure 3.3G-I). In both sexes, serum TAG was significantly reduced in mice fed FPC diet, but no differences were observed in the LAL overexpression group (Figure 3G, Supplemental Figure 3.3J). Ketone bodies were elevated in the LAL overexpression group in male mice fed the FPC diet (Figure 3.3H) but were unchanged in females (Supplemental Figure 3.3K). As LAL is released with lysosomal exocytosis, we also

measured serum LIPA activity (Figure 3.3I, Supplemental Figure 3.3L) to determine whether increased hepatic LAL impacted circulating LAL but found that it was not significantly changed across groups regardless of sex. Further, LAL protein abundance in heart and iWAT tissue was measured in male mice (Figure 3.3J-K). No significant differences were identified between groups, although there was large mouse to mouse variation in iWAT LAL expression levels. These data indicate that hepatic LAL overexpression does not result in increased LAL throughout the body and does not have a major effect on adiposity or serum metabolites.

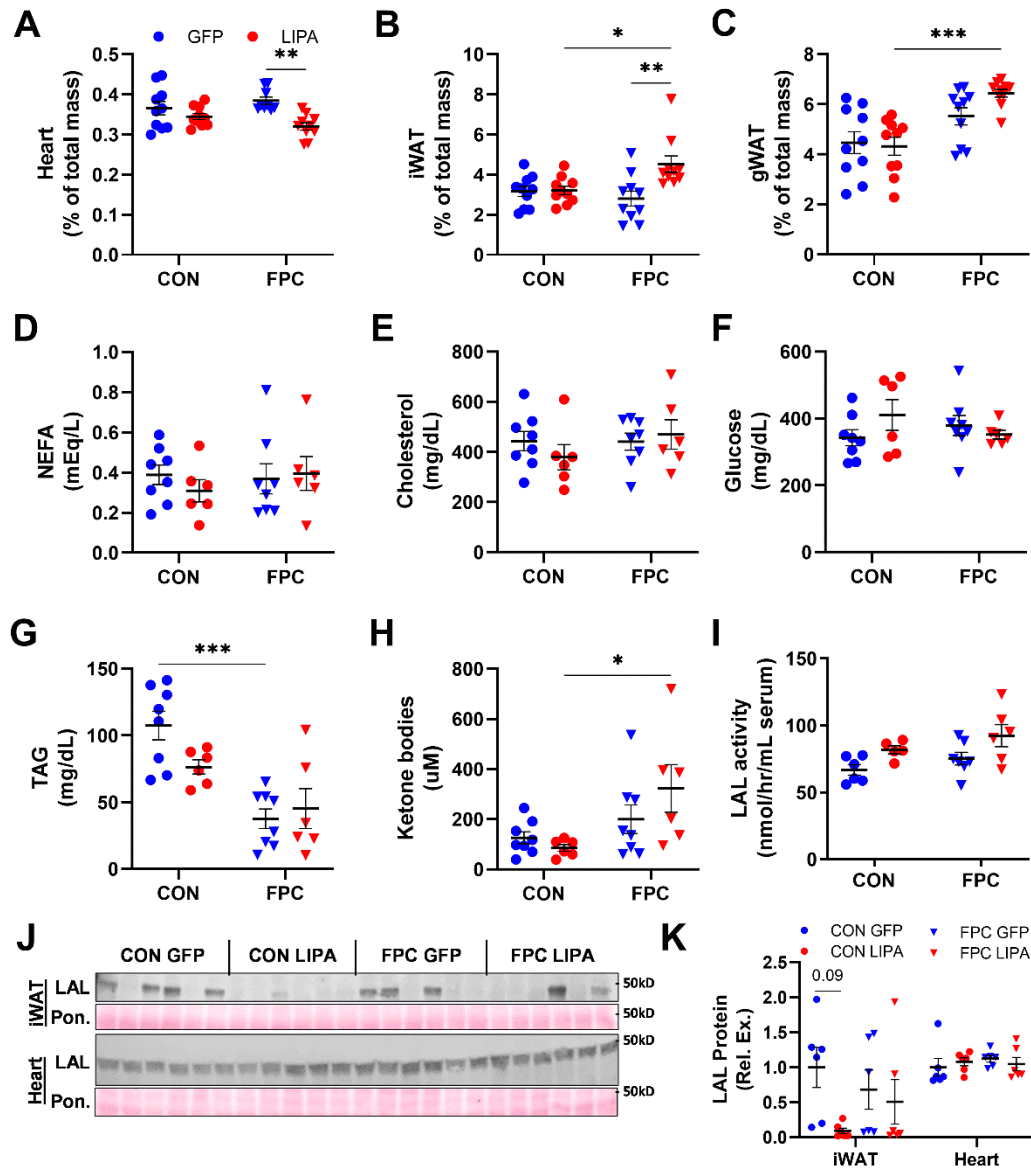


**Figure 3.3: Whole body treatment effects.**

Weights for (A) heart, (B) inguinal WAT, and (C) gonadal WAT normalized to body weight. Serum levels for (D) NEFA, (E) cholesterol, (F) fasting glucose, (G) TAG, and (H) ketone bodies. (I) Serum LAL activity measured via 4-MUO hydrolysis assay. (J) Western blots and (K) quantification for LAL expression in iWAT and heart tissue. All data shown are from male mice. Statistical comparisons are indicated by horizontal lines and significant values are depicted as \* $P < 0.05$ , \*\* $P < 0.01$ , \*\*\* $P < 0.005$ , \*\*\*\* $P < 0.001$ .

### *LAL overexpression alters the hepatic transcriptome*

To further investigate the effect of both the FPC diet and LAL overexpression on changes in the hepatic transcriptome, RNAseq analysis was conducted. Since our primary focus was on testing if LAL overexpression could remedy NAFLD, we conducted RNAseq analysis on livers from the CON-GFP, FPC-GFP, and FPC-LIPA groups to validate the effects of the FPC diet and to determine the effects of LIPA within the NAFLD-promoting FPC diet in male mice. There were 1335 genes differentially expressed (DE) between the CON-GFP and FPC-GFP groups (Figure 3.4A), and 1879 between the FPC-GFP and FPC-LIPA groups (Figure 3.4B). Ingenuity Pathway Analysis (IPA) revealed that the most significantly changed pathways as a result of the FPC diet were related to immune infiltration, hepatic fibrosis, stellate cell activation, and inflammation (Figure 3.4C). These changes were largely expected as they are associated with the development of NAFLD. DE gene lists also underwent GO analysis, which revealed similar increases in immune pathways related to leukocyte activation and inflammation (Supplemental Figure 3.4A-C)

Using IPA, we identified the top pathways altered in response to LAL overexpression in the mice fed the FPC diet (Figure 3.4D). While the most significant pathways were associated with protein translation and oxidative metabolism, many IPA pathways were related to immune cell infiltration and inflammation. This suggested that LAL overexpression resulted in substantial changes in the immune cell infiltration and inflammation, especially as these pathways were largely related to leukocyte extravasation/diapedesis and communication between immune cell populations. Similar inflammation-related pathways were identified in the GO analysis of DE genes (Supplemental Figure 3.4D-F). To determine potential drivers of the observed changes, we performed an IPA Upstream Regulator analysis and found cholesterol to be one of

the top endogenous chemicals predicted to be upregulated was cholesterol (Figure 3.4E) suggesting that alternate pathways of cholesterol signaling that we were unable to capture may be responsible for some of the observed phenotype.

While similar pathways were significantly changed with the FPC diet or LAL overexpression, only 186 genes were significantly changed under both the FPC and LIPA conditions. Of these genes, 32 are involved in the immune response (GO:0002376) and have been plotted as a heatmap to show the changes in this gene list across groups (Figure 3.4F). Most of the genes in this group increase in expression with FPC and LIPA, potentially reflecting an exacerbation of hepatic inflammation.

To further examine the changes in inflammation that resulted from LAL overexpression, we generated a heatmap of the genes differentially expressed between FPC GFP and FPC LIPA that were enriched in the diapedesis and lymphocyte extravasation (Figure 3.4G). We found that LAL overexpression resulted in increased expression of genes encoding for immune activation, pro-inflammatory cytokines, chemokines, and toll-like receptors. Taken together, these changes suggest that LAL overexpression is significantly driving the pro-inflammatory response associated with the FPC diet.

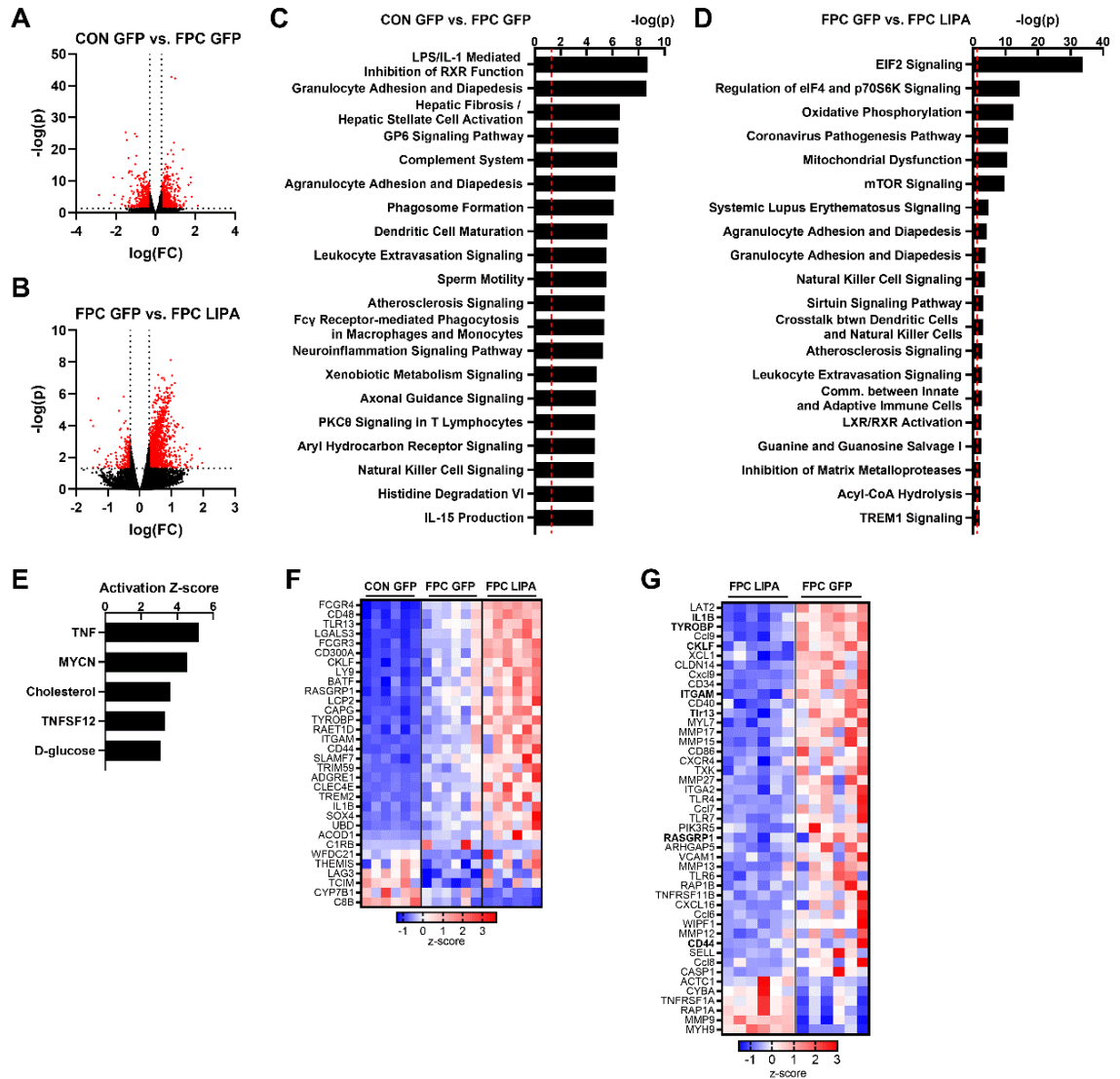
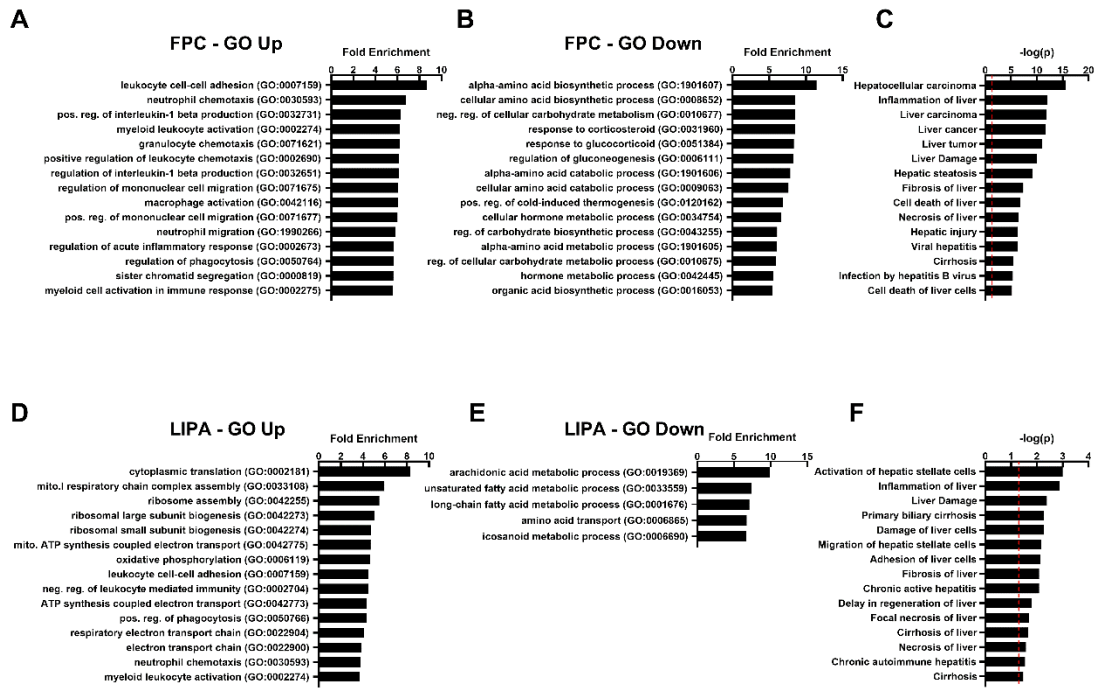


**Figure 3.4: LAL overexpression altered the hepatic transcriptome.**

Volcano plots of differentially expressed genes when comparing (A) FPC GFP to CON GFP and (B) LIPA FPC to GFP FPC. Top canonical pathways predicted to be changed by IPA based on transcriptome changes between (C) FPC GFP to CON GFP and (D) LIPA FPC to GFP FPC. (E) Top predicted upstream regulators of LIPA induced gene changes. (F) Heatmap based on z-score for immune related genes that were DE due to both FPC and LIPA effects. (G) DE genes in the Leukocyte extravasation, Agranulocyte/Granulocyte Adhesion and Diapedesis, and TREM1 signaling IPA groups. Bolded gene names in (F) are also present in (E). All data shown are from male livers.



**Supplemental Figure 3.4: Gene ontology analysis of transcriptomic data.**

GO analysis of DE genes (A) increased and (B) decreased with FPC. (C) Top terms returned using a liver specific Tox Function analysis in IPA for the FPC DE genes. GO analysis of DE genes (D) increased and (E) decreased with LIPA. (F) Top terms returned using a liver specific Tox Function analysis in IPA for the LIPA DE genes.

### LAL overexpression *promotes hepatic immune infiltration and inflammation*

To better understand how LAL overexpression instigates hepatic inflammation, we characterized the immune cell infiltrates in the liver. First, we measured the protein content and mRNA expression of several inflammatory markers. Western blots were performed for CD45 and F4/80, which are a leukocyte and a macrophage marker, respectively (Figure 3.5A-B). LAL overexpression increased the expression of CD45 in the livers of mice on both diets and F4/80 in the FPC fed group. Female mice showed a similar increase in CD45 expression in hepatic lysate (Supplemental Figure 3.5A-B). Next, we performed qPCR for a subset of inflammatory and fibrotic genes (TNF $\alpha$ , F4/80, IL1 $\beta$ , Col1a1, and Acta2) including tissue from CON-LIPA group (Figure 3.5C, Supplemental Figure 3.5C). Both TNF $\alpha$  and IL1 $\beta$  were highly expressed in response to LAL overexpression in male mice fed the FPC diet (Figure 3.5C). However, this effect was not seen in female mice, which had increased TNF $\alpha$  and F4/80 mRNA levels in response to the FPC diet, not LAL overexpression (Supplemental Figure 3.5C). Male mice showed significant increases in Col1a1 mRNA in response to the FPC diet, but there was no significant change in Acta2 expression due to high mouse to mouse variability (Figure 3.5C).

We then isolated the immune cells from the livers and performed CyTOF to identify the major immune subsets (Figure 3.5D). The abundance of natural killer T cells (NKT; Figure 3.5E) was not affected by dietary treatment but trended to increase with LAL expression. The amounts of natural killer (NK; Figure 3.5F) cells, B cells (Figure 3.5G), CD4+ T cells (Figure 3.5H), CD8+ T cells (Figure 3.5I), Kupffer cells (KC; Figure 3.5J), polymorphonuclear cells (PMN; Figure 3.5K), and plasmacytoid dendritic cells (pDC; Figure 3.5L) present in the liver were increased with LAL overexpression, but unaltered on the FPC diet alone. Monocytes and monocyte derived macrophages (Mo/MFs) were

significantly increased by the FPC diet and by LAL overexpression (Figure 3.5M). Overall, these findings suggest that LAL overexpression results in a substantial accumulation of all major immune cell subsets. As the infiltration of monocyte and monocyte-derived macrophages (Mo/MF population) is associated with proinflammatory signaling, these data suggest that LAL overexpression promotes inflammation through an increase in monocyte recruitment, as suggested by our IPA analysis.

Examination of the relative abundance of immune cell subsets showed that LAL overexpression increased the percent of B cells, while the frequency of NK and CD8+ T cells decreased (Figure 3.5N). The FPC diet elicited similar trends in the Mo/MF frequency and total abundance. To further characterize the Mo/MFs population, we used an alternative gating strategy to quantify Ly6Chi (Figure 3.5O) and Ly6Clo (Figure 3.5P) monocytes. These monocytes are associated with inflammatory and restorative phenotypes, respectively<sup>149</sup>. Both of these populations increased as a percentage of total CD45+ cells with the FPC diet, but only the restorative Ly6Clo population decreased with LAL overexpression. Additionally, this increased immune cell infiltration was not observed in iWAT or heart tissue (Supplemental Figure 3.5D-E), suggesting that the liver is the primary site of inflammation. Collectively, these data show that LAL overexpression enhanced the pro-inflammatory liver phenotype of mice on the FPC diet.

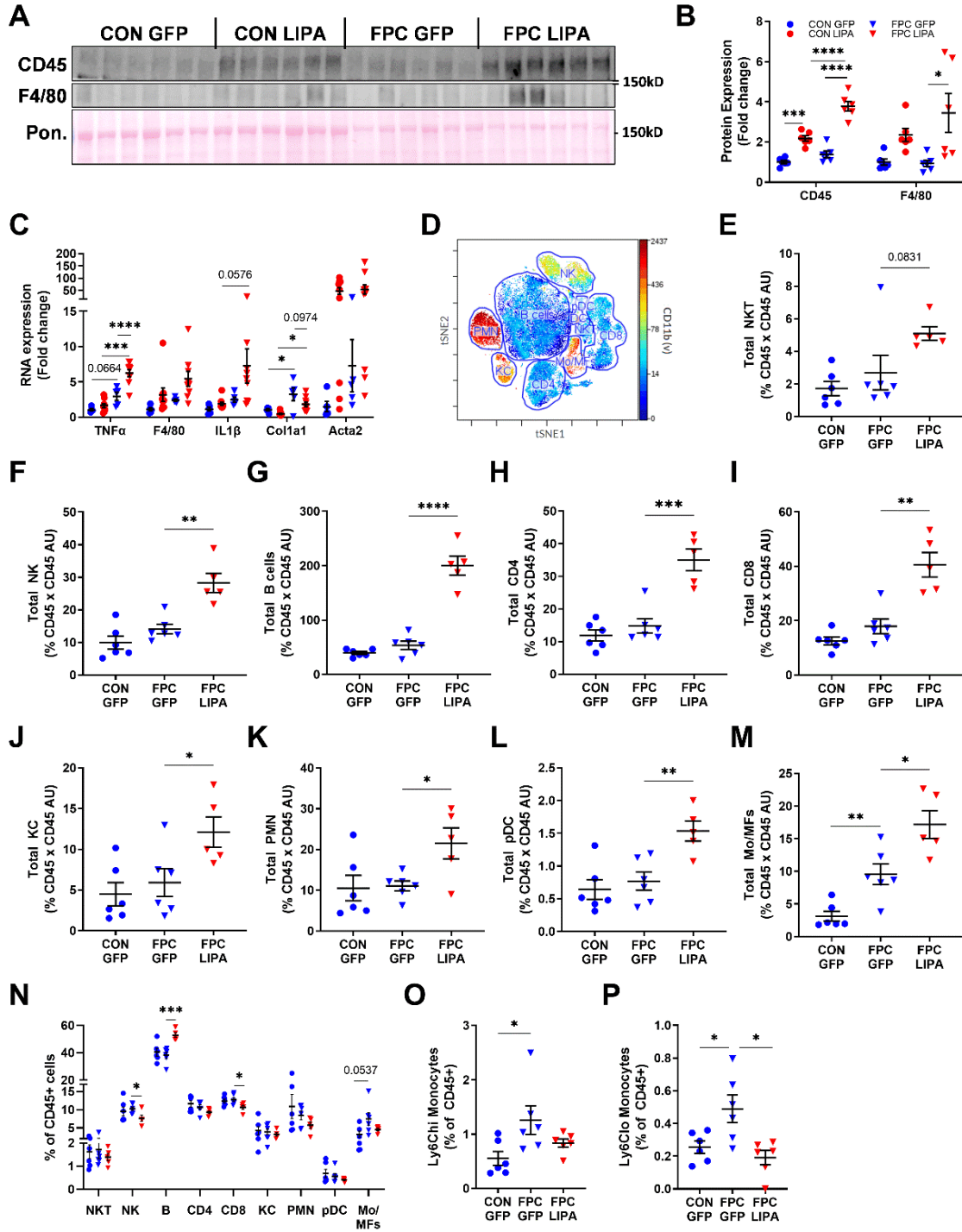
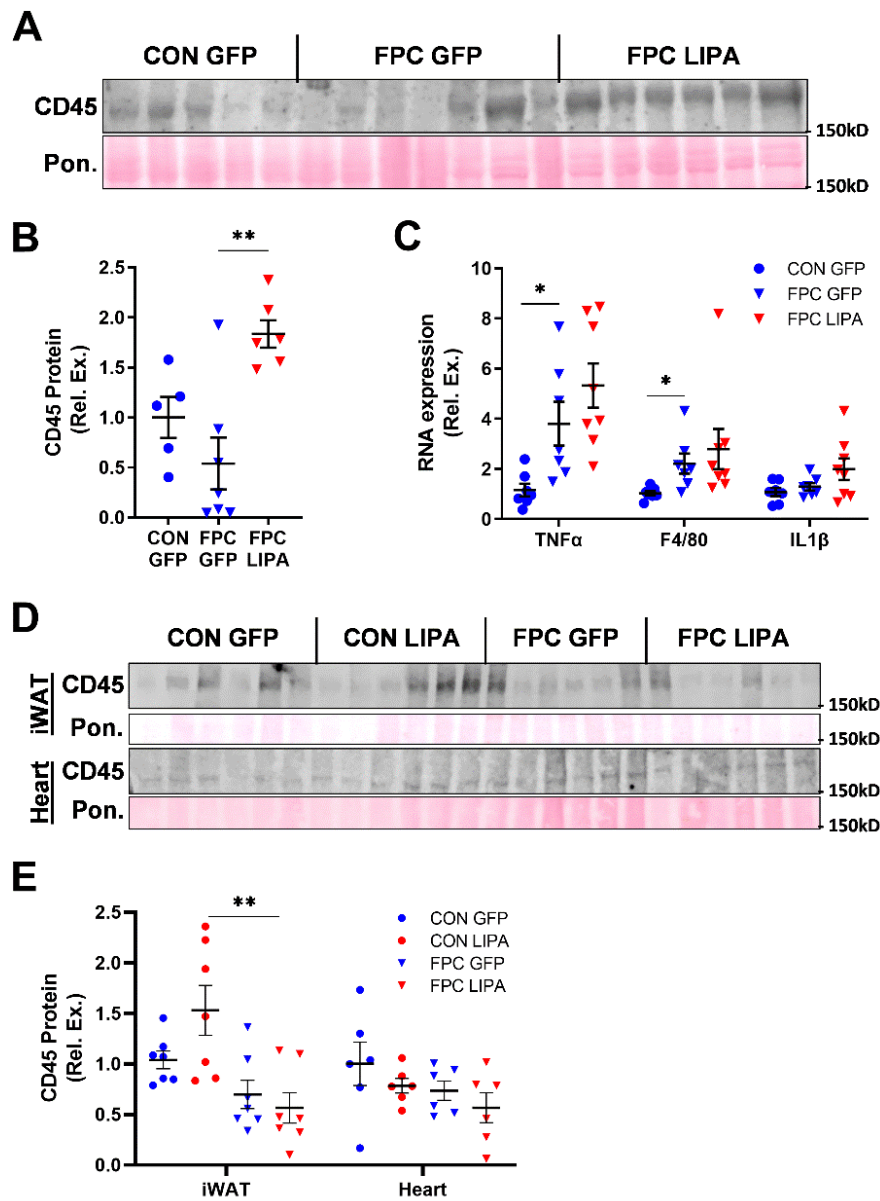


**Figure 3.5: LAL overexpression promoted immune cell infiltration and inflammation.**

(A) Westerns for immune markers in hepatic protein lysates and (B) quantification. (C) Hepatic RNA levels of immune and fibrotic markers determined by qPCR. (D) Representative plot of immune cell populations measured via CyTOF. Mass cytometry

analyses normalized to CD45 protein levels for (E) NKT cells, (F) NK cells, (G) B cells, (H) CD4+ cells, (I) CD8+ cells, (J) KCs, (K) PMNs, (L) pDC, and (M) Mo/MFs. (N) Immune cell populations as a percent of the total CD45+ cell pool. Ly6Chi (O) and Ly6Clo (P) monocytes as a percentage of the total CD45+ pool. All data shown are from male mice. Statistical comparisons are indicated by horizontal lines and significant values are depicted as \*P < 0.05, \*\*P < 0.01, \*\*\*P < 0.005, \*\*\*\*P < 0.001.



**Supplemental Figure 3.5: Immune measurements in females and systemic infiltration in males.**

(A) Western for CD45 in hepatic protein lysates and (B) quantification. (C) Hepatic RNA levels of immune markers determined by qPCR. (D) Representative western blots and (E) quantification for CD45 expression in iWAT and heart tissue. Data in A-D are from female mice, D-E are male mice. Statistical comparisons are indicated by horizontal lines and significant values are depicted as \*P < 0.05, \*\*P < 0.01, \*\*\*P < 0.005, \*\*\*\*P < 0.001.

*LAL overexpression Drives Autolysosome Accumulation and Lysosomal Lipid Droplets*

As NAFLD is often associated with the disruption of autophagy, we assessed livers for changes in protein markers of autophagy (Figure 3.6A, Supplemental Figure 3.6A).

Upstream signaling was assessed by measuring Ulk1 phosphorylation by mTOR at Ser757, which inhibits the initiation of autophagy. Phospho-Ulk1 trended towards being reduced in the FPC-LIPA group when compared to every other group (Figure 3.6B).

Atg5 and LC3 lipidation were measured as indicators of autophagosome formation and abundance. The FPC diet resulted in a significant increase in Atg5 expression in male mice (Figure 3.6C, Supplemental Figure 3.6B) and LC3II/I ratio in both sexes (Figure 3.6D, Supplemental Figure 3.6C), indicating an increase in the abundance of autophagic machinery. LAL overexpression on the FPC diet significantly increased LC3 lipidation, represented by the LC3II/I ratio, in male mice, whereas female mice trended toward a reduction, suggesting there may be sex-specific differences in autophagy that require further examination. As the FPC diet did not alter upstream activation as measured by phospho-Ulk1, this suggests that autophagy is inhibited at a downstream step, which matches previous studies showing that a high fat diet inhibits autophagic flux<sup>150</sup>.

Here, we also quantified LC3-II alone as an approximation of mature autophagosomes and early autolysosomes and observed that, regardless of dietary conditions, LAL overexpression significantly increases LC3-II expression in male mice (Figure 3.6E). Female mice do not exhibit a difference in LC3-II expression with LAL overexpression (Supplemental Figure 3.6D). The data from male mice suggest that LIPA is either promoting autophagosome formation or inhibiting LC3 removal and breakdown from the autophagosome membrane after lysosomal fusion. However, as we only see a trend in phospho-Ulk1 in the FPC-LIPA group, it seems less likely that LIPA is regulating

autophagosome formation, and more likely that lysosomal lipids are accumulating and stalling autophagy.

To further investigate the impact of LAL overexpression, TEM of male liver samples was performed to identify changes in autophagic machinery (Figure 3.6F). We observed an increase in autophagosomes in the CON-LIPA group compared to the CON-GFP group, again suggesting that LAL overexpression either drives autophagosome formation or prevents breakdown (Figure 3.6G). Additionally, autophagosomes were largely absent from FPC livers. In both FPC groups, we identified an increase in LD-laden lysosomes, with the FPC-LIPA group containing more (Figure 3.6H). These data suggest that LAL overexpression, despite increasing LAL enzymatic activity, negatively impacts lysosomal lipid degradation especially under FPC feeding conditions.

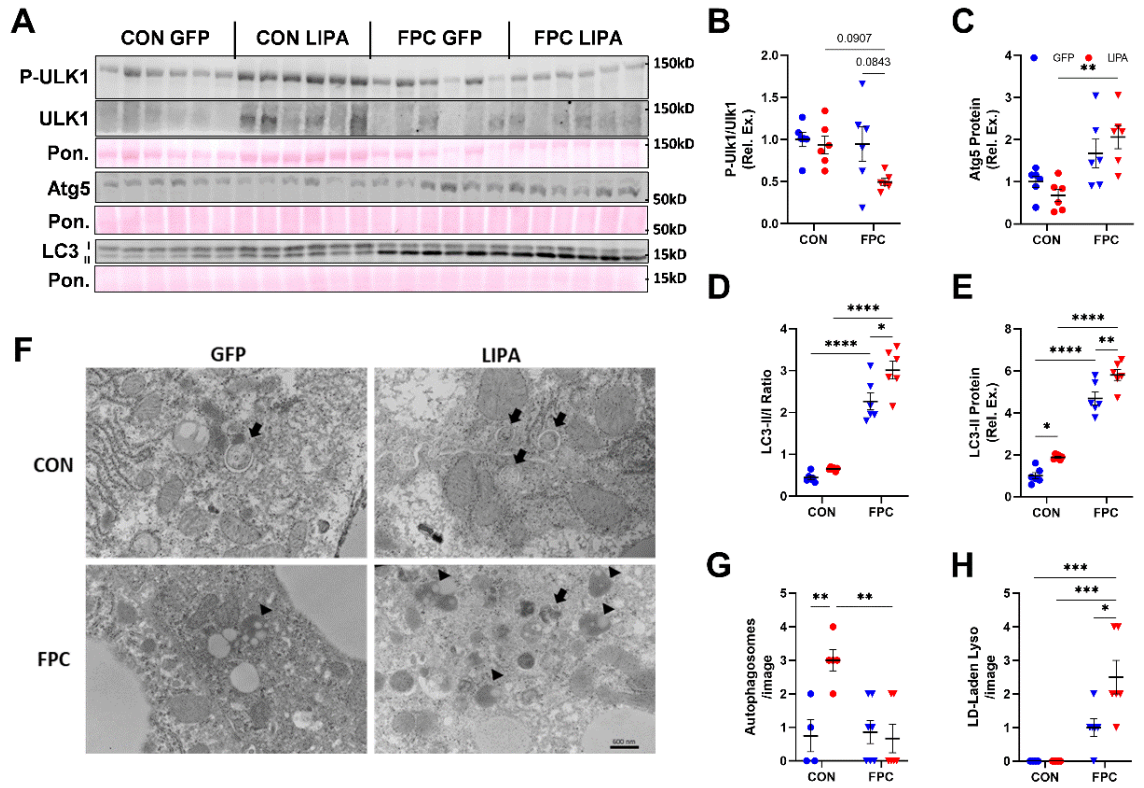
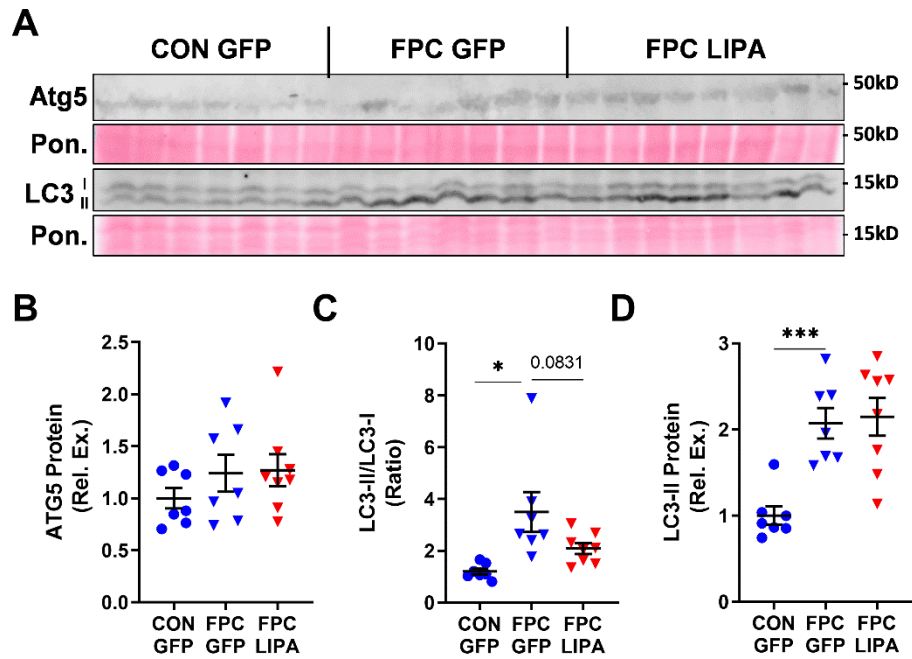


**Figure 3.6: LAL overexpression alters autophagosome abundance.**

(A) Western blots probing for phospho (Ser757)-Ulk1, total Ulk1, LC3, and Atg5 expression. (B) Quantification of the fold change in Ulk1 phosphorylation. (C) Quantification of Atg5 expression. LC3 expression quantified as both (D) LC3-II/I ratio and (E) LC3-II expression. (F) Representative TEM images (600 nm scale bar) displaying autophagosomes (arrow) and lipid laden lysosomes (arrowhead). Numbers of (G) autophagosomes and (H) lipid laden lysosomes per image (n=2-3 images/mouse, 3 mice/group). All data shown are from male mice. Statistical comparisons are indicated by horizontal lines and significant values are depicted as \*P < 0.05, \*\*P < 0.01, \*\*\*P < 0.005, \*\*\*\*P < 0.001.



**Supplemental Figure 3.6: Autophagic measurements in females.**

(A) Autophagic proteins measured via Western blot. (B) Quantified Atg5 expression. LC3 expression quantified as both (C) LC3-II/I ratio and (D) LC3-II. All data shown are from female mice. Statistical comparisons are indicated by horizontal lines and significant values are depicted as \* $P < 0.05$ , \*\* $P < 0.01$ , \*\*\* $P < 0.005$ , \*\*\*\* $P < 0.001$ .

## Discussion

In this study, we sought to determine whether the overexpression of LAL attenuated the development of fatty liver disease in mice on a Western diet. However, LAL overexpression did not prevent the accumulation of hepatic TAG or cholesterol due to the FPC diet, although LAL alone drove changes in LD size and the composition of CE populations. This was surprising as the importance of lysosomal derived sterols in regulating cholesterol homeostasis and hepatic cholesterol levels has previously been established, although the involvement of SREBP2 in this system is controversial<sup>78,99</sup>. However, these studies were based on loss of function, in contrast to the overexpression model used in the current study. Previous research has shown that SREBP2 regulation is activated when ER cholesterol dips below 5% of the total lipid content<sup>40</sup>. Thus, it is possible that the control GFP groups would not be below this threshold, so overexpressing LAL would not make a difference in SREBP2 activation.

Unexpectedly, the overexpression of LAL alone increases autophagosome and lysosomal accumulation to some degree. However, this increase was not associated with reduced hepatomegaly and lipid accumulation in the liver, suggesting that despite the increases in autophagic measures, promoting LAL expression is not sufficient to prevent NAFLD. The reduced number of small LDs coupled with the increase in autophagic measures further supports the assertion that lipophagic degradation preferentially targets small LDs<sup>63</sup>. The mechanism by which LAL overexpression alters autophagy remains to be elucidated. Previous studies have shown that rescuing lysosomal pH, which was increased with steatosis, restored autophagy flux<sup>151</sup>. This leads us to question whether therapies aimed at restoring lysosomal pH may be more viable than enhancing LAL abundance or activity.

The alterations in PUFA and MUFA content of CE suggest that LAL overexpression preferentially changes CE composition, especially when compared to the lack of changes seen in the TAG pool. It remains unclear whether there is a change in synthesis or breakdown that is altering the CE pool. There is no evidence suggesting that the process by which LDs are engulfed by autophagosomes or lysosomes is a selective process. LAL enzymatic selectivity for different substrates has only been biochemically using a fluorescent assay, although no FA longer than oleate was used<sup>152</sup>. As such, we cannot rule out that LAL has a specific preference for degrading CEs containing saturated FAs. It is worth noting that the changes resulting from LAL overexpression shift the CE pool to resemble more closely that of mice on the FPC diet. However, the CE pool is much smaller than the TAG pool, so it is difficult to establish whether these changes hold biological significance.

While the total amount of all immune cells was increased on the FPC diet with LAL expression, B cells showed one of the highest increases in response to LAL overexpression. While the development of hepatic inflammation during NAFLD development and progression involves numerous immune and parenchymal cell types, B cells are becoming increasingly recognized for their role in NAFLD-induced inflammation<sup>134</sup>. In addition to a general increase in immune cells likely promoting inflammation, LAL overexpression also reduced pro-resolution Ly6Clo monocytes, which may have further contributed to the state of elevated hepatic inflammation. These changes in hepatic immune cells mirror the robust increase in numerous proinflammatory pathways revealed from the RNAseq analysis, which reinforces that LAL overexpression promotes an inflammatory phenotype.

Our data strongly indicate that LAL overexpression drives hepatic inflammation, however, we have not identified a specific mechanism at work. Previous studies have shown that disruption of hepatocyte LAL expression drives immune infiltration as a result of excess cholesterol<sup>99</sup>, and that the expression of LAL in macrophages<sup>153</sup> or hepatocytes<sup>122</sup> in *Lipa* deficient mice reduces this inflammation. As hepatic cholesterol levels do not change with LAL overexpression, we do not think that cholesterol accumulation is responsible for the observed inflammation. However, as we measured total hepatic cholesterol, our data does not rule out the possibility of localized or cell type specific fluctuations in cholesterol driving the observed inflammation.

Overall, we have shown that hepatic LAL overexpression is unable to prevent the development of NAFLD on a Western diet, providing evidence against using recombinant LAL as a potential treatment for NAFLD. We also show that overexpression drives inflammation and promotes a large influx of immune cells into the liver. This is contrary to overexpression of LIPA in adipose tissue which showed reduced inflammation and no changes in autophagy<sup>128</sup> suggesting that the liver may be particularly sensitive to alterations of lysosomal lipid degradation and signaling.

### **Data availability**

RNAseq data is available in the NCBI GEO database (GSE180377). This article contains supplemental data.

### **Acknowledgements**

The authors thank the University of Minnesota Research Animal Facility staff for animal care, Colleen Forster for her assistance with histology preparation, the University of Minnesota Genomics Core for performing RNA sequencing, the University of Minnesota

Informatics Institute (Dr. Juan Abrahante) for RNAseq analysis, and the University of Minnesota University Imaging Centers (Dr. Gail Celio, SCR\_020997) for EM sample preparation and imaging. All viral vectors used in this study were generated by the University of Minnesota Viral Vector and Cloning Core (Minneapolis, MN). We also thank Mara Mashek for help with viral injections and mouse care.

## CHAPTER FOUR

### Conclusions and Perspectives

Michael Lopresti wrote this chapter in its entirety

Upwards of 25% of the American population has non-alcoholic fatty liver disease (NAFLD). Without treatment, lipid metabolism becomes further dysregulated, and the accumulation of cholesterol and hepatic inflammation can result in non-alcoholic steatohepatitis (NASH), a stepping stone to cirrhosis and hepatocellular carcinoma. Ultimately, this can result in the need for liver transplantation. As no specific treatment has been identified for NAFLD, there has been a lot of research into hepatic lipid breakdown and the progression of NASH. Lipophagy is known to play a key role in the breakdown of hepatic lipid droplets and has increasingly been examined as a potential therapeutic target. While the molecular mechanisms regulating lipid droplet (LD) engulfment by lysosomes and autophagosomes are still undetermined, the lysosomal degradation of lipids is well characterized.

There is only one identified lipase in the lysosome: lysosomal acid lipase (LAL). As LAL breaks down all triacylglycerol (TAG) and cholesteryl ester (CE) that enter the lysosome, it plays a key role in both lipophagy and low-density lipoprotein (LDL) degradation. Disruptions in autophagic flux and lysosome function have previously been connected to the progression of NAFLD and the accumulation of lipid<sup>154,155</sup>. This disruption results in the blockage of lysosomal lipid degradation and may initiate the excessive cholesterol synthesis associated with NASH progression. The increase in hepatic cholesterol goes hand in hand with rising inflammation and often exacerbate each other. The cholesterol and lipid released from dying hepatocytes are endocytosed by infiltrating macrophages and can drive further inflammation by disrupting immune function.

As the key enzymatic step in lysosomal CE breakdown, LAL plays a vital role in hepatocytes to regulate cholesterol levels as LDL is absorbed. Previous work has extensively characterized the regulation of SREBP2 (sterol regulatory element binding

protein 2) as a result of NPC (Niemann-Pick type C) mutations<sup>78</sup>, and here we provide complementary studies confirming that the lysosomal cholesterol pool is a key source of hydroxycholesterols to regulate SREBP2. In metabolically healthy hepatocytes, this lysosomal cholesterol is derived from LDL uptake and degradation. LAL ablation and inhibition drive SREBP2 activation and cholesterol synthesis by modulating oxysterols produced by LDL degradation.

Notably, endogenous CE stored in the LD does not appear to regulate SREBP2 under conditions of LDL deficiency. This could be a result of the low CE:TAG ratio present in non-steroidogenic cell populations like hepatocytes<sup>156</sup>. Even with lipophagic breakdown of LDs when LDL is absent, there doesn't appear to be enough cholesterol released to modulate SREBP2 activity. On the other hand, hepatocytes with a higher CE:TAG ratio, like those present in a NASH liver, are likely unable to properly hydrolyze the CE and TAG as a result of increased lysosomal pH that accompanies lipid accumulation<sup>157,158</sup>. As such, the LD pool of CE is unlikely to play a major regulatory role in maintaining cellular cholesterol, though this requires further confirmation.

The disruption in SREBP2 activation we observed with LAL inhibition was affected by alterations in the insulin signaling pathway, suggesting that mTOR may be driving SREBP2 under these conditions. While the regulation of mTORC1 (molecular target of rapamycin complex 1) by lysosomal cholesterol has previously been shown, these experiments utilize MCD ( $\beta$ -methylcyclodextrin) to deplete cells of cholesterol<sup>32</sup>. Other work has indicated that MCD has numerous effects on cells including the direct activation of AMPK (AMP kinase), which may provide an alternate mechanism for changes in mTORC1 activity<sup>117</sup>. In our experiments with LAL KD or inhibition, we saw no effect of disrupted lysosomal cholesterol metabolism on mTOR. This could indicate that

the lysosomal cholesterol sensor is able to sense increases in CE, or that the impact of lysosomal cholesterol on mTOR activity was overstated.

Given the central role LAL plays in the events that regulate the development of NAFLD, namely lysosomal dysfunction and cholesterol synthesis, we expected the overexpression of LAL to slow NAFLD progression. LAL overexpression didn't reduce hepatic lipid or cholesterol synthesis, instead resulting in increased hepatic inflammation. While we did see signs of increased autophagic induction, the lack of lipid reduction and accumulation of lipid laden lysosomes suggest that lysosomal function was not restored. This suggests that the limiting factor isn't LAL itself, rather that the lipid filled lysosomes blunt the LAL enzymatic activity. This indicates that increasing LAL isn't a viable treatment for the prevention of fatty liver disease, at least not via a hepatic overexpression. The accumulation of lipid in lysosomes has been shown to raise pH and prevent proper lysosome function<sup>123,157-159</sup>. Previous work shows that nanoparticle mediated reacidification of the lysosomes restores flux<sup>151</sup>, which may be a more effective therapeutic target to restore autophagic flux.

In recent months, other groups have also examined the potential for LAL overexpression to prevent fat accumulation and inflammation, with drastically different findings than ours. The overexpression of LAL in adipose tissue in mice on a high fat diet resulted in reduced serum cholesterol and TAG and decreased fat mass. White adipose tissue showed reduced inflammatory markers. Strikingly, brown adipose tissue alone showed reduced HMG-CoA reductase and LDL receptor expression<sup>128</sup>. These results suggest a much more favorable outcome with adipose LAL overexpression, and clearly demonstrate how different the functions of adipose tissue and liver are.

Another study examined hepatic LAL overexpression in ApoE (apolipoprotein E) KO mice, an atherosclerotic mouse model<sup>160</sup>. As with the adipose tissue overexpression, this resulted in decreased circulating cholesterol and TAG. Notably, this hepatic overexpression reduced inflammation, counter to our data, although the only measure we had common was the expression of TNF $\alpha$  (tumor necrosis factor  $\alpha$ ) mRNA. Similar to our results, increases were seen in the expression of autophagic proteins. Of concern when comparing models is that a lentiviral system was used for overexpression, and the authors did not demonstrate hepatic specificity. Additionally, ApoE KO mice exhibit an extreme cholesterol accumulation phenotype, with atherosclerosis occurring within a few months of birth, and with increased systemic inflammation. This severe whole-body phenotype may outweigh the more subtle effects of hepatic LAL overexpression, resulting in the differences between our studies. Despite these concerns, the differences between our study and these regarding the effect on inflammation are notable and require further research.

The accumulation of immune cells in the liver resulting from hepatocyte specific LAL overexpression was unexpected. Inflammation driven by high hepatic cholesterol or FAs was expected, but no differences were observed in total liver cholesterol or any lipid species. As no changes were seen, the culprit driving the inflammation mice overexpressing LAL was not identified. There could be localized changes in cholesterol that are driving this that we are unable to measure, though this would need to be accompanied by an increase in re-esterification as total levels were unchanged. The blockage of lysosomal degradation could have reduced the production of an unmeasured lysosomal metabolite essential for keeping the immune system at bay. The overexpression of LAL likely resulted in higher extracellular LAL in the liver due to lysosomal exocytosis. High extracellular LAL could be a signal in and of itself to prompt

inflammation. A key step in determining this mechanism would be to identify what cell types are producing inflammatory signals. As there is no obvious lead, the answers to the mechanism at work would benefit from single cell analyses of RNA or a comprehensive lipidomics panel on hepatic tissue.

In conclusion, LAL plays an essential role in the degradation of hepatic lipids and the regulation of whole-body lipid metabolism. While this work did not identify LAL overexpression as a viable therapeutic, it showed a previously unidentified link between hepatic LAL and immune infiltration. As inflammation is a key player in the progression of liver disease, the identification and prevention of inflammatory pathways is essential, and this work reveals a previously unidentified mechanism for recruiting immune cells to the liver. Our data shows that restoring LAL expression does not alleviate steatosis in the face of lysosomal dysfunction, leading us to suggest restoring lysosomal pH as a next step in developing a specific treatment to mitigate NAFLD progression.

## Bibliography

1. Younossi, Z. M. *et al.* Global epidemiology of nonalcoholic fatty liver disease—Meta-analytic assessment of prevalence, incidence, and outcomes. *Hepatology* **64**, 73–84 (2016).
2. Younossi, Z. M. *et al.* The economic and clinical burden of nonalcoholic fatty liver disease in the United States and Europe. *Hepatology* **64**, 1577–1586 (2016).
3. Ding, C. *et al.* A Cell-type-resolved Liver Proteome. *Mol. Cell. Proteomics* **15**, 3190–3202 (2016).
4. Smith, G. I. *et al.* Insulin resistance drives hepatic de novo lipogenesis in nonalcoholic fatty liver disease. *J. Clin. Invest.* **130**, 1453–1460 (2020).
5. Wilfling, F. *et al.* Triacylglycerol synthesis enzymes mediate lipid droplet growth by relocalizing from the ER to lipid droplets. *Dev. Cell* **24**, 384–399 (2013).
6. Xu, W. *et al.* Differential Roles of Cell Death-inducing DNA Fragmentation Factor- $\alpha$ -like Effector (CIDE) Proteins in Promoting Lipid Droplet Fusion and Growth in Subpopulations of Hepatocytes. *J. Biol. Chem.* **291**, 4282–4293 (2016).
7. Itabe, H., Yamaguchi, T., Nimura, S. & Sasabe, N. Perilipins: a diversity of intracellular lipid droplet proteins. *Lipids Health Dis.* **16**, 83 (2017).
8. Tsai, T. H. *et al.* The constitutive lipid droplet protein PLIN2 regulates autophagy in liver. *Autophagy* **13**, 1130–1144 (2017).
9. Wang, C. *et al.* Perilipin 5 improves hepatic lipotoxicity by inhibiting lipolysis. *Hepatology* **61**, 870–882 (2015).
10. Sathyanarayan, A., Mashek, M. T. & Mashek, D. G. ATGL Promotes Autophagy/Lipophagy via SIRT1 to Control Hepatic Lipid Droplet Catabolism. *Cell Rep.* **19**, 1–9 (2017).
11. Najt, C. P. *et al.* Lipid Droplet-Derived Monounsaturated Fatty Acids Traffic via PLIN5 to Allosterically Activate SIRT1. *Mol. Cell* **77**, 810-824.e8 (2020).
12. Zhang, E. *et al.* Hepatic PLIN5 signals via SIRT1 to promote autophagy and prevent inflammation during fasting. *J. Lipid Res.* **61**, 338–350 (2020).
13. Li, X. *et al.* Opposing roles of cell death-inducing DFF45-like effector B and perilipin 2 in controlling hepatic VLDL lipidation. *J. Lipid Res.* **53**, 1877–1889 (2012).
14. de Faria, E., Fong, L. G., Komaromy, M. & Cooper, A. D. Relative roles of the LDL receptor, the LDL receptor-like protein, and hepatic lipase in chylomicron remnant removal by the liver. *J. Lipid Res.* **37**, 197–209 (1996).

15. Elshourbagy, N. A., Meyers, H. V & Abdel-Meguid, S. S. Cholesterol: the good, the bad, and the ugly - therapeutic targets for the treatment of dyslipidemia. *Med. Princ. Pract. Int. J. Kuwait Univ. Heal. Sci. Cent.* **23**, 99–111 (2014).
16. Dietschy, J. M. Regulation of cholesterol metabolism in man and in other species. *Klin. Wochenschr.* **62**, 338–345 (1984).
17. Gowans, G. J., Hawley, S. A., Ross, F. A. & Hardie, D. G. AMP is a true physiological regulator of AMP-activated protein kinase by both allosteric activation and enhancing net phosphorylation. *Cell Metab.* **18**, 556–566 (2013).
18. Carling, D., Zammit, V. A. & Hardie, D. G. A common bicyclic protein kinase cascade inactivates the regulatory enzymes of fatty acid and cholesterol biosynthesis. *FEBS Lett.* **223**, 217–222 (1987).
19. Marsin, A.-S. *et al.* Phosphorylation and activation of heart PFK-2 by AMPK has a role in the stimulation of glycolysis during ischaemia. *Curr. Biol.* **10**, 1247–1255 (2000).
20. Wu, N. *et al.* AMPK-dependent degradation of TXNIP upon energy stress leads to enhanced glucose uptake via GLUT1. *Mol. Cell* **49**, 1167–1175 (2013).
21. Toyama, E. Q. *et al.* AMP-activated protein kinase mediates mitochondrial fission in response to energy stress. *Science (80-. )*. **351**, 275–281 (2016).
22. Kim, J., Kundu, M., Viollet, B. & Guan, K.-L. AMPK and mTOR regulate autophagy through direct phosphorylation of Ulk1. *Nat. Cell Biol.* **13**, 132–141 (2011).
23. Gwinn, D. M. *et al.* AMPK phosphorylation of raptor mediates a metabolic checkpoint. *Mol. Cell* **30**, 214–226 (2008).
24. Inoki, K., Zhu, T. & Guan, K.-L. TSC2 Mediates Cellular Energy Response to Control Cell Growth and Survival. *Cell* **115**, 577–590 (2003).
25. Condon, K. J. & Sabatini, D. M. Nutrient regulation of mTORC1 at a glance. *J. Cell Sci.* **132**, (2019).
26. Sancak, Y. *et al.* Ragulator-Rag complex targets mTORC1 to the lysosomal surface and is necessary for its activation by amino acids. *Cell* **141**, 290–303 (2010).
27. Sancak, Y. *et al.* The Rag GTPases bind raptor and mediate amino acid signaling to mTORC1. *Science* **320**, 1496–1501 (2008).
28. Kim, E., Goraksha-Hicks, P., Li, L., Neufeld, T. P. & Guan, K.-L. Regulation of TORC1 by Rag GTPases in nutrient response. *Nat. Cell Biol.* **10**, 935–945 (2008).

29. Menon, S. *et al.* Spatial control of the TSC complex integrates insulin and nutrient regulation of mTORC1 at the lysosome. *Cell* **156**, 771–785 (2014).
30. Potter, C. J., Pedraza, L. G. & Xu, T. Akt regulates growth by directly phosphorylating Tsc2. *Nat. Cell Biol.* **4**, 658–665 (2002).
31. Inoki, K., Li, Y., Zhu, T., Wu, J. & Guan, K.-L. TSC2 is phosphorylated and inhibited by Akt and suppresses mTOR signalling. *Nat. Cell Biol.* **4**, 648–657 (2002).
32. Castellano, B. M. *et al.* Lysosomal cholesterol activates mTORC1 via an SLC38A9-Niemann-Pick C1 signaling complex. *Science (80-. )*. **355**, 1306–1311 (2017).
33. Wang, S. *et al.* Lysosomal amino acid transporter SLC38A9 signals arginine sufficiency to mTORC1. *Science (80-. )*. **347**, 188–194 (2015).
34. Holz, M. K., Ballif, B. A., Gygi, S. P. & Blenis, J. mTOR and S6K1 Mediate Assembly of the Translation Preinitiation Complex through Dynamic Protein Interchange and Ordered Phosphorylation Events. *Cell* **123**, 569–580 (2005).
35. Kim, D.-H. *et al.* mTOR interacts with raptor to form a nutrient-sensitive complex that signals to the cell growth machinery. *Cell* **110**, 163–175 (2002).
36. Cunningham, J. T. *et al.* mTOR controls mitochondrial oxidative function through a YY1–PGC-1 $\alpha$  transcriptional complex. *Nature* **450**, 736–740 (2007).
37. Porstmann, T. *et al.* SREBP activity is regulated by mTORC1 and contributes to Akt-dependent cell growth. *Cell Metab.* **8**, 224–236 (2008).
38. Shimomura, I., Shimano, H., Horton, J. D., Goldstein, J. L. & Brown, M. S. Differential expression of exons 1a and 1c in mRNAs for sterol regulatory element binding protein-1 in human and mouse organs and cultured cells. *J. Clin. Invest.* **99**, 838–845 (1997).
39. Sato, R. *et al.* Assignment of the membrane attachment, DNA binding, and transcriptional activation domains of sterol regulatory element-binding protein-1 (SREBP-1). *J. Biol. Chem.* **269**, 17267–17273 (1994).
40. Radhakrishnan, A., Goldstein, J. L., McDonald, J. G. & Brown, M. S. Switch-like control of SREBP-2 transport triggered by small changes in ER cholesterol: a delicate balance. *Cell Metab.* **8**, 512–521 (2008).
41. Adams, C. M. *et al.* Cholesterol and 25-hydroxycholesterol inhibit activation of SREBPs by different mechanisms, both involving SCAP and Insigs. *J. Biol. Chem.* **279**, 52772–52780 (2004).

42. Shimomura, I., Shimano, H., Korn, B. S., Bashmakov, Y. & Horton, J. D. Nuclear sterol regulatory element-binding proteins activate genes responsible for the entire program of unsaturated fatty acid biosynthesis in transgenic mouse liver. *J. Biol. Chem.* **273**, 35299–35306 (1998).
43. Moon, Y. A., Shah, N. A., Mohapatra, S., Warrington, J. A. & Horton, J. D. Identification of a mammalian long chain fatty acyl elongase regulated by sterol regulatory element-binding proteins. *J. Biol. Chem.* **276**, 45358–45366 (2001).
44. Lee, J. N., Zhang, X., Feramisco, J. D., Gong, Y. & Ye, J. Unsaturated fatty acids inhibit proteasomal degradation of Insig-1 at a postubiquitination step. *J. Biol. Chem.* **283**, 33772–33783 (2008).
45. Li, S., Brown, M. S. & Goldstein, J. L. Bifurcation of insulin signaling pathway in rat liver: mTORC1 required for stimulation of lipogenesis, but not inhibition of gluconeogenesis. *Proc. Natl. Acad. Sci. U. S. A.* **107**, 3441–3446 (2010).
46. Owen, J. L. *et al.* Insulin stimulation of SREBP-1c processing in transgenic rat hepatocytes requires p70 S6-kinase. *Proc. Natl. Acad. Sci. U. S. A.* **109**, 16184–16189 (2012).
47. Edwards, P. A., Tabor, D., Kast, H. R. & Venkateswaran, A. Regulation of gene expression by SREBP and SCAP. *Biochim. Biophys. Acta* **1529**, 103–113 (2000).
48. Engelking, L. J. *et al.* Schoenheimer effect explained--feedback regulation of cholesterol synthesis in mice mediated by Insig proteins. *J. Clin. Invest.* **115**, 2489–2498 (2005).
49. Song, B.-L., Javitt, N. B. & DeBose-Boyd, R. A. Insig-mediated degradation of HMG CoA reductase stimulated by lanosterol, an intermediate in the synthesis of cholesterol. *Cell Metab.* **1**, 179–189 (2005).
50. Jensen, M. D., Haymond, M. W., Gerich, J. E., Cryer, P. E. & Miles, J. M. Lipolysis during fasting. Decreased suppression by insulin and increased stimulation by epinephrine. *J. Clin. Invest.* **79**, 207–213 (1987).
51. Chakrabarti, P., English, T., Shi, J., Smas, C. M. & Kandror, K. V. Mammalian target of rapamycin complex 1 suppresses lipolysis, stimulates lipogenesis, and promotes fat storage. *Diabetes* **59**, 775–781 (2010).
52. Lee, I. H. *et al.* A role for the NAD-dependent deacetylase Sirt1 in the regulation of autophagy. *Proc. Natl. Acad. Sci.* **105**, 3374–3379 (2008).
53. Jung, C. H. *et al.* ULK-Atg13-FIP200 complexes mediate mTOR signaling to the autophagy machinery. *Mol. Biol. Cell* **20**, 1992–2003 (2009).

54. Singh, R. *et al.* Autophagy regulates lipid metabolism. *Nature* **458**, 1131–1135 (2009).
55. Schroeder, B. *et al.* The small GTPase Rab7 as a central regulator of hepatocellular lipophagy. *Hepatology* **61**, 1896–1907 (2015).
56. Ma, S. Y. *et al.* Disruption of Plin5 degradation by CMA causes lipid homeostasis imbalance in NAFLD. *Liver Int. Off. J. Int. Assoc. Study Liver* **40**, 2427–2438 (2020).
57. Kaushik, S. & Cuervo, A. M. Degradation of lipid droplet-associated proteins by chaperone-mediated autophagy facilitates lipolysis. *Nat. Cell Biol.* **17**, 759–770 (2015).
58. Kaushik, S. & Cuervo, A. M. Degradation of lipid droplet-associated proteins by chaperone-mediated autophagy facilitates lipolysis. *Nat. Cell Biol.* **17**, 759–770 (2015).
59. Terlecky, S. R., Chiang, H. L., Olson, T. S. & Dice, J. F. Protein and peptide binding and stimulation of in vitro lysosomal proteolysis by the 73-kDa heat shock cognate protein. *J. Biol. Chem.* **267**, 9202–9209 (1992).
60. Cuervo, A. M. & Dice, J. F. A receptor for the selective uptake and degradation of proteins by lysosomes. *Science* **273**, 501–503 (1996).
61. Cuervo, A. M. & Dice, J. F. Unique properties of lamp2a compared to other lamp2 isoforms. *J. Cell Sci.* **113 Pt 24**, 4441–4450 (2000).
62. Goodman, J. M. The importance of microlipophagy in liver. *Proc. Natl. Acad. Sci. U. S. A.* **118**, (2021).
63. Schott, M. B. *et al.* Lipid droplet size directs lipolysis and lipophagy catabolism in hepatocytes. *J. Cell Biol.* **218**, 3320–3335 (2019).
64. Ganley, I. G. *et al.* ULK1.ATG13.FIP200 complex mediates mTOR signaling and is essential for autophagy. *J. Biol. Chem.* **284**, 12297–12305 (2009).
65. Itakura, E. & Mizushima, N. Characterization of autophagosome formation site by a hierarchical analysis of mammalian Atg proteins. *Autophagy* **6**, 764–776 (2010).
66. Obara, K., Sekito, T. & Ohsumi, Y. Assortment of phosphatidylinositol 3-kinase complexes--Atg14p directs association of complex I to the pre-autophagosomal structure in *Saccharomyces cerevisiae*. *Mol. Biol. Cell* **17**, 1527–1539 (2006).
67. Russell, R. C. *et al.* ULK1 induces autophagy by phosphorylating Beclin-1 and activating VPS34 lipid kinase. *Nat. Cell Biol.* **15**, 741–750 (2013).
68. Hemelaar, J., Lelyveld, V. S., Kessler, B. M. & Ploegh, H. L. A single protease,

- Apg4B, is specific for the autophagy-related ubiquitin-like proteins GATE-16, MAP1-LC3, GABARAP, and Apg8L. *J. Biol. Chem.* **278**, 51841–51850 (2003).
69. Sou, Y., Tanida, I., Komatsu, M., Ueno, T. & Kominami, E. Phosphatidylserine in addition to phosphatidylethanolamine is an in vitro target of the mammalian Atg8 modifiers, LC3, GABARAP, and GATE-16. *J. Biol. Chem.* **281**, 3017–3024 (2006).
  70. Lőrincz, P. & Juhász, G. Autophagosome-Lysosome Fusion. *J. Mol. Biol.* **432**, 2462–2482 (2020).
  71. Warner, T. G., Dambach, L. M., Shin, J. H. & O'Brien, J. S. Purification of the lysosomal acid lipase from human liver and its role in lysosomal lipid hydrolysis. *J. Biol. Chem.* **256**, 2952–2957 (1981).
  72. Goldstein, J. L., Dana, S. E., Faust, J. R., Beaudet, A. L. & Brown, M. S. Role of lysosomal acid lipase in the metabolism of plasma low density lipoprotein. Observations in cultured fibroblasts from a patient with cholesteryl ester storage disease. *J. Biol. Chem.* **250**, 8487–8495 (1975).
  73. Cui, W. *et al.* Lipophagy-derived fatty acids undergo extracellular efflux via lysosomal exocytosis. *Autophagy* **17**, 690–705 (2021).
  74. Infante, R. E. *et al.* NPC2 facilitates bidirectional transfer of cholesterol between NPC1 and lipid bilayers, a step in cholesterol egress from lysosomes. *Proc. Natl. Acad. Sci.* **105**, 15287 LP – 15292 (2008).
  75. Pfeffer, S. R. NPC intracellular cholesterol transporter 1 (NPC1)-mediated cholesterol export from lysosomes. *J. Biol. Chem.* **294**, 1706–1709 (2019).
  76. Jelinek, D. *et al.* Physiological and coordinate downregulation of the NPC1 and NPC2 genes are associated with the sequestration of LDL-derived cholesterol within endocytic compartments. *J. Cell. Biochem.* **108**, 1102–1116 (2009).
  77. Ramirez, C. M. *et al.* Quantitative role of LAL, NPC2, and NPC1 in lysosomal cholesterol processing defined by genetic and pharmacological manipulations. *J. Lipid Res.* **52**, 688–698 (2011).
  78. Frolov, A. *et al.* NPC1 and NPC2 regulate cellular cholesterol homeostasis through generation of low density lipoprotein cholesterol-derived oxysterols. *J. Biol. Chem.* **278**, 25517–25 (2003).
  79. Liscum, L. & Faust, J. R. Low density lipoprotein (LDL)-mediated suppression of cholesterol synthesis and LDL uptake is defective in Niemann-Pick type C fibroblasts. *J. Biol. Chem.* **262**, 17002–17008 (1987).
  80. Feltes, M., Gale, S. E., Moores, S., Ory, D. S. & Schaffer, J. E. Monitoring the

- itinerary of lysosomal cholesterol in Niemann-Pick Type C1-deficient cells after cyclodextrin treatment. *J. Lipid Res.* **61**, 403–412 (2020).
81. Roussel, A. *et al.* Crystal structure of human gastric lipase and model of lysosomal acid lipase, two lipolytic enzymes of medical interest. *J. Biol. Chem.* **274**, 16995–17002 (1999).
  82. Rajamohan, F. *et al.* Crystal structure of human lysosomal acid lipase and its implications in cholesteryl ester storage disease. *J. Lipid Res.* **61**, 1192–1202 (2020).
  83. Lohse, P., Chahrokh-Zadeh, S. & Seidel, D. Human lysosomal acid lipase/cholesteryl ester hydrolase and human gastric lipase: identification of the catalytically active serine, aspartic acid, and histidine residues. *J. Lipid Res.* **38**, 892–903 (1997).
  84. Zschenker, O., Bähr, C., Hess, U.-F. & Ameis, D. Systematic mutagenesis of potential glycosylation sites of lysosomal acid lipase. *J. Biochem.* **137**, 387–394 (2005).
  85. Strom, T. B. *et al.* Lysosomal acid lipase does not have a propeptide and should not be considered being a proprotein. *Proteins* (2019) doi:10.1002/prot.25821.
  86. PATRICK, A. D. & LAKE, B. D. Deficiency of an Acid Lipase in Wolman's Disease. *Nature* **222**, 1067–1068 (1969).
  87. Pericleous, M., Kelly, C., Wang, T., Livingstone, C. & Ala, A. Wolman's disease and cholesteryl ester storage disorder: the phenotypic spectrum of lysosomal acid lipase deficiency. *Lancet Gastroenterol. Hepatol.* **2**, 670–679 (2017).
  88. Aslanidis, C. *et al.* Genetic and Biochemical Evidence That CESD and Wolman Disease Are Distinguished by Residual Lysosomal Acid Lipase Activity. *Genomics* **33**, 85–93 (1996).
  89. Bowden, K. L. *et al.* Lysosomal acid lipase deficiency impairs regulation of ABCA1 gene and formation of high density lipoproteins in cholesteryl ester storage disease. *J. Biol. Chem.* **286**, 30624–30635 (2011).
  90. Balwani, M. *et al.* Clinical effect and safety profile of recombinant human lysosomal acid lipase in patients with cholesteryl ester storage disease. *Hepatology* **58**, 950–957 (2013).
  91. Valayannopoulos, V. *et al.* Sebelipase alfa over 52 weeks reduces serum transaminases, liver volume and improves serum lipids in patients with lysosomal acid lipase deficiency. *J. Hepatol.* **61**, 1135–1142 (2014).

92. Carter, A., Brackley, S. M., Gao, J. & Mann, J. P. The global prevalence and genetic spectrum of lysosomal acid lipase deficiency: a rare condition that mimics NAFLD. *J. Hepatol.* (2018) doi:S016882781832453X.
93. Saito, S., Ohno, K., Suzuki, T. & Sakuraba, H. Structural bases of Wolman disease and cholesteryl ester storage disease. *Mol. Genet. Metab.* **105**, 244–248 (2012).
94. Vinje, T., Laerdahl, J. K., Bjune, K., Leren, T. P. & Strøm, T. B. Characterization of the mechanisms by which missense mutations in the lysosomal acid lipase gene disrupt enzymatic activity. *Hum. Mol. Genet.* **28**, 3043–3052 (2019).
95. Du, H. *et al.* Lysosomal acid lipase-deficient mice: depletion of white and brown fat, severe hepatosplenomegaly, and shortened life span. *J. Lipid Res.* **42**, 489–500 (2001).
96. Chuang, J.-C., Lopez, A. M. & Turley, S. D. Quantitation of the rates of hepatic and intestinal cholesterol synthesis in lysosomal acid lipase-deficient mice before and during treatment with ezetimibe. *Biochem. Pharmacol.* **135**, 116–125 (2017).
97. Aqul, A. *et al.* Hepatic entrapment of esterified cholesterol drives continual expansion of whole body sterol pool in lysosomal acid lipase-deficient mice. *Am. J. Physiol. Gastrointest. Liver Physiol.* **307**, G836-47 (2014).
98. Pajed, L. *et al.* Hepatocyte-specific deletion of lysosomal acid lipase leads to cholesteryl ester but not triglyceride or retinyl ester accumulation. *J. Biol. Chem.* **294**, 9118–9133 (2019).
99. Leopold, C. *et al.* Hepatocyte-specific lysosomal acid lipase deficiency protects mice from diet-induced obesity but promotes hepatic inflammation. *Biochim. Biophys. Acta - Mol. Cell Biol. Lipids* **1864**, 500–511 (2019).
100. Shteyer, E., Villenchik, R., Mahamid, M., Nator, N. & Safadi, R. Low Serum Lysosomal Acid Lipase Activity Correlates with Advanced Liver Disease. *Int. J. Mol. Sci.* **17**, 312 (2016).
101. Tovoli, F. *et al.* A Relative Deficiency of Lysosomal Acid Lipase Activity Characterizes Non-Alcoholic Fatty Liver Disease. *Int. J. Mol. Sci.* **18**, 1134 (2017).
102. Gomaraschi, M. *et al.* Lipid accumulation impairs lysosomal acid lipase activity in hepatocytes: Evidence in NAFLD patients and cell cultures. *Biochim. Biophys. Acta. Mol. Cell Biol. Lipids* **1864**, 158523 (2019).
103. Carotti, S. *et al.* Lipophagy Impairment Is Associated With Disease Progression in NAFLD. *Front. Physiol.* **11**, 850 (2020).

104. Min, H.-K. *et al.* Increased hepatic synthesis and dysregulation of cholesterol metabolism is associated with the severity of nonalcoholic fatty liver disease. *Cell Metab.* **15**, 665–674 (2012).
105. Ioannou, G. N., Haigh, W. G., Thorning, D. & Savard, C. Hepatic cholesterol crystals and crown-like structures distinguish NASH from simple steatosis. *J. Lipid Res.* **54**, 1326–1334 (2013).
106. Puri, P. *et al.* A lipidomic analysis of nonalcoholic fatty liver disease. *Hepatology* **46**, 1081–1090 (2007).
107. Caballero, F. *et al.* Enhanced free cholesterol, SREBP-2 and StAR expression in human NASH. *J. Hepatol.* **50**, 789–796 (2009).
108. Wouters, K. *et al.* Dietary cholesterol, rather than liver steatosis, leads to hepatic inflammation in hyperlipidemic mouse models of nonalcoholic steatohepatitis. *Hepatology* **48**, 474–486 (2008).
109. Song, Y., Liu, J., Zhao, K., Gao, L. & Zhao, J. Cholesterol-induced toxicity: An integrated view of the role of cholesterol in multiple diseases. *Cell Metab.* (2021) doi:10.1016/j.cmet.2021.09.001.
110. Musso, G., Gambino, R. & Cassader, M. Cholesterol metabolism and the pathogenesis of non-alcoholic steatohepatitis. *Prog. Lipid Res.* **52**, 175–191 (2013).
111. Eid, W. *et al.* mTORC1 activates SREBP-2 by suppressing cholesterol trafficking to lysosomes in mammalian cells. *Proc. Natl. Acad. Sci. U. S. A.* **114**, 7999–8004 (2017).
112. Viaud, M. *et al.* Lysosomal Cholesterol Hydrolysis Couples Efferocytosis to Anti-Inflammatory Oxysterol Production. *Circ. Res.* **122**, 1369–1384 (2018).
113. Davis, O. B. *et al.* NPC1-mTORC1 Signaling Couples Cholesterol Sensing to Organelle Homeostasis and Is a Targetable Pathway in Niemann-Pick Type C. *Dev. Cell* **56**, 260-276.e7 (2021).
114. Folch, J., Lees, M. & Sloane Stanley, G. H. A simple method for the isolation and purification of total lipides from animal tissues. *J. Biol. Chem.* **226**, 497–509 (1957).
115. Nagarajan, S. R. *et al.* Lipid and glucose metabolism in hepatocyte cell lines and primary mouse hepatocytes: a comprehensive resource for in vitro studies of hepatic metabolism. *Am. J. Physiol. Endocrinol. Metab.* **316**, E578–E589 (2019).
116. Ioannou, G. N. *et al.* Cholesterol crystallization within hepatocyte lipid droplets

- and its role in murine NASH. *J. Lipid Res.* **58**, 1067–1079 (2017).
117. Dai, S. *et al.* Methyl- $\beta$ -cyclodextrin restores impaired autophagy flux in Niemann-Pick C1-deficient cells through activation of AMPK. *Autophagy* **13**, 1435–1451 (2017).
  118. Zhao, T., Du, H., Ding, X., Walls, K. & Yan, C. Activation of mTOR pathway in myeloid-derived suppressor cells stimulates cancer cell proliferation and metastasis in *lal(-/-)* mice. *Oncogene* **34**, 1938–1948 (2015).
  119. Schulze, R. J., Sathyanarayan, A. & Mashek, D. G. Breaking fat: The regulation and mechanisms of lipophagy. *Biochim. Biophys. Acta - Mol. Cell Biol. Lipids* **1862**, 1178–1187 (2017).
  120. Martinez-Lopez, N. & Singh, R. Autophagy and Lipid Droplets in the Liver. *Annu. Rev. Nutr.* **35**, 215–237 (2015).
  121. Radović, B. *et al.* Lysosomal acid lipase regulates VLDL synthesis and insulin sensitivity in mice. *Diabetologia* **59**, 1743–1752 (2016).
  122. Du, H., Zhao, T., Ding, X. & Yan, C. Hepatocyte-Specific Expression of Human Lysosome Acid Lipase Corrects Liver Inflammation and Tumor Metastasis in *lal(-/-)* Mice. *Am. J. Pathol.* **185**, 2379–2389 (2015).
  123. Koga, H., Kaushik, S. & Cuervo, A. M. Altered lipid content inhibits autophagic vesicular fusion. *FASEB J. Off. Publ. Fed. Am. Soc. Exp. Biol.* **24**, 3052–3065 (2010).
  124. Yang, L., Li, P., Fu, S., Calay, E. S. & Hotamisligil, G. S. Defective hepatic autophagy in obesity promotes ER stress and causes insulin resistance. *Cell Metab.* **11**, 467–478 (2010).
  125. Wang, X. *et al.* Defective lysosomal clearance of autophagosomes and its clinical implications in nonalcoholic steatohepatitis. *FASEB J. Off. Publ. Fed. Am. Soc. Exp. Biol.* **32**, 37–51 (2018).
  126. Inami, Y. *et al.* Hepatic steatosis inhibits autophagic proteolysis via impairment of autophagosomal acidification and cathepsin expression. *Biochem. Biophys. Res. Commun.* **412**, 618–625 (2011).
  127. Carotti, S. *et al.* An overview of deregulated lipid metabolism in nonalcoholic fatty liver disease with special focus on lysosomal acid lipase. *Am. J. Physiol. Gastrointest. Liver Physiol.* **319**, G469–G480 (2020).
  128. Gamblin, C. *et al.* Lysosomal Acid Lipase Drives Adipocyte Cholesterol Homeostasis and Modulates Lipid Storage in Obesity, Independent of Autophagy.

- Diabetes* **70**, 76–90 (2021).
129. Kanda, T. *et al.* Apoptosis and non-alcoholic fatty liver diseases. *World J. Gastroenterol.* **24**, 2661–2672 (2018).
  130. Rajamaki, K. *et al.* Cholesterol crystals activate the NLRP3 inflammasome in human macrophages: a novel link between cholesterol metabolism and inflammation. *PLoS One* **5**, e11765 (2010).
  131. Leroux, A. *et al.* Toxic lipids stored by Kupffer cells correlates with their pro-inflammatory phenotype at an early stage of steatohepatitis. *J. Hepatol.* **57**, 141–149 (2012).
  132. Remmerie, A. *et al.* Osteopontin Expression Identifies a Subset of Recruited Macrophages Distinct from Kupffer Cells in the Fatty Liver. *Immunity* **53**, 641-657.e14 (2020).
  133. Tran, S. *et al.* Impaired Kupffer Cell Self-Renewal Alters the Liver Response to Lipid Overload during Non-alcoholic Steatohepatitis. *Immunity* **53**, 627-640.e5 (2020).
  134. Barrow, F. *et al.* Microbiota-Driven Activation of Intrahepatic B Cells Aggravates Nonalcoholic Steatohepatitis through Innate and Adaptive Signaling. *Hepatology* (2021) doi:10.1002/hep.31755.
  135. Baeck, C. *et al.* Pharmacological inhibition of the chemokine CCL2 (MCP-1) diminishes liver macrophage infiltration and steatohepatitis in chronic hepatic injury. *Gut* **61**, 416–426 (2012).
  136. Reid, D. T. *et al.* Kupffer Cells Undergo Fundamental Changes during the Development of Experimental NASH and Are Critical in Initiating Liver Damage and Inflammation. *PLoS One* **11**, e0159524 (2016).
  137. Tosello-Tramont, A.-C., Landes, S. G., Nguyen, V., Novobrantseva, T. I. & Hahn, Y. S. Kupffer cells trigger nonalcoholic steatohepatitis development in diet-induced mouse model through tumor necrosis factor-alpha production. *J. Biol. Chem.* **287**, 40161–40172 (2012).
  138. Karlmark, K. R. *et al.* Hepatic recruitment of the inflammatory Gr1+ monocyte subset upon liver injury promotes hepatic fibrosis. *Hepatology* **50**, 261–274 (2009).
  139. Chandler, R. J. *et al.* Liver-directed adeno-associated virus serotype 8 gene transfer rescues a lethal murine model of citrullinemia type 1. *Gene Ther.* **20**, 1188–1191 (2013).

140. Wang, X. *et al.* Hepatocyte TAZ/WWTR1 Promotes Inflammation and Fibrosis in Nonalcoholic Steatohepatitis. *Cell Metab.* **24**, 848–862 (2016).
141. McQuin, C. *et al.* CellProfiler 3.0: Next-generation image processing for biology. *PLoS Biol.* **16**, e2005970 (2018).
142. Abernathy, B. E., Schoenfuss, T. C., Bailey, A. S. & Gallaher, D. D. Poly lactose Exhibits Prebiotic Activity and Reduces Adiposity and Nonalcoholic Fatty Liver Disease in Rats Fed a High-Fat Diet. *J. Nutr.* **151**, 352–360 (2021).
143. Krämer, A., Green, J., Pollard, J. & Tugendreich, S. Causal analysis approaches in ingenuity pathway analysis. *Bioinformatics* **30**, 523–530 (2014).
144. Ashburner, M. *et al.* Gene ontology: tool for the unification of biology. The Gene Ontology Consortium. *Nat. Genet.* **25**, 25–29 (2000).
145. Riedel, G. *et al.* An Extended  $\Delta$ CT-Method Facilitating Normalisation with Multiple Reference Genes Suited for Quantitative RT-PCR Analyses of Human Hepatocyte-Like Cells. *PLoS One* **9**, e93031 (2014).
146. Ghazarian, M. *et al.* Type I Interferon Responses Drive Intrahepatic T cells to Promote Metabolic Syndrome. *Sci. Immunol.* **2**, (2017).
147. Sato, T. A modified method for lead staining of thin sections. *J. Electron Microsc.* (Tokyo). **17**, 158–159 (1968).
148. Wild, P. S. *et al.* A genome-wide association study identifies LIPA as a susceptibility gene for coronary artery disease. *Circ. Cardiovasc. Genet.* **4**, 403–412 (2011).
149. Kazankov, K. *et al.* The role of macrophages in nonalcoholic fatty liver disease and nonalcoholic steatohepatitis. *Nat. Rev. Gastroenterol. Hepatol.* **16**, 145–159 (2019).
150. Miyagawa, K. *et al.* Lipid-Induced Endoplasmic Reticulum Stress Impairs Selective Autophagy at the Step of Autophagosome-Lysosome Fusion in Hepatocytes. *Am. J. Pathol.* **186**, 1861–1873 (2016).
151. Zeng, J., Shirihai, O. S. & Grinstaff, M. W. Degradable Nanoparticles Restore Lysosomal pH and Autophagic Flux in Lipotoxic Pancreatic Beta Cells. *Adv. Healthc. Mater.* **8**, 1801511 (2019).
152. Sheriff, S., Du, H. & Grabowski, G. A. Characterization of lysosomal acid lipase by site-directed mutagenesis and heterologous expression. *J. Biol. Chem.* **270**, 27766–27772 (1995).
153. Yan, C. *et al.* Macrophage-specific expression of human lysosomal acid lipase

- corrects inflammation and pathogenic phenotypes in *lal*<sup>-/-</sup> mice. *Am. J. Pathol.* **169**, 916–926 (2006).
154. Ding, H. *et al.* Hepatic autophagy fluctuates during the development of non-alcoholic fatty liver disease. *Ann. Hepatol.* **19**, 516–522 (2020).
  155. González-Rodríguez, A. *et al.* Impaired autophagic flux is associated with increased endoplasmic reticulum stress during the development of NAFLD. *Cell Death Dis.* **5**, e1179 (2014).
  156. Khor, V. K. *et al.* The proteome of cholesteryl-ester-enriched versus triacylglycerol-enriched lipid droplets. *PLoS One* **9**, e105047 (2014).
  157. Las, G., Serada, S. B., Wikstrom, J. D., Twig, G. & Shirihai, O. S. Fatty acids suppress autophagic turnover in  $\beta$ -cells. *J. Biol. Chem.* **286**, 42534–42544 (2011).
  158. Cox, B. E., Griffin, E. E., Ullery, J. C. & W. Gray, J. Effects of cellular cholesterol loading on macrophage foam cell lysosome acidification. *J. Lipid Res.* **48**, 1012–1021 (2007).
  159. Yamamoto, T. *et al.* High-Fat Diet-Induced Lysosomal Dysfunction and Impaired Autophagic Flux Contribute to Lipotoxicity in the Kidney. *J. Am. Soc. Nephrol.* **28**, 1534–1551 (2017).
  160. Li, F. *et al.* Hepatic lysosomal acid lipase drives the autophagy-lysosomal response and alleviates cholesterol metabolic disorder in ApoE deficient mice. *Biochim. Biophys. acta. Mol. cell Biol. lipids* **1866**, 159027 (2021).